

Author's Response:

The following replies have been posted in response to the three Referees. The Referee's comments (in bold) are followed by our response. Changes to the manuscript are highlighted in green.

5 These responses are followed by 1) the revised manuscript with track changes enabled.

Reply to Referee #1

10 The authors present a very comprehensive and thoughtfully planned study to evaluate the performance of the three common N₂O isotope laser spectrometers, Picarro CRDS, Los Gatos ICOS, and Aerodyne QCLAS. Most importantly, they found that significant matrix and trace gas composition affected the precision and accuracy of all instruments with these interferences scaling with N₂O mole fraction. The authors do a great service for the community by proposing a step-by-step workflow to properly deal with these interferences.

15 I really appreciated Table 4 overviewing the many experiments performed because it helped orient me as I read through Section 2.4. Testing of instruments. Although I hesitate to ask the authors to add any more to this already massive manuscript, I think that readers would benefit from an additional overview table summarizing the main findings for each of the three types of N₂O isotope
20 laser spectrometers. This would help readers implement step 1 of the proposed workflow, choosing the right laser spectrometer for one's application, and also help readers implement the general workflow as appropriate for the specific spectrometer type (e.g., dealing with CH₄ interference is less important for QCLAS). Some readers may view this instrument intercomparison as an effort to determine which spectrometer outperforms the others. The addition of this summary table would
25 also help convey the important point that there is not one spectrometer with superior performance across all applications. The manuscript is well-written, but given the complex and detailed nature of the study, the experimental set-ups and results were inherently confusing to wade through. I have inserted specific comments in the attached PDF supplement to help highlight the take-home messages from the experiments and to clarify some points for readers who may be less familiar with
30 N₂O isotope laser spectrometry.

Authors' response: Following your suggestion, we have incorporated Table 8 into the manuscript (please note that the original Tables 8, 9 and 10 have now been placed in the Supplementary). We anticipate that the information provided in Table 8 will assist readers in better understanding the advantages and
35 limitations of each instrument when applied to certain measurement applications. It will be incorporated into the text on P60L4:

P60 L4: "A summary of results is presented in Table 8. Our results highlight that [...]"

40

45

50

Table 8. Summary of main findings presented in this study.

Detection scheme (model; manufacturer)	OA-ICOS I (N2OIA-30e-EP)	CRDS I & II (G5131-i)	QCLAS I (CW-QC-TILDAS-SC-D)	TREX-QCLAS I (CW-QC-TILDAS-76-CS)
Allan precision (300 s) $\delta^{15}\text{N}^{\alpha}$, $\delta^{15}\text{N}^{\beta}$, $\delta^{18}\text{O}$ [‰] 326.5 ppb N_2O ~ 1000 ppb N_2O ~ 10000 ppb N_2O	0.79 – 1.69 0.28 – 0.67 0.12 – 0.17	0.32 – 0.46 0.21 – 0.89 n.d.	0.39 – 3.45 ^{a)} 0.19 – 0.83 ^{a)} 0.02 – 0.48 ^{a)}	n.d. n.d. n.d.
Repeatability (326.5 ppb N_2O) N_2O [ppb] $\delta^{15}\text{N}^{\alpha}$, $\delta^{15}\text{N}^{\beta}$, $\delta^{18}\text{O}$ [‰]	0.07 1.19 – 2.17	0.26 – 0.30 0.52 – 0.83	0.16 5.35 – 8.57	1.29 0.37 – 0.60
Temperature effect (326.5 ppb N_2O) N_2O [ppb K^{-1}] $\delta^{15}\text{N}^{\alpha}$, $\delta^{15}\text{N}^{\beta}$, $\delta^{18}\text{O}$ [‰ K^{-1}]	0.01 0.36 – 2.60	0.02 0.25 – 0.65	0.10 31.29 – 37.32	n.d. n.d.
N_2O mole fraction dependence $\delta^{15}\text{N}^{\alpha}$, $\delta^{15}\text{N}^{\beta}$, $\delta^{18}\text{O}$ [‰ ppb ($\Delta 1/\text{N}_2\text{O}$)]	-8296 – 2544	-458 – 1353	-66386 – 15833	n.d.
O_2 matrix effect (330 ppb N_2O) N_2O [ppb % $^{-1}$ (ΔO_2)] $\delta^{15}\text{N}^{\alpha}$, $\delta^{15}\text{N}^{\beta}$, $\delta^{18}\text{O}$ [‰ % $^{-1}$ (ΔO_2)]	-0.044 0.874 – 1.270	0.24 – 0.305 -0.279 – (-1.364)	0.351 -1.111	n.s. n.s.
CO_2 trace gas effects (330 ppb N_2O) N_2O [ppb ppm $^{-1}$ (ΔCO_2)] $\delta^{15}\text{N}^{\alpha}$, $\delta^{15}\text{N}^{\beta}$, $\delta^{18}\text{O}$ [‰ ppm $^{-1}$ (ΔCO_2)]	0.0011 -0.009 – 0.026	0.0005 n.s. – (-0.0019)	n.s. n.s. – 0.0154	n.s. n.s.
CH_4 trace gas effects (330 ppb N_2O) N_2O [ppb ppm $^{-1}$ (ΔCH_4)] $\delta^{15}\text{N}^{\alpha}$, $\delta^{15}\text{N}^{\beta}$, $\delta^{18}\text{O}$ [‰ ppm $^{-1}$ (ΔCH_4)]	n.s. ^{b)} 0.173	-0.039 – (-0.056) 0.085 – 2.50	n.s. n.s.	n.s. n.s.
CO trace gas effects (330 ppb N_2O) N_2O [ppb ppm $^{-1}$ (ΔCO)] $\delta^{15}\text{N}^{\alpha}$, $\delta^{15}\text{N}^{\beta}$, $\delta^{18}\text{O}$ [‰ ppm $^{-1}$ (ΔCO)]	-0.29 n.s.	-0.15 – (-0.24) -0.53 – (-2.41)	-0.19 n.s. – (-4.04)	n.s. n.s.

a) Includes QCLAS I, II and III

b) Likely due to inaccuracies during dynamic dilution (see text for details)

n.d. not determined

n.s. not statistically significant at $p < 0.05$ and/or $r^2 < 0.5$ **Referee comment 1 - Page 4 Line 25: Start a new paragraph here.**

Authors' response: Agreed and revised.

Referee comment 2 - Page 5 Line 9: Readers could potentially benefit from a brief explanation of the principles of the spectroscopic approach compared to IRMS. This would provide some context for the trace gas effects described later.

Authors' response: We agree with this suggestion. In keeping with Referee #1 and Referee #2's comments regarding the length of our manuscript, we have opted to only briefly explain the spectroscopic approach in comparison to IRMS to limit the length of the manuscript. This paragraph (with minor re-structuring) now reads:

(New Paragraph) P4 L27: "The advancement of mid-infrared laser spectroscopic techniques was enabled by the invention and availability of non-cryogenic light sources which have been coupled with different detection schemes, such as direct absorption quantum cascade laser absorption spectroscopy (QCLAS; Aerodyne Research Inc. [ARI]; Wächter et al., 2008), cavity ring-down spectroscopy (CRDS; Picarro Inc.) and off-axis integrated-cavity-output spectroscopy (OA-ICOS; ABB Los Gatos Research Inc.; Baer et al., 2002) to realize compact field-deployable analyzers. In short, the emission wavelength of a laser light source is rapidly and repetitively scanned through a spectral region containing the spectral lines of the target N_2O isotopocules. The laser light is coupled into a multi-path cell filled with the sample gas, and the mixing ratios of individual isotopic species are determined from the detected absorption using Beer's Law. The wavelengths of spectral lines of N_2O isotopocules with distinct ^{17}O , ^{18}O or position-

specific ^{15}N substitution are unique due to the existence of characteristic rotational-vibrational spectra (Rothman et al., 2005). Thus, unlike IRMS, laser spectroscopy does not require mass-overlap correction. However, the spectral lines may have varying degrees of overlap with those of other gaseous species, which, if unaccounted for, may produce erroneous apparent absorption intensities. One advantage of laser spectroscopy is that instruments can analyze the N_2O isotopic composition in gaseous mixtures (e.g. ambient air) in a flow-through mode, providing real-time data with minimal or no sample pretreatment, which is highly attractive to better resolve the temporal complexity of N_2O production and consumption processes (Decock and Six, 2013; Heil et al., 2014; Köster et al., 2013; Winther et al., 2018).

Referee comment 3 - Page 5 Line 16: Temperature? Humidity? Expand on this a little more for the uninitiated.

Authors' response: We apologise for the unclear explanation. Our intention was to highlight that fluctuations in ambient temperature may cause drift effects due to moving interference fringes when using these instruments (see Werle et al., 1993). We did not intend to highlight the effects of humidity in point (3), because fluctuations in humidity would cause spectral interferences due to overlapping water vapor spectral peaks that are mentioned in point (4), rather than causing drift effects. The following changes have been made to the manuscript:

“(3) laser spectrometers are subject to drift effects (e.g. due to moving interference fringes), particularly under fluctuating laboratory temperatures, which limits their performance (Werle et al., 1993).”

Referee comment 4 - Page 5 Line 18: This approach needs to be defined, especially if the purpose of this paper is to educate people new to this field.

Authors' response: This was also a concern of Referee #2, and therefore we reply to all concerns here. We agree that this approach should be defined. However, because this topic has been discussed to great lengths elsewhere (Sturm, 2013; Wen et al., 2013; Griffith et al. 2012; Flores et al., 2017; Griffith, 2018), and to limit manuscript length, we will refrain from providing too much information in our manuscript.

As outlined in Griffith (2018), calibration of spectrometers can be achieved two ways: calibrating on derived isotopologue/isotopocule ratios or delta values (Approach A; what we referred to as a "δ-calibration approach"), or calibrating on derived individual isotopocule amount fractions (Approach B). In Approach A, raw measured delta values are calculated from measured uncalibrated isotopologue/isotopocule amount fractions, and then calibrated against the delta values of the reference gases. In Approach B, raw measured amount fractions of isotopocules are calibrated against a set of reference gases with known isotopocule amount fractions, prior to deriving ratio or delta values.

In our manuscript, we applied Approach A for three reasons: 1) N_2O isotope reference materials provide delta values but not amount fractions (Ostrom et al., 2018); 2) to remain consistent with the IRMS community, who calibrate results using Approach A; and 3) not all laser spectrometers tested (such as G5131-I and II, CRDS, Picarro Inc.) make the amount fraction data available to the user. It is therefore reasonable to assume that most users of these instruments will undertake Approach A.

However, as discussed in Sturm (2013; Atmos. Meas. Tech. Discuss., 6, C170–C176) and Wen et al. (2013), Approach A introduces a concentration dependence to delta values in potentially two ways: 1) if the analyzer measurements of isotopologue/isotopocule mole fractions are linear, yet the relationship between measured and true mole fractions have a non-zero intercept (Eq. 14 in Griffith et al., 2012); and/or 2) if the instrument response has non-zero offsets in integrated peak area due to baseline structures (such as fringe effects). This effect was observed in several studies in our laboratory, e.g. Tuzson et al. (2008), Wächter et al. (2008) and Eyer et al. (2016). The effect is dominant at low amount fractions, but less prominent at higher amount fractions, as shown in the Eq. below:

$$\delta a_{eff} = \left(\frac{\frac{[^{15}\text{N}^{14}\text{N}^{16}\text{O}] - [\text{A}]}{[^{14}\text{N}^{14}\text{N}^{16}\text{O}]} - 1}{r_A} \right) = \left(\frac{\frac{[^{15}\text{N}^{14}\text{N}^{16}\text{O}]}{[^{14}\text{N}^{14}\text{N}^{16}\text{O}]} - 1}{r_A} \right) - \frac{[\text{A}]}{r_A}$$

$$\delta a_{eff} = \delta a - \frac{[\text{A}]}{r_A} \cdot \frac{1}{[^{14}\text{N}^{14}\text{N}^{16}\text{O}]}$$

where δa_{eff} is the apparent delta value including the baseline effect; δa is the true delta value; $[^{15}\text{N}^{14}\text{N}^{16}\text{O}]$ refers to the amount fraction for the isotopocule $^{15}\text{N}^{14}\text{N}^{16}\text{O}$ (used here as an example) derived from its integrated peak area; $[^{14}\text{N}^{14}\text{N}^{16}\text{O}]$ refers to the amount fraction of the isotopocule $^{14}\text{N}^{14}\text{N}^{16}\text{O}$; r_A is the isotopocule amount fraction in the standard gas; and the offset caused by base-line structure is expressed as amount fraction $[\text{A}]$. Transformation provides $\frac{[\text{A}]}{r_A}$, which is a constant that scales linearly with the variable $\frac{1}{[^{14}\text{N}^{14}\text{N}^{16}\text{O}]}$.

Accordingly, we observed an inverse concentration dependence in all spectrometers, as shown in Fig. 5. In contrast, as outlined by Griffith (2018), Approach B removes this concentration dependence, removing the need for correction. Although this could potentially simplify the workflow procedure, we did not test nor compare approaches for the reasons given above.

We have therefore made the following changes to the manuscript:

P5 L18: “(3) if apparent delta values retrieved from a spectrometer are calculated from raw uncalibrated isotopocule mole fractions, referred to here as a δ -calibration approach, an inverse concentration dependence may be introduced. This can arise if the analyzer measurements of isotopocule mole fractions are linear, yet the relationship between measured and true mole fractions have a non-zero intercept (e.g. Griffith et al., 2012; Griffith, 2018), such as due to baseline structures (e.g. interfering fringes; Tuzson et al. 2008).”

We have omitted the following because it is discussed in the Discussion on P60:

P33 L16: “[...] analyzers tested, ~~which is characteristic of optical analyzers calibrated using a δ calibration scheme (Griffith et al., 2012; Griffith, 2018).~~ However, examination of the residuals from the linear regression revealed varying degrees of residual curvature, highlighting that further non-linear terms would be required to adequately describe, and correct for, this mole fraction dependence ~~(see Griffith et al., 2012).~~”

P60 L14: “The experiments performed in this study were undertaken using a standardized protocol. Calibration was performed on isotope δ values derived from raw uncalibrated isotopocule amount fractions, thus requiring $[\text{N}_2\text{O}]$ dependence corrections. Alternative approaches aimed at calibrating isotopocule amount fractions prior to deriving δ values were not included in our study, but have the potential to remove the need for this correction (e.g. Wen et al., 2013; Flores et al., 2017; Griffith, 2018) if appropriate reference materials become available.”

P66 L16: “[...] (if calibration relies on raw δ values derived from uncalibrated isotopocule amount fractions; i.e. a δ -calibration approach).

We have added the following reference:

Tuzson, B., Mohn, J., Zeeman, M.J., Werner, R.A., Eugster, W., Zahniser, M.S., Nelson, D.D., McManus, J.B., and Emmenegger, L.: High precision and continuous field measurements of $\delta^{13}\text{C}$ and $\delta^{18}\text{O}$ in carbon dioxide with a cryogen-free QCLAS, Appl. Phys. B, 92, 451, doi:10.1007/s00340-008-3085-4, 2008.

Referee comment 5 - Page 10 Line 14: What does cw mean?

Authors' response: The term "cw" stands for continuous wave. This was first abbreviated on P9 L16.

Referee comment 6 - Page 11 Line 10: This is a weird place to stick this sentence. Unclear if this is describing one of the studies mentioned in the previous sentence.

Authors' response: We agree that this sentence may be ambiguous in whether it is referring to Yamamoto et al. (2014) or not. Our intention was to highlight the data treatment required by Yamamoto et al. (2014) in order to obtain the precision levels achieved with their QCLAS system. These included correcting for mole fraction dependence and drift. These authors also highlighted the necessity to carefully control the operating temperature of their instrument. We have subsequently made the following changes to the manuscript:

P11 L10: "[...] with a closed chamber system. To achieve the precision and accuracy levels reported in their study, Yamamoto et al. (2014) corrected their measurements for mixing ratio dependence and minimized instrumental drift by measuring N₂ gas every 1 hr for background-correction. These authors also showed that careful temperature control of their instrument in an air-conditioned cabinet was necessary for achieving optimal results."

Referee comment 7 - Page 15 Line 1: This would be easier to digest in a table.

Authors' response: We agree that this would be much better suited to a table. Again, because of the length of our report, we have opted to include the following table and accompanying text as Supplementary Material 2. Changes are as follows:

P14 L25: "The isotopic composition of high [N₂O] isotope reference gases in synthetic air (S1-a₉₀ppm, S2-a₉₀ppm) was analyzed in relation to N₂O isotope standards (Cal1 – Cal3) in an identical matrix gas (matrix a) using laser spectroscopy (CW-QC-TILDAS-200; ARI, Billerica, USA). The composition of Cal1 – Cal3 are outlined in Supplementary Material 2."

Supplementary Material 2:

Supplementary Material 2: Analysis of high [N₂O] isotope reference gases, ambient reference gasses, PA1 and PA2

As detailed in Sect. 2.2.2, the isotopic composition of high [N₂O] isotope reference gases in synthetic air (S1-a₉₀ppm, S2-a₉₀ppm) was analyzed in relation to N₂O isotope standards (Cal1, 2 and 3) in the same gas matrix (matrix a) using laser spectroscopy (CW-QC-TILDAS-200; ARI, Billerica, USA). Ambient mole fraction N₂O isotope reference gases (S1-c₃₃₀ppb, S2-c₃₃₀ppb) and PA1 and PA2 were analyzed by TREX-QCLAS (Sect. 2.1.4) using N₂O isotope standards (Cal1 to 5) shown in Table S2-1. Cal1 – Cal5 have been previously measured by Sakae Toyoda at Tokyo Institute of Technology."

Table S2-1. N₂O isotope standards (Cal1 – Cal5) used for the analysis of reference gases (S1, S2) and pressurized air (PA1, PA2). The standards (Cal1 – Cal5) used for analysis of the respective gases are indicated by a tick (✓)

N ₂ O isotope standard used for calibration	$\delta^{15}\text{N}^a$ vs AIR-N ₂ [‰]	$\delta^{15}\text{N}^b$ vs AIR-N ₂ [‰]	$\delta^{18}\text{O}$ vs VSMOW [‰]	S1-a ₉₀ ppm	S2-a ₉₀ ppm	S1-c ₃₃₀ ppb	S2-c ₃₃₀ ppb	PA1	PA2
Cal1 in matrix a	2.06±0.05	1.98±0.20	36.12±0.32	✓		✓			
Cal2 in matrix a	-48.59±0.25	-46.11±0.43	27.37±0.11	✓	✓	✓	✓		
Cal3 in matrix a	25.73±0.24	25.44±0.36	35.86±0.22		✓		✓		
Cal4 in matrix a	16.29±0.07	-2.59±0.06	39.37±0.04					✓	✓
Cal5 in matrix a	-51.09±0.07	-48.12±0.04	30.81±0.03					✓	✓

Referee comment 8 - Page 15 Line 15: Some more context about why this was done would help orient the reader.

Authors' response: Due to differences in the gas matrix, S1-b_{90ppm}, S1-c_{90ppm} and S2-c_{90ppm} cannot be analysed directly by QCLAS, but only after dilution to ambient mixing ratios by TREX-QCLAS. To avoid higher uncertainty levels, the delta values of S1-a_{90ppm} and S2-a_{90ppm} were assigned to S1-b_{90ppm}, S1-c_{90ppm} and S2-c_{90ppm} since all 90 ppm mixtures were generated from the same source of pure N₂O diluted with the different gas matrices a, b and c. We would therefore not expect any deviation in delta values during this dilution process. The absence of significant deviations was assured by analysis of all reference gases as described in the manuscript. To help the reader to understand this issue, a short sub-sentence was added to Page 15 Line 15:

P15 L15: "[...] acquired for S1-a_{90ppm} and S2-a_{90ppm} were assigned, since all S1 and S2 reference gases (irrespective of gas matrix) were generated from the same source of pure N₂O gas. Direct analysis of S1-b_{90ppm}, S1-c_{90ppm} and S2-c_{90ppm} by QCLAS was not feasible as no N₂O isotope standards in matrix b and c were available. The absence of significant difference [...]"

Referee comment 9 - Page 16 Line 6: This would be easier to digest in a table.

Authors' response: Please refer to our response for Comment 7. Changes to the main text and Supplementary Material 2 are as follows:

P16 L4: "Ambient mole fraction N₂O isotope reference gases (S1-c_{330ppb}, S2-c_{330ppb}) and PA1 and PA2 were analyzed by TREX-QCLAS (Sect. 2.1.4) using N₂O isotope standards (Cal1 – Cal5) as outlined in Supplementary Material 2."

Supplementary Material 2: Comment 7 addresses this.

*Note: While addressing these Referee comments, we also noticed that on P16 L6, reference gases S1-c_{330ppb} and S2-c_{330ppb} were incorrectly written as S1-c_{330ppm} and S2-c_{330ppm}. We have rectified this mistake in the Supplementary Material.

Referee comment 10 - Page 20 Table 4: Why were three QCLAS mentioned earlier in the text if only one tested?

Authors' response: To clarify – we conducted all experiments on QCLAS I, but only conducted the Allan Variance experiments at ambient concentrations for QCLAS II and III, as stated in Table 4. The reason for doing this was so that we could test whether the drift experienced by QCLAS I (a 2012 model) was reproducible using newer models of QCLAS (2014 and 2016 models). In hindsight, all experiments should have been performed on either QCLAS II or III given that they achieved greater precision than QCLAS I. One advantage of our experimental setup was that the experiments were performed simultaneously for OA-ICOS I, CRDS I, CRDS II and QCLAS I, and thus all these instruments measured the same gas mixtures allowing for direct comparison of results. The testing for reproducibility of drift in the QCLAS systems was conducted on QCLAS II and III after the initial experimental period had finished and instruments had been returned to their respective labs. Thus, we could not re-run our experiments.

We acknowledge that by mentioning QCLAS II and III in the main text, and then not showing any results for the instruments, that this may cause confusion. Therefore, we agree that clarification is warranted. We have therefore added the following sentences to the updated manuscript:

Starting P10 L9: "Three QCLAS instruments (ARI, USA; CW-QC-TILDAS-SC-D) were used in this study. One instrument (QCLAS I), purchased in 2013, was provided by Karlsruhe Institute of Technology, Germany and two instruments, purchased in 2014 (QCLAS II) and 2016 (QCLAS III), were supplied by ETH Zürich, Switzerland (Table 1). QCLAS I was used in all experiments presented in this study, while QCLAS II and III were only used to assess the reproducibility of drift reported in Sect. 3.1."

Referee comment 11 - Page 21 Line 16: How quickly did the temperature change?

Authors' response: We thank the Referee for making this comment, as it allowed us to review the data more closely and identify an error in P21 L 15: the laboratory temperature was turned off for 10hrs, not 30hrs as stated.

The initial rise in temperature of the laboratory from 21°C to 30°C occurred over a 10 hr period while the air-conditioning was turned off at ~22:00 on 7/07/2018. This equates to an increase of roughly 0.9°C per hour. Detectable increases in the laboratory temperature occurred within 15 minutes of turning off the air conditioning due to the simultaneous operation of over 6 laser spectrometers and auxiliary devices in the laboratory releasing significant amounts of heat to the room. Once the air conditioning in the laboratory was turned back on at ~08:00 on 8/07/2018, the temperature returned to 21°C over a period of 16 hrs, equating to a decrease of roughly 0.6°C per hour. Unfortunately, due to unforeseeable delays in operating the instruments, we were only able to start the 24 hr analyser measurement period shortly before 00:00 on 8/07/2018 as shown in Fig. 4. Thus, we only captured the last stages of the rising limb of the temperature change in the laboratory, which should be clarified to the reader.

In light of this, we have made the following changes to the updated manuscript:

P21 L15: “[...] conditioning of the laboratory was turned off for 10 h. This led to a rise in temperature from 21°C to 30°C, equating to an increase in temperature of approximately 0.9°C per hour. The increase in laboratory room temperature was detectable shortly after the air conditioning was turned off due to considerable heat being released from several other instruments located in the laboratory. Thereafter, the air conditioning was restarted and the laboratory temperature returned to 21°C over the course of 16 h, equating to a decrease of roughly 0.6°C per hour, with most pronounced effects observable shortly after restart of air conditioning when temperature changes were highest.”

Fig. 4. Caption: “[...] Cell temperatures for each instrument are also plotted for comparison. The analyzers began acquiring measurements at 00:00 on 8/07/2018, capturing the end of the rising limb of the laboratory temperature.”

Referee comment 12 - Page 27 Line 7: Suggest starting a new paragraph here since the rest of this paragraph focuses on the QCLAS only. This will help make the information more digestible as well since this is otherwise a long paragraph.

Authors' response: We agree with this suggestion and will start a new paragraph here.

Referee comment 13 - Page 32 Fig. 4: Text too microscopic to read. should use landscape format.

Authors' response: Please refer to Referee #2 Comment 11.

Referee comment 14 - Page 34 Fig. 5: The text in the figure is too microscopic to read.

Authors' response: We agree. Please refer to Referee #2 Comment 11.

Referee comment 15 - Page 36 Fig. 6: Should use landscape format to show this figure because text too microscopic.

Authors' response: Please refer to Referee #2 Comment 11.

Referee comment 16 - Page 42 Fig. 8: Cannot read the microscopic text. Use landscape format.

Authors' response: Please refer to Referee #2 Comment 11.

5 Referee comment 17 - Page 43 Fig. 9: Cannot read the microscopic text. Use landscape format. This same comment applies for the following figures as well.

Authors' response: Please refer to Referee #2 Comment 11.

10 Referee comment 18 - Page 57 Line 3: This is a really important result to highlight.

Authors' response: We agree that this is an important result to highlight, and, as such, had re-emphasised this in the Discussion (Sect. 4.4) on P65 L16: "Our results show that large uncertainties exist for N₂O source apportionment using Keeling analysis performed at near-ambient N₂O mole fractions.". In keeping with all Referee's comments to limit the size of the manuscript, we wish to refrain from adding any further text highlighting this point.

Referee comment 19 - Page 60 Line 23: On the order of? It would be helpful to give some numbers here to remind the readers of the order of magnitude.

Authors' response: While we agree with the Referee's comment, we would prefer not to go into excessive detail regarding the magnitude of numbers here, because there are many numbers that could be quoted (5 analyzers were tested at 5 different O₂ compositions, and at 3 different N₂O concentrations). Thus, we would prefer to leave this as a general statement regarding the magnitude of the effect, as follows:

P60 L24: "[...] matrix. Although the magnitude of this effect ultimately varied across the analysers and was dependent on N₂O mixing ratios, the effect of a change in O₂ composition of 20.5 % was typically on the order of 10 to 30 ‰ for δ values."

30 Referee comment 20 - Page 63 Line 16: But this depends on the absorbance cell size. Supercells will require more flushing. And also depends on the pressures operated at.

Authors' response: That is correct. The volumes reported do reflect these different operating pressures, as well as the different flows, as mentioned in the text starting from P63 L14. To clarify this, we re-wrote parts of this paragraph:

*Please note that the following includes corrections implemented as part of our Reply to RC3 Comment 1.

40 P63 L11: "Researchers should also consider the sample gas volume required for a given measurement application using a specific laser spectrometer. In our experience, ensuring that five laser cavity cell volumes have been flushed prior to measurement is *best practice* to negate any memory effects when these instruments are operated using continuous flow-through configurations (as opposed to discrete sample measurements in a closed laser cavity). By following this procedure and using the operating parameters selected in this study (Table 1), the sample gas volume required for a single 300 s measurement is approximately 80 mL for CRDS II, 150 mL for CRDS I, 600 mL for OA-ICOS I and 1200 mL for QCLAS I. The different sample volumes required for CRDS I and CRDS II is due to the different selected flow rates. By comparison, TREX-QCLAS I requires approximately 5 L of sample gas to allow for N₂O preconcentration. These sample gas volumes represent typical numbers for atmospheric applications; however, instrument parameter settings such as flow rate and cell pressure, which ultimately change the required sample volume, can be optimized depending on the measurement application. This is particularly the case for QCLAS instruments, which can be operated with different user-adjustable settings. For applications requiring discrete sample analysis (e.g. the headspace analysis of $\delta^{15}\text{N}$ and $\delta^{18}\text{O}$

in N₂O derived from dissolved NO₃⁻), high N₂O concentration gas samples with lower volumes can be introduced to these instruments using injection ports and dilution gases (e.g. Soto et al., 2015; Wassenaar et al., 2018); however we did not test these capabilities in our study. Thus, users should carefully consider the available volume of the sample gas, although the possibility exists to dilute high concentration samples to increase gas volume. Researchers should also ensure that gas samples contain N₂O within the operational ranges of the different laser spectrometers (Table 1)."

Referee comment 21 - Page 64 Line 5: differ from

Authors' response: This sentence has been deleted and replaced with Fig. 15.

Referee comment 22 - Page 64 Line 8: But CH₄ is issue for only ICOS and CRDS?

Authors' response: Correct. The workflow seeks to cover all possible sources of measurement error tested in our study. CH₄ co-measurement is only relevant if the user is using a spectrometer employing a spectral range where N₂O isotopocule lines overlap with those of CH₄. This also applies for other substances. To clarify this, a general statement was added at the beginning of Section 4.3 P63 L25. Please note that we have included a new Fig. 15 to depict this workflow (see RC2 Comment 11):

P63 L23: "In-line with our results, we propose a step-by-step workflow that can be followed by researchers to acquire N₂O isotopocule measurements (Fig. 15). This workflow seeks to cover all sources of potential error tested in our study. Not all steps will be applicable because interference effects vary across analyzers. For QCLAS analyzers, which offer high versatility, interference effects can also be approached by multi-line analysis, inclusion of interfering spectral lines or adaption of pressure broadening parameters in the spectral fitting algorithm. For specific applications, such as incubation experiments with He, accessory injection units and setups using TREX, related actions have to be taken. While we tested several mono-variant and some bi-variant (e.g. changes in [CH₄] and [N₂O]) systems in our study, more complex systems (e.g. [CH₄] and [O₂], or even [CH₄], [O₂] and [N₂O]) were not tested, and deviations from additive behavior are to be expected. Depending on the desired precision, users may vary the measurement and averaging times, and calibration frequency.

Referee comment 23 - Page 66 Line 26: Perhaps this point can be moved elsewhere because the placement here undercuts the final message of the paper.

Authors' response: We agree and will move this point to P65 L12. We shall also rephrase it so that it does not undercut our findings so much:

P65 L12: "[...] performance, as shown in Supplementary Material 3. It is worth noting that, although the results of our study are representative of the performance of the instruments tested, the magnitude of reported effects and performances are likely to vary within the same analyser models."

The original paragraph has been deleted in line with Comment 24 below:

"It is important to note that the results of this study should be interpreted for these analyzer models only, and results are likely to vary slightly across the same make. Newer analyzers and models may yield better performance than reported here. As illustrated by the noticeable improvement between the CRDS I (2015 model) and CRDS II (2018 model), it is foreseeable that the performance of N₂O isotope laser spectrometers will continue to improve into the future. Future studies should focus on quantifying the error contributions to N₂O isotopocule analysis using laser spectroscopy."

Referee comment 24 - Page 67 Line 3: This last sentence doesn't seem to fit the rest of this paragraph and is a weak ending. Suggest just deleting this last sentence.

Authors' response: We have deleted this sentence.

Reply to Referee #2:

The paper reports the results of a detailed intercomparison study on the performance of commercially available isotopic N₂O analyzers based on laser spectroscopic methods. Such analyzers allow for continuous measurement of absolute trace gas concentrations (here N₂O) and isotope ratios (here, $\delta^{15}\text{N}$, $\delta^{18}\text{O}$) under field conditions. Isotopic analysis of N₂O is challenging, but is of high interest for source and sink identification in the biogeochemical community.

The extensive study was very well planned and conducted and produced large amount of data. As a result, a very extensive paper has been compiled by the authors. The paper is clearly structured and well-written. However, in order to limit the length of the paper to a bearable level, I suggest to shorten the main part by moving part of the Figure content and some Tables into the Supplement.

The presented results underline the necessity to carefully check analyzer performance, even for such sophisticated instruments as the ones used in this study. Although absorption based techniques should be essentially calibration-free (as they are simply based on Beer-Lambert law), the measurement of isotope ratios is prone to even smallest inaccuracies of the analyzers. This becomes quite obvious in case of the presented large uncertainties in the Keeling type experiments for source identification.

The paper ends with a clear conclusion and recommendation for the use of laser-based isotopic N₂O analyzers in practical applications. This is very useful and helps to design reasonable calibration strategies for future experiments. The paper is very technical, and not too much effort was spent to elaborate physical/spectroscopic explanations for the worked-out gas matrix effects and cross sensitivity issues. This may be well considered outside the scope of this paper, however, at least some brief statements about possible explanations are desirable.

However, overall this very good-excellent paper is a pleasure to read and for sure it is very well suited for publication in AMT, subject to changes (sorry for the long list – but it is a long paper. . .) as outlined in the following:

Specific Comments:

Referee Comment 1 – Page 4 Line 16: There is no principle reason why laser spectroscopy should be limited to the MIR spectral range. Of course, isotope specific measurements can also be performed in the NIR, albeit the used instruments are based on strong rovibrational transitions of the asymmetric stretch vibrational band of N₂O. Detection in the NIR range, due to the fact that overtone or combination bands with lower line strengths must be probed, will be less sensitive, however, due to lower spectral congestion, interference issues may be less dramatic.

Authors' response: We thank the Referee for their comment. Indeed, isotope measurements can be performed in other spectral ranges, and thus is not limited to the MIR. In our study, we focussed on commercially available analyzers that all operate in the MIR to achieve highest sensitivity. There are research grade instruments operating in the NIR, as stated by the reviewer. Therefore, we will re-word this sentence to highlight that other spectral regions may be used:

P4 L16: "N₂O isotopocules can be analyzed by isotope-ratio mass spectrometry (IRMS) and laser spectroscopic techniques, with currently available commercial spectrometers operating in the mid-infrared (MIR) region to achieve highest sensitivities."

Referee Comment 2 – Page 5 Line 18: Whereas items (1), (2), and (4) seem to be clear to me, this is not the case for item (3). Is it possible to include a short explanation why changes in the total N₂O

mole fraction also affect the determined delta values? Is this directly related to the “delta calibration approach” (what is this?)?

Authors' response: Please refer to our response to RC1 – Comment 4, where we address the delta calibration approach and N₂O mole fraction dependence.

Referee Comment 3 – Page 5 Line 21: While pressure broadening changes the absorption line shape of a specific rovibrational transition, the integral absorption should not be affected. As such, I would expect that instruments like the Picarro-CRDS that presumably measures peak absorption (at least this is the case for the corresponding isotopic CO₂ instrument) are more prone to gas matrix effects than instruments that are based on integral absorption (I think this is the case for the Los Gatos-OA-ICOS, for example). This should be explained at some point in the manuscript.

Authors' response: The authors agree that the specific detection scheme used by the analysers (CRDS, OA-ICOS, QCLAS), as well as the data acquisition and treatment, affect the analysers' response to changes in matrix gas composition (e.g. O₂). The importance of the data acquisition / treatment versus detection scheme can be seen by the different responses of CRDS I and II on changes in O₂ (Fig. 6). Because details on data acquisition / treatment are not accessible by users for all instruments, we prefer to provide readers with: 1) the observational data; 2) an explanation of the underlying fundamental causes; and 3) methods to correct these effects. For research grade instruments, with open-source data acquisition / treatment, it would be feasible to implement more sophisticated correction schemes, such as adapting pressure-broadening coefficients based on O₂ analysis. This, however, is beyond the scope of our study. To inform the reader that data acquisition / treatment can be advanced for open-source analysers, particularly the QCLAS systems tested, we added some statements to the text:

P10 L24: "QCLAS instruments offer great liberty to the user as the system can also be operated with different parameter settings, such as the selection of spectral lines for quantification, wavenumber calibration, sample flow rate and pressure. Thereby different applications can be realized, from high flow eddy covariance studies or high mole fraction process studies to high-precision measurements coupled to a customized inlet system. In addition, spectral interferences and gas matrix effects can be taken into consideration by multi-line analysis, inclusion of the respective spectroscopic parameters in the spectral evaluation or adjustment of the pressure broadening coefficients. The spectrometers used in this study (QCLAS I – III) were tested under standard settings but were not optimized for the respective experiments. QCLAS I was operated as a single laser instrument using laser one, to optimize spectral resolution of the frequency sweeps".

In addition, the following section was added to the discussions (in addition to corrections implemented in Referee #1 Comment 22):

P P63 L23: "In-line with our results, we propose a step-by-step workflow that can be followed by researchers to acquire N₂O isotopocule measurements. This workflow seeks to cover all sources of potential error tested in our study. Not all steps will be applicable because interference effects vary across analyzers. For QCLAS analyzers, which offer high versatility, interference effects can also be approached by multi-line analysis, inclusion of interfering spectral lines or adaption of pressure broadening parameters in the spectral fitting algorithm. For specific applications, such as incubation experiments with He, accessory injection units and setups using TREX, related actions have to be taken. While we tested several mono-variant (e.g changes in [CH₄] at constant [N₂O]) and some bi-variant (e.g. changes in [CH₄] and [N₂O]) systems in our study, more complex systems (e.g. changes in [CH₄], [O₂] and [N₂O]) were not tested, and deviations from additive behavior are to be expected. Depending on the desired precision, users may vary the measurement and averaging times, and calibration frequency."

Referee Comment 4 – Table 1: From a spectroscopic point of view, it would be interesting to include the rotational quantum number and term energy (i.e. the energy of the lower state) of the probed transitions. On the one hand, pressure broadening and with it the gas matrix effect is known to

sensitively depend on the rotational excitation of the probed molecules. On the other hand, the term energy largely determines the population of the lower state and with it is an important quantity to rationalize a potential temperature sensitivity of the instruments. According values can be taken from the HITRAN database.

Authors' response: We agree that rotational quantum numbers (J) and lower state energies (E'') of probed transitions provide information on pressure broadening (gas matrix effects) and temperature sensitivity. Therefore, we will provide the respective numbers in a new Supplementary Material 11 and add the following statements and restructuring to the manuscript:

P60 Line 4: "Our results highlight that the precision at which laser-based analyzers acquire N_2O isotopocule measurements is a function of N_2O mole fraction, the selected measuring and averaging times and calibration frequency according to measurement stability. The degree of accuracy obtained using different laser spectrometers is ultimately a function of the robustness of corrections aimed at removing matrix and trace gas effects, and the selected calibration procedure aimed at standardizing the data to international scales.

****New paragraph****

All spectrometers tested displayed temperature effects on isotope measurements, which can be attributed to differences in the lower state energies of the probed N_2O isotopocule lines (Supplementary Material 11) (e.g. Wächter et al. 2008). The temperature sensitivities of all analyzers tested necessitates that, especially when deployed in the field, they be operated under temperature-controlled conditions (such as in maintained field stations), and/or their dependence adequately characterized and corrected."

P60 Line 24: "[...] O_2 composition of the gas matrix. The underlying reason for this effect is differences in N_2 versus O_2 (and Ar) broadening parameters of the probed N_2O isotopocule lines. In short, the N_2 , O_2 (and Ar) broadening parameters depend on rotational quantum numbers of the respective N_2O lines (Henry et al., 1985; Supplementary Material 11). Thus, differences in the rotational quantum numbers for a pair of isotopocules (e.g. $^{14}N^{15}N^{16}O$ / $^{14}N^{14}N^{16}O$) relate to a difference in their N_2 , O_2 and Ar broadening parameters. Consequently, differences in the O_2 or Ar content of the sample gas matrix and that of the reference gas affect measured isotope ratios and lead to changes in apparent delta values. Nonetheless, the magnitude of effects reported for the CRDS analyzers in this study varied [...]"

The following reference will be added to the updated manuscript:
Henry, A., Margottin-Maclou, M., and Lacome, N.: N_2 - and O_2 -broadening parameters in the ν_3 band of $^{14}N_2^{16}O$, J. Mol. Spectrosc., 111, 291–300, doi:10.1016/0022-2852(85)90006-2, 1985.

Supplementary Material 11:

"Supplementary Material 11: Lower state energies of probed N_2O isotopocule lines

The lower state energies of probed N_2O isotopocule lines are provided in Table S11-1. Differences in the rotational quantum numbers for a pair of isotopocules (such as $^{14}N^{15}N^{16}O$ / $^{14}N^{14}N^{16}O$) lead to changes in N_2 , O_2 and Ar broadening parameters (Henry et al., 1985). If the sample gas matrix is different to that of the reference gas, deviations in the apparent delta values will arise.

Table S11-1. Wavenumber positions, line strength, branch / rotational quantum numbers and lower state energies of selected N₂O isotopocule lines applied for different laser spectrometers as retrieved from HITRAN2016 database.

	Line positions (cm ⁻¹)	Line strength (cm ⁻¹ /(molecule cm ⁻²))	Branch / rotational quantum number	Lower-state energy (cm ⁻¹)
OA-ICOS I				
¹⁴ N ¹⁴ N ¹⁶ O	2192.401	4.92E-20	P / 19	748.33
	2192.436	4.92E-20	P / 19	748.03
	2192.483	3.38E-19	P / 33	469.91
¹⁴ N ¹⁵ N ¹⁶ O	2192.309	3.31E-21	R / 18	143.27
¹⁵ N ¹⁴ N ¹⁶ O	2192.330	2.97E-21	P / 11	53.44
¹⁴ N ¹⁴ N ¹⁸ O	2192.133	1.11E-21	P / 28	321.10
CRDS I & II				
¹⁴ N ¹⁴ N ¹⁶ O	2196.21	5.16E-20	P / 15	689.55
	2196.24	5.16E-20	P / 15	689.36
¹⁴ N ¹⁵ N ¹⁶ O	2195.762	2.73E-21	R / 23	231.22
¹⁵ N ¹⁴ N ¹⁶ O	2195.796	2.20E-21	P / 7	22.67
¹⁴ N ¹⁴ N ¹⁸ O	2195.951	1.43E-21	P / 24	237.29
QCLAS I, II & III				
¹⁴ N ¹⁴ N ¹⁶ O	2188.045	2.60E-21	P / 9	1205.92
¹⁴ N ¹⁵ N ¹⁶ O	2187.943	3.29E-21	R / 12	65.36
¹⁵ N ¹⁴ N ¹⁶ O	2187.846	3.27E-21	P / 16	110.11
¹⁴ N ¹⁴ N ¹⁸ O	2203.281	1.79E-21	P / 16	107.59
TREX-QCLAS I				
¹⁴ N ¹⁴ N ¹⁶ O	2203.100	2.71E-21	R / 8	1198.37
	2203.114	1.44E-21	R / 8	1314.95
¹⁴ N ¹⁵ N ¹⁶ O	2203.359	9.80E-22	R / 35	527.64
¹⁵ N ¹⁴ N ¹⁶ O	2203.205	7.02E-22	R / 1	0.81
¹⁴ N ¹⁴ N ¹⁸ O	2203.281	1.79E-21	P / 16	107.59

5

Referee Comment 5 – Table 6 and Figure 3: How often these experiments have been repeated? How reproducible was the drift behavior of the QCLAS analyzers?

10 Authors' response: During reconnaissance testing in the ~two months prior to the final measurement campaign, we performed the Allan deviation testing on three separate occasions. These experiments yielded similar results (for both Allan “minimums”, and 300s and 600s averaging times) for all analyzers. As further confirmation of the drift behavior in QCLAS I, the QCLAS II and QCLAS III analyzers were tested for their Allan deviation after the measurement campaign. As shown in Fig. 3, the drift behavior, albeit to different magnitudes, was evident. Moreover, a QCLAS system (CW-QC-TILDAS-SC-S-
15 N₂OISO; Aerodyne Research Inc.) used by Yamamoto et al. (2014) showed similar drift (their Figure 2).

During our communications with Aerodyne Inc. technicians, we were made aware that they had developed an automatic spectral correction method to correct for data that was influenced by changing baseline structure. For this reason, we included a brief description of their methodology (courtesy of
20 Aerodyne Inc.), and an example of the same Allan deviation data for QCLAS I which had been re-processed by Aerodyne technicians using their correction methodology (see Table 6). This correction technique significantly decreased the magnitude of drift experienced by QCLAS I.

Accordingly, we will make the following additions to the updated manuscript:

25

Fig. 3 Caption: “[...] The dashed lines represent a slope of -0.5 (log-log scale) and indicate the expected behavior for Gaussian white noise in each analyzer. The Allan deviations of all analyzers tested were reproducible on three separate occasions prior to the test results presented here.”

- 5 **Referee Comment 6 – Figure 4: I wonder how the cell temperatures have been measured? In the middle of the cell? one or two pint measurements? Is anything known about possible T-gradients across the measurement cells? It seems that the experiment has only been conducted once. Do the authors believe that the measured trends in the signals are robust? Actually, for practical applications it would also have been interesting to perform an experiment at static (but different) temperatures.**

Authors’ response: The authors agree with Referee #2 that gas temperature measurements are delicate, as sensor temperature may deviate from the actual gas temperature due to inaccuracies and wall effects. Also, the gas temperature might not be homogeneous, calling for multiple temperature sensors. 15 Nonetheless, plotting the cell temperature as additional supporting parameter, allows us to rationalize the observed T effects on N₂O mixing ratios and delta values. The temperature experiment was only conducted once to test and demonstrate the detrimental effects of lab temperature changes on analyzer performance and call for a air-condition lab environment. The authors do not claim or encourage to correct data based on the observed experiments, as the magnitude might depend on cooling / heating rate ($\Delta T / \Delta t$), starting / end temperature etc. As such, we will remove the following statement from P60 L6 in the Discussion: 20

P60 L6: “[...] The temperature sensitivities of all analyzers tested necessitates that, especially when such instruments are deployed in the field, laser spectrometers in general be operated under temperature-controlled conditions (such as in maintained field stations), ~~and/or their dependence adequately characterized and corrected.~~” 25

- 30 **Referee Comment 7 – Section 3.2: Please give some more information about possible reasons for the observed temperature effects.**

Authors’ response: The authors agree and added lower state energies for the probed N₂O isotopocule lines to the supplementary information and a statement to the discussion section (see our response to Comment 4, above). 35

- 40 **Referee Comment 8 – Page 33 Line 20: Again, the reason for the N₂O mole fraction dependence is not fully clear to me without further explanation. I am sure that this is explained in some detail in the cited Griffith et al. papers, however, is it possible to roughly outline the main reason for this in 1-2 sentences?**

Authors’ response: The authors agree, please refer to our response to RC1 – Comment 4, where we address the delta calibration approach and N₂O mole fraction dependence.

- 45 **Referee Comment 9 – Figure 6: Actually, I am surprised to see the strong effect of O₂ content for the integrating OA-ICOS experiment as well, in particular for the total N₂O data (see also my comment above). Do the authors have a physical/spectroscopic explanation for this effect?**

Authors’ response: We will here refer to the same line of reasoning as given in response to Comments 3 and 4 (above). 50

- Referee Comment 10 – Page 35 Line 6: The authors state that minor gas matrix effects have been observed for Ar (in comparison with O₂). Well, as the Ar content has been changed by only 1% in comparison to 21% for O₂. Therefore, I think, this statement is not fully valid. Overall, the effect**

(on a mole fraction basis) is not very much different. May be the authors allude to the maximum effect expected for real-world measurement conditions. Although the depicted trends seem to be instrument-specific in some cases (e.g., the different slopes of the gas matrix effects for variable N₂O content, which cannot be explained by a simple pressure broadening effect), I would appreciate to elaborate a little bit more on physical/spectroscopic reasons that may (at least partly) explain some of the observations.

Authors' response: The authors agree that the statement with respect to the limited effect of Ar on [N₂O] and delta values refers to the anticipated maximum changes in [Ar] of 1 %; i.e. the difference between a ambient air sample with argon and a calibration gas mixed in N₂/O₂. We do not foresee situations where measurements of N₂O isotopes would coincide with a gas matrix consisting higher than 1 % argon. Details on the underlying physical/spectroscopic causes are given in our response to RC2 – Comment 3 and 4. In addition, we added the following statements to the manuscript:

P35 L7: "The range investigated was between approximately 0 % and 0.95 % Ar, as anticipated for an N₂O in synthetic air (no Ar) reference gas versus a whole air (with Ar) sample gas. The effects observed for 0.95 % change in [Ar] were significantly smaller than that observed for O₂, but might extend to a similar range for sample and reference gases with higher differences in [Ar]. The interference effects were found to be best described by second-order polynomial functions, though we expect that a linear fit would serve equally well if a larger change in [Ar] was investigated. Although most functions to describe the dependence on Ar across all instruments were statistically significant ($p < 0.05$), maximum effects did not transgress the repeatability (1σ) of the Anchor gas measurements."

P39 L24: "Although we could have tested for effects for [Ar] changes greater than 0.95%, we limited our experiments to [Ar] expected in tropospheric samples."

P61 L5: "Although the Ar effects characterized in this study were not large (a maximum ~1 % change in [Ar]), it is nonetheless recommended as a precautionary measure that researchers ensure, where possible, the standard calibration gas Ar composition is similar to that of the sample gas."

Referee Comment 11 – In most Figures, the complete datasets for N₂O, delta 15N_{alpha}, delta15N_{beta} and deltaN18O are given for all five instruments. Even though it is interesting to see all these results, keeping in mind the length of the paper, the authors may consider to somewhat lower the total number of subplots in each Figure by showing only selected trends. This would also allow one to somewhat increase the font size of the captions that are often hard to read anyway. Of course, the complete dataset should be included in the Supplement.

Authors' response: In line with both Referee #1 and #2, we have increased the text size and lowered the number of subplots in Figs. 3 – 14 so that the data may be viewed more easily. We also agree that the overall number of figures should be reduced, so we have transferred the original Figs. 7, 10 and 11 (Ar, CO, H₂O effects) to the new Supplementary Material 4. Thus, no data for Ar, CO and H₂O will be depicted in the main manuscript. We will refer the reader at the beginning of Sect. 3 (Results) to a new Supplementary Material 4 which provides the complete datasets:

P26 L17: "**3. Results**

Note: due to the large number of results acquired in this Section, only selected results are shown in Figs. 3 to 14. The complete datasets (including [N₂O], $\delta^{15}\text{N}^{\alpha}$, $\delta^{15}\text{N}^{\beta}$ and $\delta^{18}\text{O}$ acquired by all instruments tested) are provided in Supplementary Material 4.

3.1 Allan precision

[...]"

The following figures will be added to Supplementary Material 4:

“Supplementary Material 4: Complete Results datasets

Allan deviation plots (Sect. 3.1)

5 Fig. S4-1: *Original Fig. 3 with original figure caption

Temperature dependence plots (Sect. 3.2)

10 Fig. S4-2: *Original Fig. 4 with original figure caption

Mole fraction dependence plots (Sect. 3.4)

15 Fig. S4-3: *Original Fig. 5 with original figure caption

O₂ dependence plots (Sect. 3.5)

20 Fig. S4-4: *Original Fig. 6 with original figure caption

Ar dependence plots (Sect. 3.5)

25 Fig. S4-5: *Original Fig. 7 with original figure caption

CO₂ dependence plots (Sect. 3.6)

30 Fig. S4-6: *Original Fig. 8 with original figure caption

CH₄ dependence plots (Sect. 3.6)

35 Fig. S4-7: *Original Fig. 9 with original figure caption

CO dependence plots (Sect. 3.6)

40 Fig. S4-8: *Original Fig. 10 with original figure caption

H₂O dependence plots (Sect. 3.6)

45 Fig. S4-9: *Original Fig. 11 with original figure caption

Two end-member mixing correlation diagrams for measured vs expected (Sect. 3.7)

50 Figs. S4-10 to S4-14: *Original Figs. 12 to 16 with original figure captions

Two end-member mixing source intercept comparison plots (Sect. 3.7)

Fig. S4-15: *Original Fig. 17 with original figure caption”.

In Figs. 3, 5, 6, 7 and 8 in the updated manuscript, we compare the response of the analyzers across one consistent isotope (e.g. comparing all $\delta^{15}\text{N}^{\alpha}$ measurements for all instruments). In the updated Fig. 4, not all analyzers were clearly and uniformly affected across equivalent measurements – therefore, we show examples of measurements that were clearly temperature-dependent for each instrument ($\delta^{18}\text{O}$ for OA-ICOS I, $\delta^{15}\text{N}^{\alpha}$ for CRDS I, $[\text{N}_2\text{O}]$ for CRDS II, and $\delta^{15}\text{N}^{\beta}$ for QCLAS I). In Figs. 9 to 14, we compare the measurements of the analyzers for $\delta^{15}\text{N}^{\text{Bulk}}$ and SP as examples.

The following figures and captions were added to the manuscript as follows:

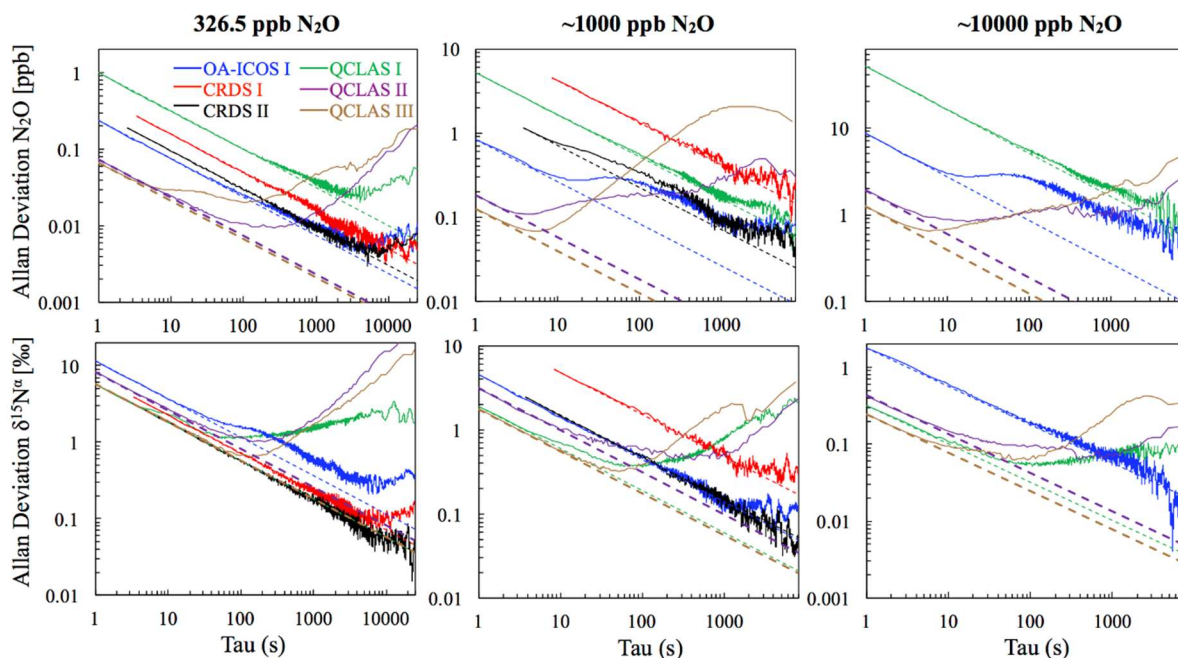


Fig. 3. Allan deviation (square root of Allan Variance) plots for the OA-ICOS I (blue), CRDS I (red), CRDS II (black), QCLAS I (green), QCLAS II (purple) and QCLAS III (brown) at different N_2O mole fractions (326.5, 1000 and 10000 ppb). The dashed lines represent a slope of -0.5 (log-log scale) and indicate the expected behavior for Gaussian white noise in each analyzer. The entire dataset is provided in Supplementary Material 4 (Fig. S4-1).

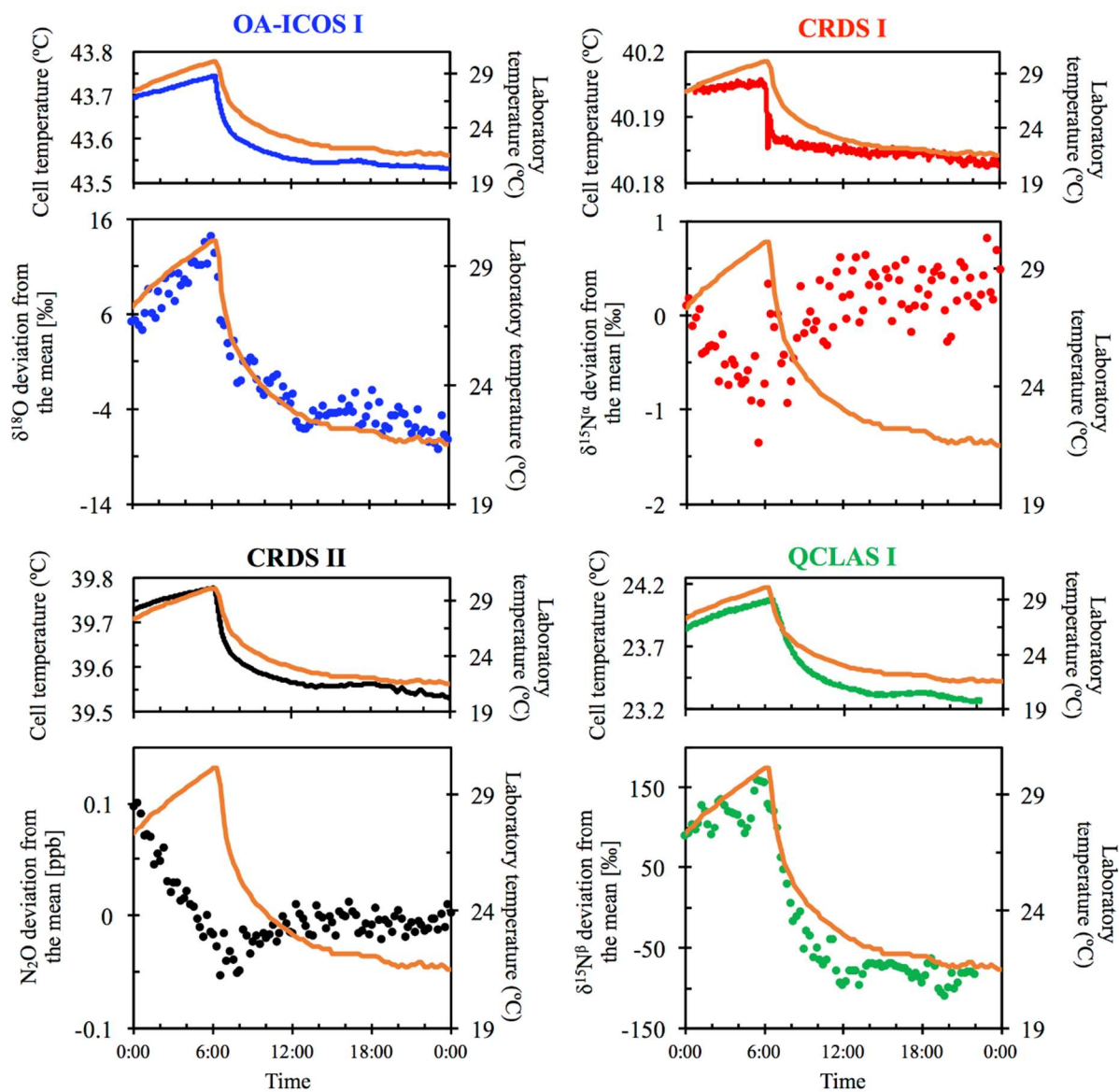


Fig. 4. Examples of the dependency of different measurements on laboratory temperature (°C) for OA-ICOS I (blue), CRDS I (red), CRDS II (black) and QCLAS I (green). The complete dataset is provided in Supplementary Material 4 (Fig. S4-2). The laboratory temperature is indicated by a solid orange line and was allowed to vary over time. Cell temperatures for each instrument are also plotted for comparison. Results are plotted as the deviation from the mean, without any anchoring to reference gases.

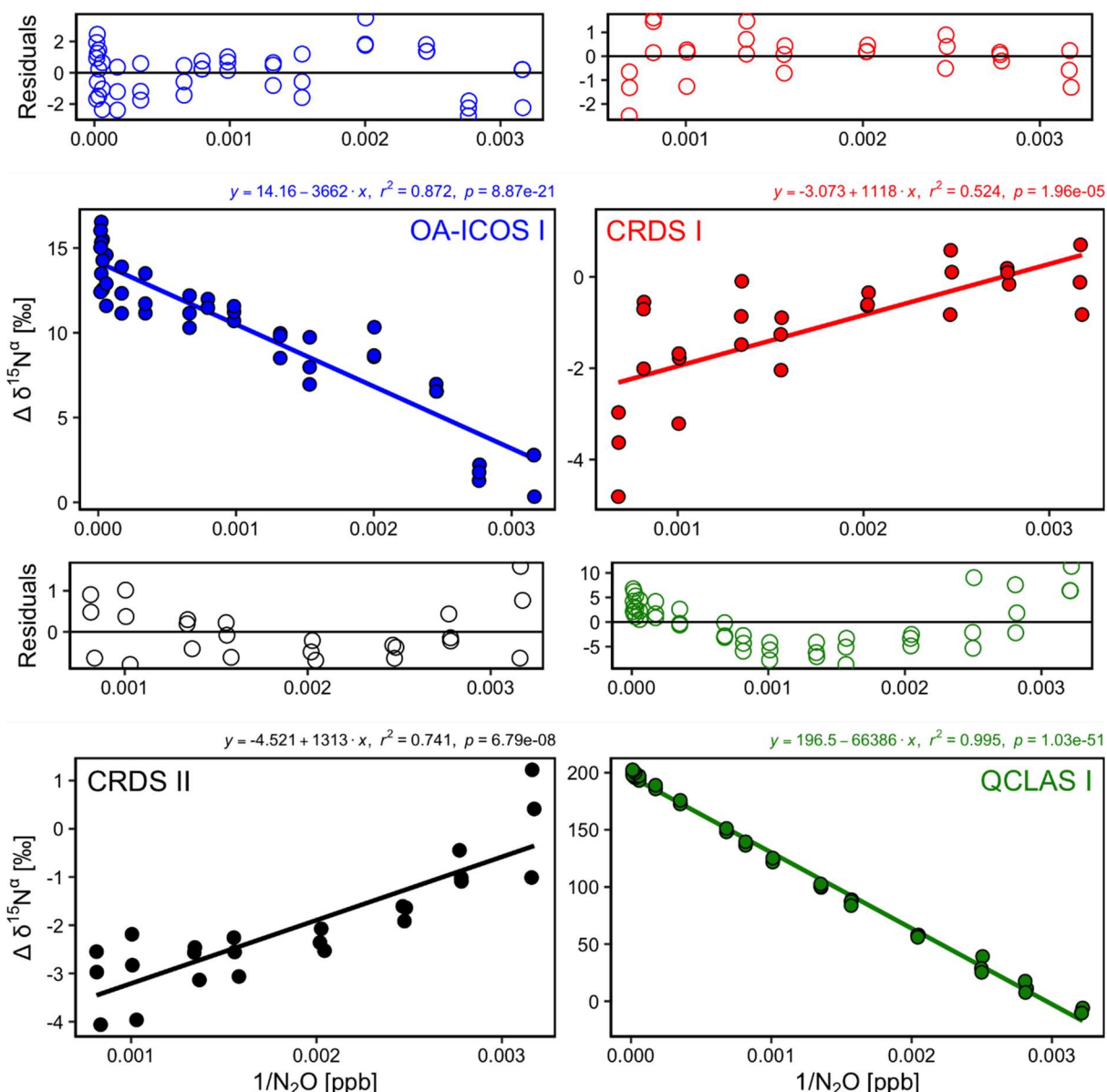


Fig. 5. Deviations of the measured $\delta^{15}\text{N}^{\alpha}$ values according to $1/[\text{N}_2\text{O}]$ for the OA-ICOS I (blue), CRDS I (red), CRDS II (black) and QCLAS I (green). Measurements span the manufacturer-specified operational ranges of the analyzers. The experiment was repeated on three separate days. A linear regression is indicated by the solid line, and a residual plot is provided above each plot. Individual linear equations, coefficients of determination (r^2) and p-values are indicated above each plot. **The entire dataset is provided in Supplementary Material 4 (Fig. S4-3).**

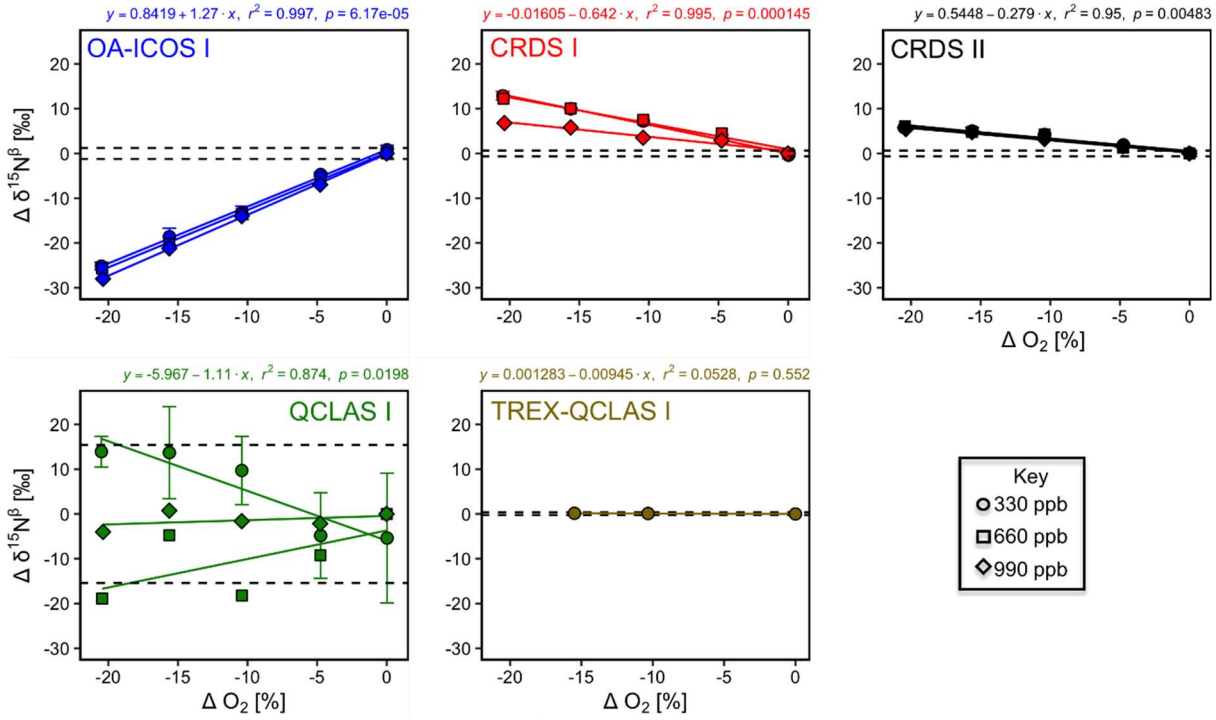


Fig. 6. Deviations of the measured $\delta^{15}\text{N}^\beta$ values according to ΔO_2 (%) at different N_2O mole fractions (330, 660 and 990 ppb) for the OA-ICOS I (blue), CRDS I (red), CRDS II (black), QCLAS I (green) and TREX-QCLAS I (brown). The remaining plots for $[\text{N}_2\text{O}]$, $\delta^{15}\text{N}^\alpha$ and $\delta^{18}\text{O}$ are provided in Supplementary Material 4 (Fig. S4-4). The standard deviation of the Anchor gas ($\pm 1\sigma$) is indicated by dashed lines. Data points represent the mean and standard deviation (1σ) of triplicate measurements. Dependencies are best-described using linear regression, which are indicated by a solid line. Individual equations, coefficients of determination (r^2) and p -values are indicated above each plot for the 330 ppb N_2O data only.

10

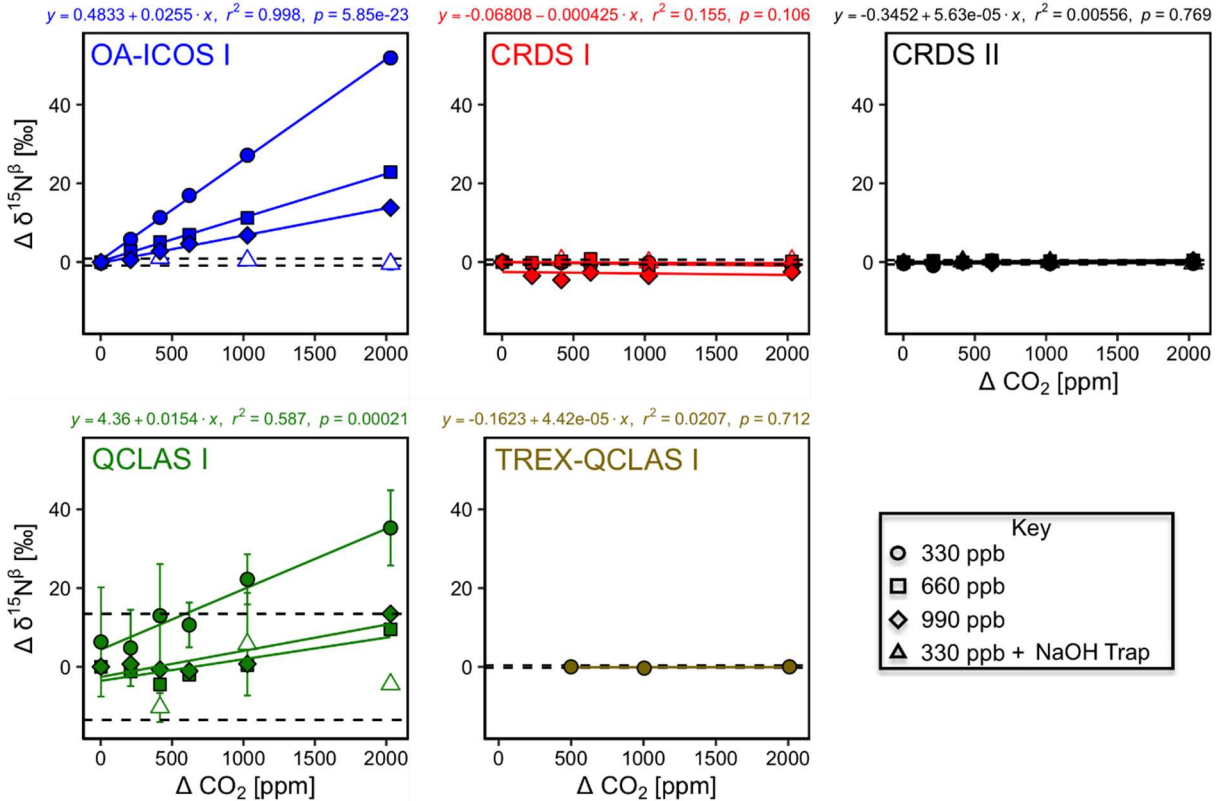


Fig. 7. Deviations of the measured $\delta^{15}\text{N}^\beta$ values according to ΔCO_2 (ppm) at different N_2O mole fractions (330, 660 and 990 ppb) for the OA-ICOS I (blue), CRDS I (red), CRDS II (black), QCLAS I (green) and TREX-QCLAS I (brown). The remaining plots for $[\text{N}_2\text{O}]$, $\delta^{15}\text{N}^\alpha$ and $\delta^{18}\text{O}$ are provided in Supplementary

Material 4 (Fig. S4-6). The standard deviation of the Anchor gas ($\pm 1\sigma$) is indicated by dashed lines. Data points represent the mean and standard deviation (1σ) of triplicate measurements. Dependencies are best-described by linear fits, which are indicated by solid lines. Individual equations, coefficients of determination (r^2) and p -values are indicated above each plot for the 330 ppb N_2O data only.

5

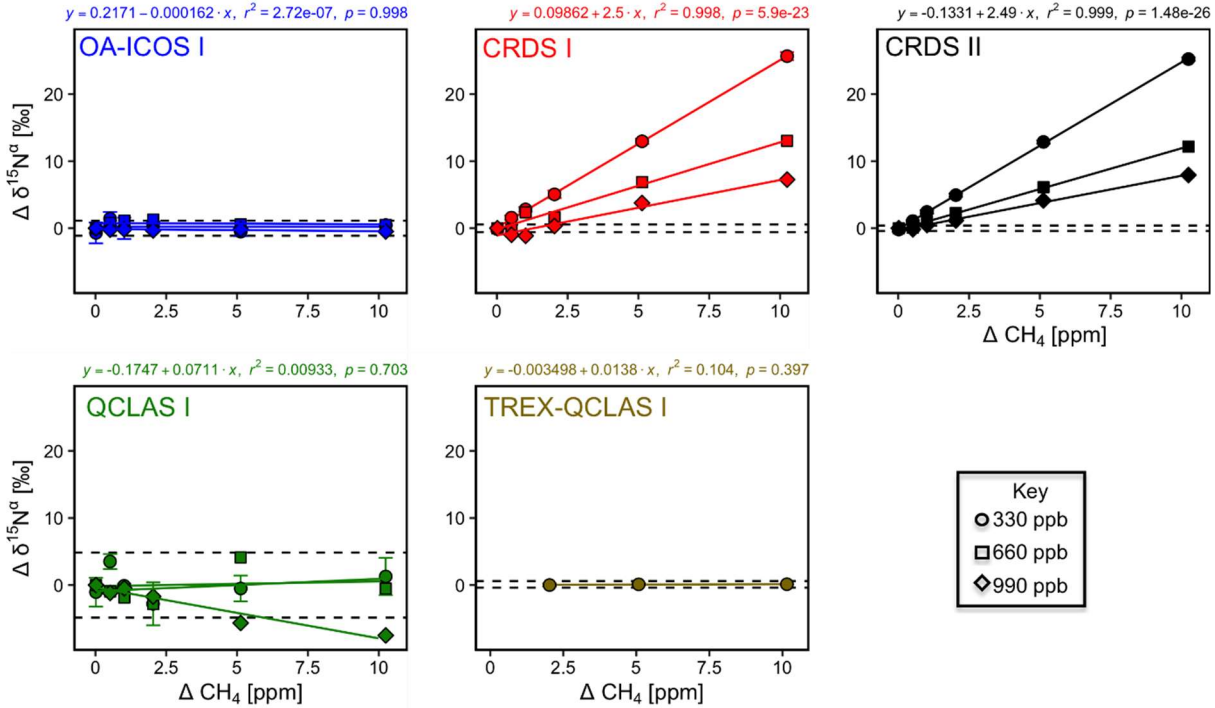
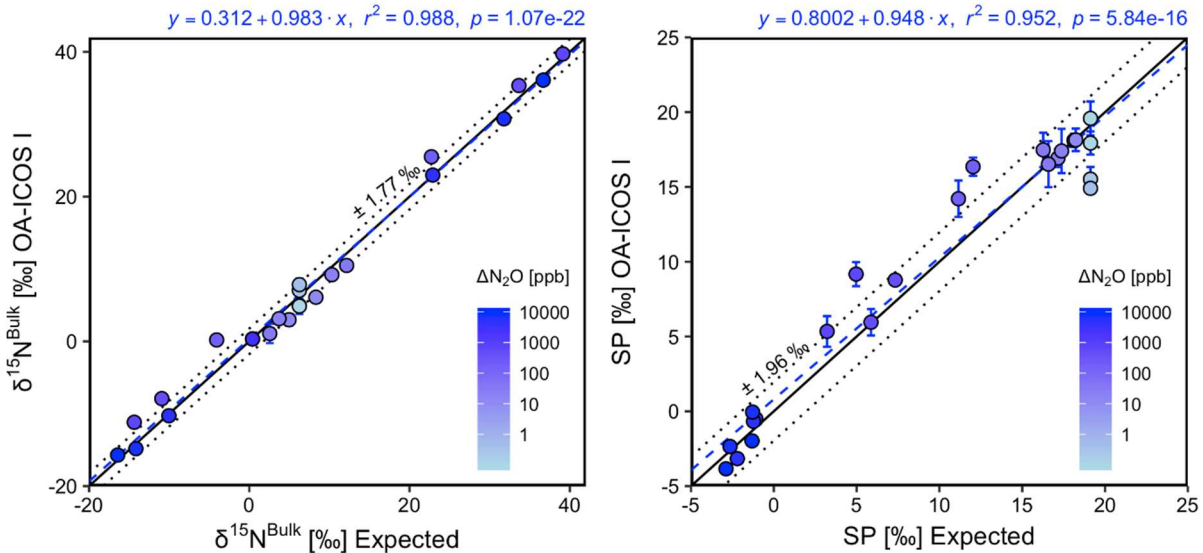


Fig. 8. Deviations of the measured $\delta^{15}N^a$ values according to ΔCH_4 (ppm) at different N_2O mole fractions (330, 660 and 990 ppb) for the OA-ICOS I (blue), CRDS I (red), CRDS II (black), QCLAS I (green) and TREX-QCLAS I (brown). The remaining plots for $[N_2O]$, $\delta^{15}N^b$ and $\delta^{18}O$ are provided in Supplementary Material 4 (Fig. S4-7). Data points represent the mean and standard deviation (1σ) of triplicate measurements. Dependencies are best-described by linear fits, which are indicated by solid lines. Individual equations, coefficients of determination (r^2) and p -values are indicated above each plot for the 330 ppb N_2O data only.

10



15

Fig. 9. Correlation diagrams for $\delta^{15}N^{bulk}$ and SP measurements at various ΔN_2O mole fractions analyzed by OA-ICOS I plotted against expected values. The remaining plots for $[N_2O]$, $\delta^{15}N^a$, $\delta^{15}N^b$ and $\delta^{18}O$ are provided in Supplementary Material 4 (Fig S4-10). The solid black line denotes the 1:1 line, while the dotted line indicates $\pm 1\sigma$ of the residuals from the 1:1 line. The dashed blue line represents a linear fit to the data. Individual equations, coefficients of determination (r^2) and p -values are indicated above each plot. Each data point represents the mean and standard deviation (1σ) of triplicate measurements.

20

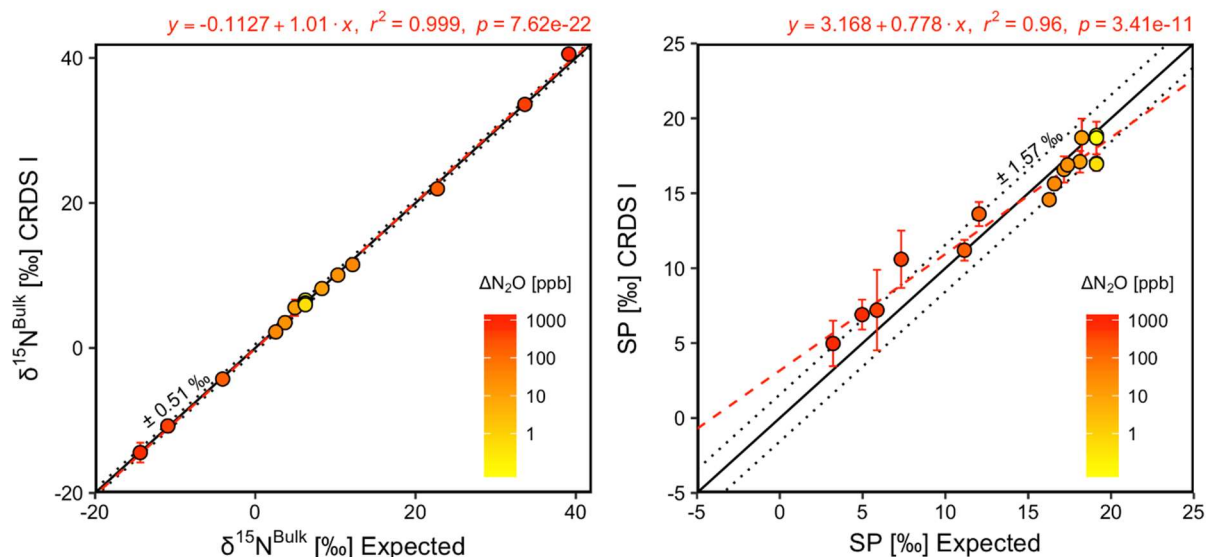


Fig. 10. Correlation diagrams for $\delta^{15}\text{N}^{\text{bulk}}$ and SP measurements at various $\Delta\text{N}_2\text{O}$ mole fractions analyzed by CRDS I plotted against expected values. The remaining plots for $[\text{N}_2\text{O}]$, $\delta^{15}\text{N}^{\alpha}$, $\delta^{15}\text{N}^{\beta}$ and $\delta^{18}\text{O}$ are provided in Supplementary Material 4 (Fig. S4-11). The solid black line denotes the 1:1 line, while the dotted line indicates $\pm 1\sigma$ of the residuals from the 1:1 line. The dashed blue line represents a linear fit to the data. Individual equations, coefficients of determination (r^2) and p -values are indicated above each plot. Each data point represents the mean and standard deviation (1σ) of triplicate measurements.

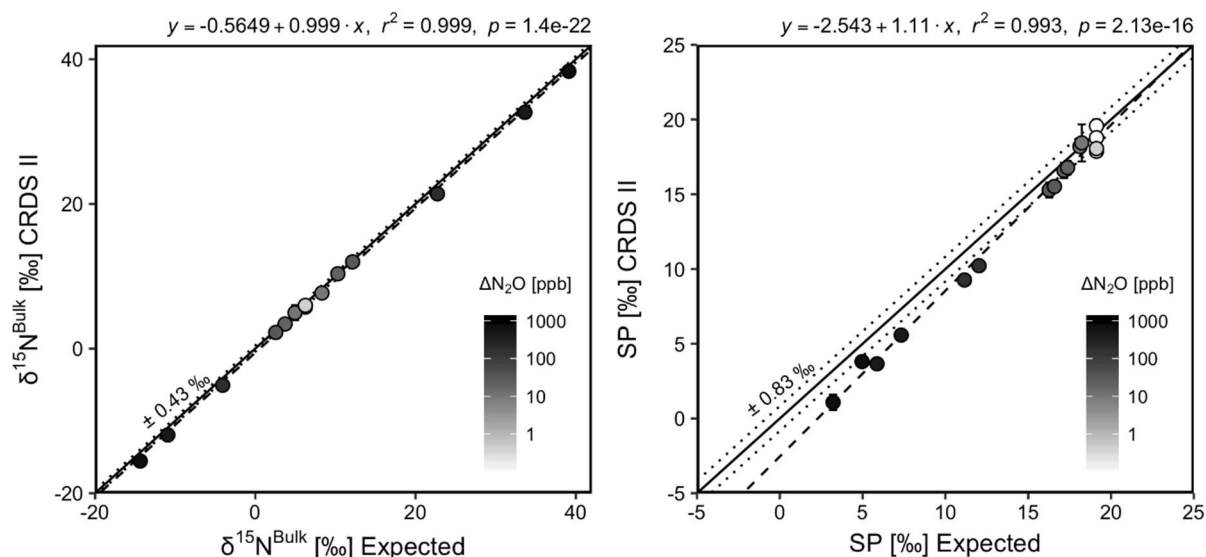


Fig. 11. Correlation diagrams for $\delta^{15}\text{N}^{\text{bulk}}$ and SP measurements at various $\Delta\text{N}_2\text{O}$ mole fractions analyzed by CRDS II plotted against expected values. The remaining plots for $[\text{N}_2\text{O}]$, $\delta^{15}\text{N}^{\alpha}$, $\delta^{15}\text{N}^{\beta}$ and $\delta^{18}\text{O}$ are provided in Supplementary Material 4 (Fig. S4-12). The solid black line denotes the 1:1 line, while the dotted line indicates $\pm 1\sigma$ of the residuals from the 1:1 line. The dashed blue line represents a linear fit to the data. Individual equations, coefficients of determination (r^2) and p -values are indicated above each plot. Each data point represents the mean and standard deviation (1σ) of triplicate measurements.

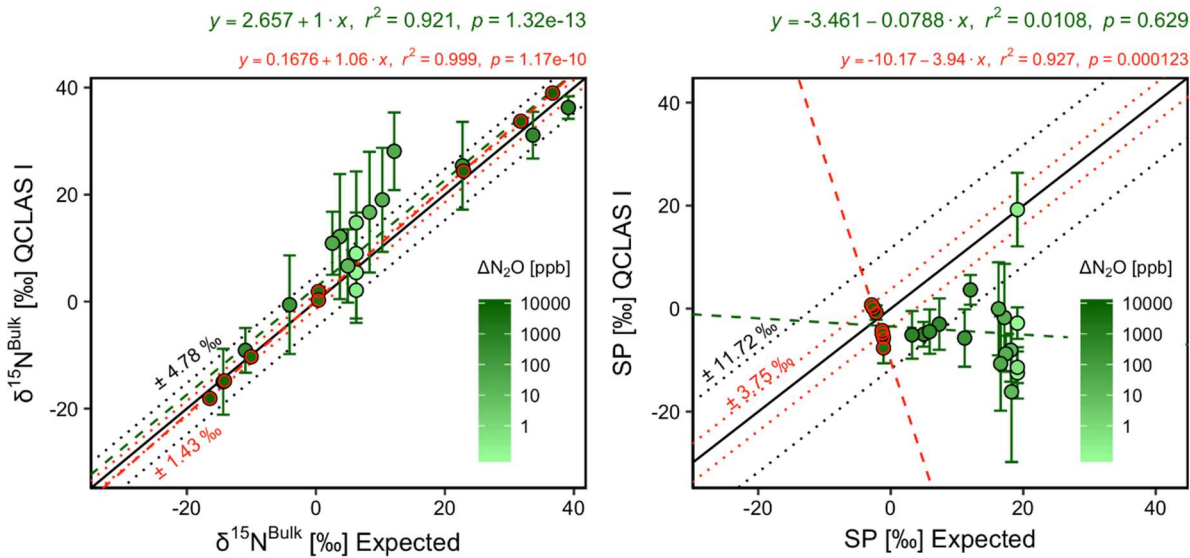


Fig. 12. Correlation diagrams for $\delta^{15}\text{N}^{\text{bulk}}$ and SP measurements at various $\Delta\text{N}_2\text{O}$ mole fractions analyzed by QCLAS I plotted against expected values. The remaining plots for $[\text{N}_2\text{O}]$, $\delta^{15}\text{N}^{\alpha}$, $\delta^{15}\text{N}^{\beta}$ and $\delta^{18}\text{O}$ are provided in Supplementary Material 4 (Fig. S4-13). The solid black line denotes the 1:1 line, while the dotted line indicates $\pm 1\sigma$ of the residuals from the 1:1 line. The dashed blue line represents a linear fit to the data. Individual equations, coefficients of determination (r^2) and p -values are indicated above each plot. Each data point represents the mean and standard deviation (1σ) of triplicate measurements. Results for Exp. 5-6 are highlighted in red, with the dashed red line indicating a linear fit to this data.

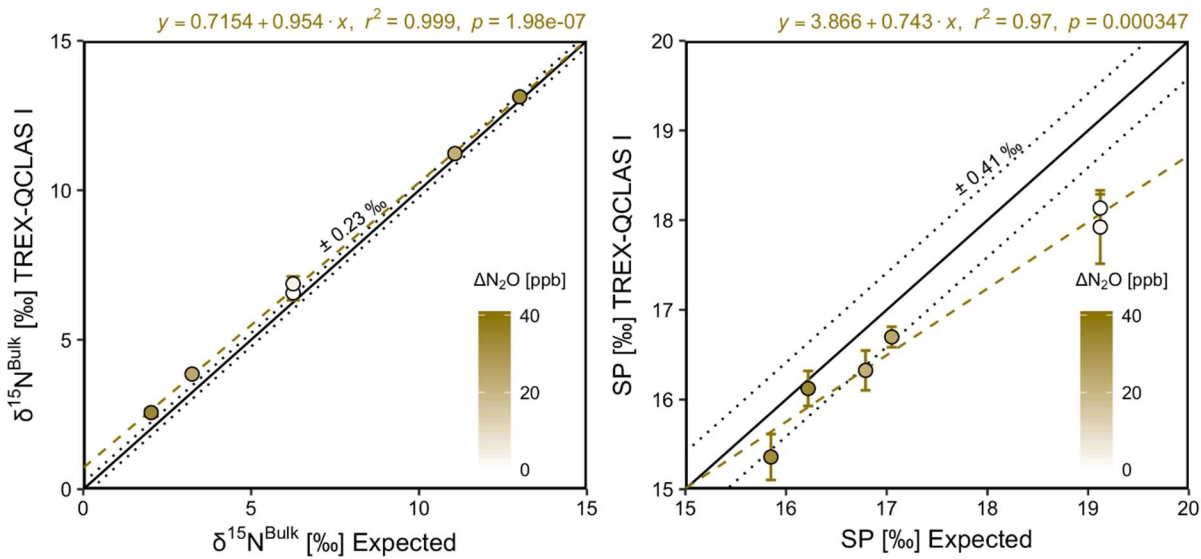


Fig. 13. Correlation diagrams for $\delta^{15}\text{N}^{\text{bulk}}$ and SP measurements at various $\Delta\text{N}_2\text{O}$ mole fractions analyzed by TREX-QCLAS I plotted against expected values. The remaining plots for $[\text{N}_2\text{O}]$, $\delta^{15}\text{N}^{\alpha}$, $\delta^{15}\text{N}^{\beta}$ and $\delta^{18}\text{O}$ are provided in Supplementary Material 4 (Fig. S4-14). The solid black line denotes the 1:1 line, while the dotted line indicates $\pm 1\sigma$ of the residuals from the 1:1 line. The dashed blue line represents a linear fit to the data. Individual equations, coefficients of determination (r^2) and p -values are indicated above each plot. Each data point represents the mean and standard deviation (1σ) of triplicate measurements.

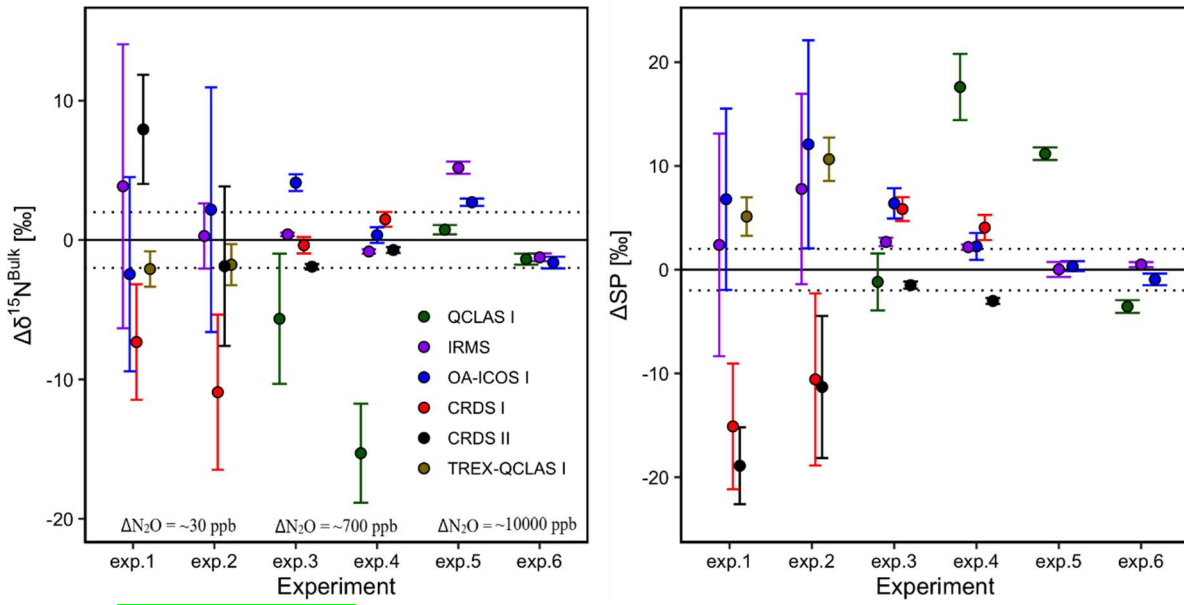


Fig. 14. $\Delta\delta^{15}\text{N}^{\text{bulk}}$ and ΔSP ($\text{Estimated}_{\text{Source}} - \text{True}_{\text{Source}}$) values derived from OA-ICOS I (blue), CRDS I (red), CRDS II (black), QCLAS I (green) and IRMS (purple) via Keeling analysis of the two end-member mixing scenario. The remaining plots for $\delta^{15}\text{N}^{\text{a}}$, $\delta^{15}\text{N}^{\text{b}}$ and $\delta^{18}\text{O}$ are provided in Supplementary Material 4 (Fig. S4-15). $\text{Estimated}_{\text{Source}} = \text{True}_{\text{Source}}$ is indicated by a solid black line at $y = 0$, and the dotted lines indicated $\pm 2\text{‰}$ deviation from $y = 0$. The change in concentration exceeding that of the background gas is indicated for experiments 1-2 ($\Delta\text{N}_2\text{O} \approx 30$ ppb), 3-4 ($\Delta\text{N}_2\text{O} \approx 700$ ppb) and 5-6 ($\Delta\text{N}_2\text{O} \approx 10000$ ppb). Note: the QCLAS I results for experiments 1 and 2 are not depicted to maintain clarity, as they exceed the selected y-axis scale.

Furthermore, to limit the word count, in Sect. 4.3 we will replace the written *Measurement workflow* with Fig. 15, which closely parallels the workflow.

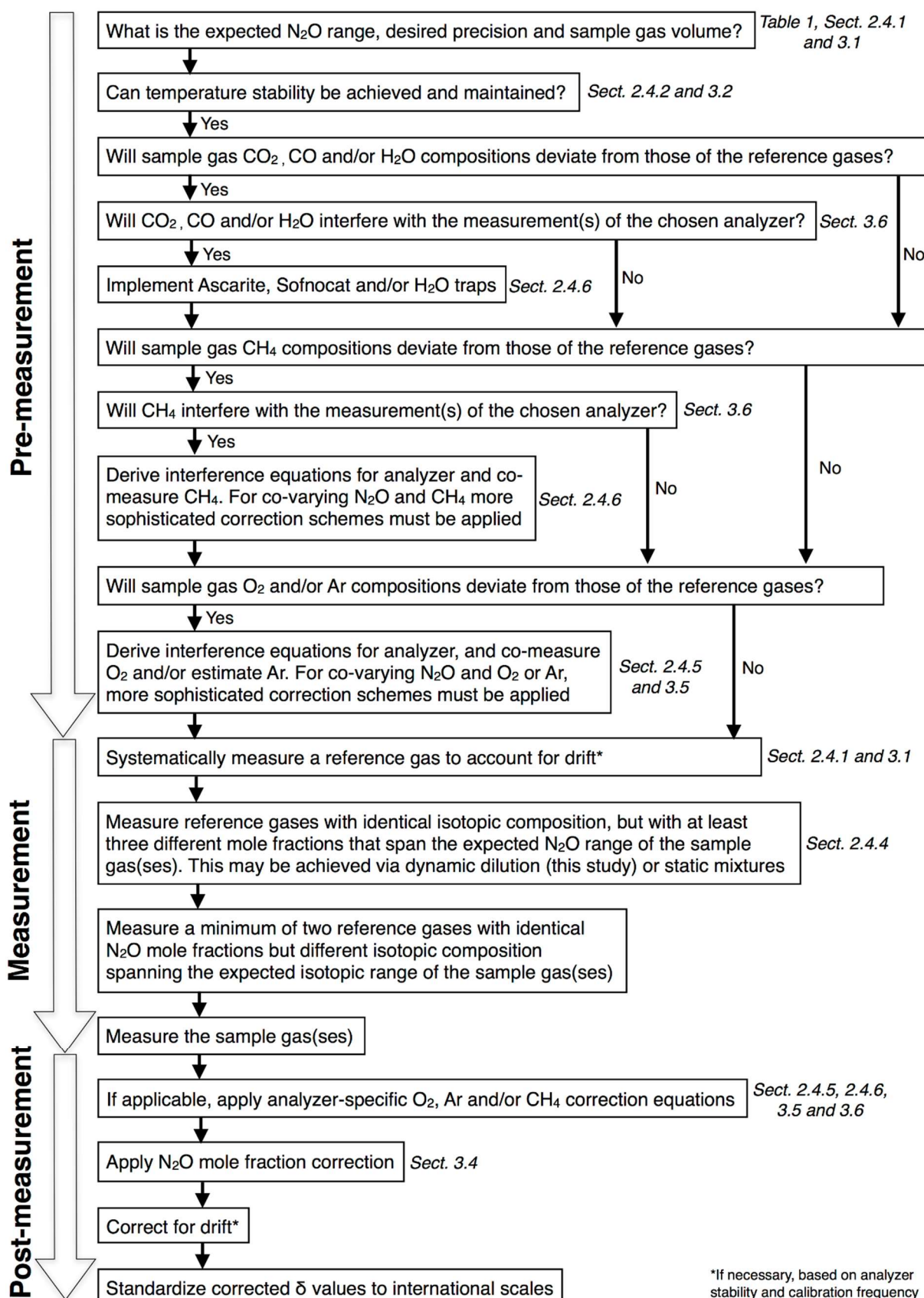


Fig. 15. Proposed measurement workflow for the operation of N₂O isotope laser spectrometers. Relevant sections of this study are shown next to each step.

- 5 Referee Comment 12 – I agree with the anonymous referee 1 that a summary table highlighting the particular advantages and limitations of each instrument would be very helpful. Such a Table should also include an item about the versatility of an instrument (how many parameters can be set/changed by the user to fit a particular experimental requirement) or the disclosure of details of

the used data evaluation algorithms (for black box instruments, it may be hard to figure out the physical reason for a specific instrumental behavior).

Authors' response: Please refer to our response to Referee 1. A summary table (new Table 8) has been included in our reply, which addresses both Referee 1 and Referee 2 comments. Regarding the versatility of analysers, we agree there is basic difference between CRDS and OA-ICOS (Picarro Inc. and ABB LGR Inc.) and QCLAS (ARI) instruments, as the latter enables greater flexibility with respect to experimental parameters. Besides instrumental variables (flows, cell pressure, temperature, etc.), many spectroscopic parameters can also be set, including spectral line selection (multi-line analysis, inclusion of interferants, pressure broadening, etc.). This is already mentioned in the text on P10 L24, and the statement was extended as detailed in Comment 3 above.

Referee Comment 13 – I think, some of the reported interferences and shortcomings of the instruments could be (at least partly) overcome by multi-line analysis. So far, laser spectroscopic instruments typically use only one selected absorption line for analysis of one species. In particular cross-sensitivity issues could be identified easier and also be less pronounced for multi-line instruments.

Authors' response: We thank the reviewer for this comment. Indeed, multi-line analysis could overcome the spectral interference effects we have reported in our manuscript. This might be feasible given the availability of commercial multi-laser instruments or with new broadly tuneable light sources. However, this technology is only currently available for research grade instruments and not yet for commercial use.

Technical Corrections:

Referee Comment 14 – Page 5 Line 5: Please add an original reference for CRDS as well.

Authors' response: We assume that the Referee is referring to P4 L28. We will add the following reference to the updated manuscript, well as in Table 1:

P4 L28: "(QCLAS; Aerodyne Research Inc. [ARI]; Wächter et al., 2008), cavity ring-down spectroscopy (CRDS; Picarro Inc.; Berden et al., 2000) [...]"

Berden, G., Peeters, R. and Meijer, G.: Cavity ring-down spectroscopy: Experimental schemes and applications, Int. Rev. Phys. Chem., 19, 565–607, doi: 10.1080/014423500750040627, 2000.

Referee Comment 15 – Page 9 Line 2 & Page 9 Line 19: I think that referring to the manufacturer website is OK. However, in addition an appropriate original reference should be included that explains details of the OA-ICOS and CRDS techniques.

Authors' response: Agreed. We have updated as follows:

P9 L2: "[...] reader is referred to the webpage of ABB-Los Gatos Research Inc. (ABB-Los Gatos Research Inc., 2019) and Baer et al. (2002)."

P9 L19: "[...] reader to the webpage of Picarro Inc. (Picarro Inc., 2019) and Berden et al. (2000)."

Referee Comment 16 – Page 8-Page 11: Next to the manufacturing date, the serial number of the used instruments should be included for future reference.

Authors' response: We will include serial numbers as follows:

P8 L6: "The N₂OIA-30e-EP (model 914-0027, serial number 15-830, ABB-Los Gatos Research Inc., USA) [...]"

P9 L12: “[...] a 2015 model (referred to as CRDS I, serial number 5001-PVU-JDD-S5001, delivered September 2015) provided by the Niels Bohr Institute, University of Copenhagen, Denmark; and a 2018 model (referred to as CRDS II, serial number 5070-DAS-JDD-S5079, delivered June 2018) provided by Karlsruhe Institute of Technology [...]”

P10 L9: “[...] Three QCLAS instruments (ARI, USA; CW-QC-TILDAS-SC-D) were used in this study. One instrument (QCLAS I, serial number 046), purchased in 2013, was provided by Karlsruhe Institute of Technology, Germany and two instruments, purchased in 2014 (QCLAS II, serial number 065) and 2016 (QCLAS III, serial number 077) [...]”

P11 L13: " A compact mini QCLAS device (CW-QC-TILDAS-76-CS; ARI, USA, serial number 074) coupled with a preconcentration system, called trace gas extractor (TREX) was provided by Empa, Switzerland.

Referee Comment 17 – Page 14 Line 3-6: The (more detailed) synthesis procedure could be moved to the Supplement.

Authors’ response: In-line with Referee #1’s comments, we will move a large portion of Sect. 2.2.2 into Supplementary Material 2. This includes P14 L3-6 as requested here by Referee #2.

Referee Comment 18 – Page 18 Line 15: The Picarro-CRDS analyzer really does not report any absolute numbers for the individual mole fractions? May be they are provided in some of the log files?

Authors’ response: We verified that mole fractions of individual isotopocules are not available in the extended log files of our G5131-i, which was confirmed by Picarro technicians. Mole fractions are certainly generated during data processing; however, because post-processing might be conducted by internal software prior to data output, we did not extract them from the reported delta values.

Referee Comment 19 – Page 19 Line 16: While the meaning of the index “true” is clear in this context, I would prefer the index “reference” instead of “true”.

Authors’ response: We agree with the Referee’s suggestion and have made the following changes in Lines 14 to 16. We also have made minor changes to the equations to highlight what corrections were performed prior to executing Eq. 4:

P19 L14:

$$\delta_{cal,G} = \frac{\delta_{ref,S1} - \delta_{ref,S2}}{\delta_{corr,S1} - \delta_{corr,S2}} * (\delta_{corr,G} - \delta_{corr,S1}) + \delta_{ref,S1} \quad (4)$$

where $\delta_{cal,G}$ is the calibrated δ value for sample gas G normalized to international isotope ratio scales; $\delta_{ref,S1}$ and $\delta_{ref,S2}$ are the respective δ values assigned to reference gases S1-c₃₃₀ppb and S2-c₃₃₀ppb; $\delta_{corr,S1}$ and $\delta_{corr,S2}$ are the δ values measured for the reference gases S1-c₃₃₀ppb and S2-c₃₃₀ppb which, if required, were drift-corrected; and $\delta_{corr,G}$ is the trace gas-corrected, mole fraction-corrected (Sect.2.4.8 only) and drift-corrected (if required) δ value measured for the sample gas G.”

Referee Comment 20– Page 21 Line 15: Please refer the reader to Fig 4 , because the actual T versus t trend is given there.

Authors' response: We believe that introducing Fig. 4 at this stage of the manuscript would disrupt the structure as the figure belongs to the results section, and therefore we would prefer not to introduce Fig. 4 here.

- 5 We refer Referee #2 to our response to Referee #1 Comment 11, as we identified some errors in the main text, which we have now rectified, as well as clarifying some details about the experiment.

Referee Comment 21 – Page 26 Line 21: Replace “greatest” by “best”?

- 10 Authors' response: We agree with the Referee's suggestion and have changed it to the following:

P26 L21: “[...] both CRDS analyzers showed the **best** precision and stability for the measurement [...]”

- 15 **Referee Comment 22 – Figure 5: The text labels are too small to be readable. I suggest to leave out the residual plots to free some space.**

Authors' response: Please refer to Referee #2 Comment 11.

- 20 **Referee Comment 23 – Page 39 Line 25: Weird sentence.**

Authors' response: We have updated the sentence as detailed in Comment 10 above.

Referee Comment 24 – Table 9+10: These Tables could be moved to the Supplement.

- 25 Authors' response: We agree that these tables should be moved to the supplement to free up space in the manuscript. We note, however, that if we move Table 9 (trace gas interference slopes) to the supplement, then it is worthwhile also moving Table 8 (gas matrix interference slopes) to the supplement as well, seeing as they describe similar effects. We will therefore move Table 8 and 9 to the new Supplementary Material 8 and Table 10 to Supplementary Material 11 in keeping with the numbering for the revised
30 Supplementary Material:

Supplementary Material 8:

“**Supplementary Material 8** – Continuity of gas matrix and trace gas corrections at higher N₂O mole fractions

- 35 Gas matrix (O₂) and trace gas (CO₂, CH₄ and CO) experiments conducted at 660 and 990 ppb N₂O showed that the interference effects on N₂O mole fraction and delta values is also dependent on N₂O mole fraction (**Tables S8-1 and S8-2**). **Figs. S8-1 to S8-4** show all data (330, 660 and 990 ppb N₂O) acquired during O₂, CO₂, CH₄ and CO dependence testing, and shows data corrected using Eqs. (7-8) for O₂ and Eq. (9) for CO₂, CH₄ and CO. [...] The O₂ constants A and B, and a, b and c estimated for
40 each analyzer are provided in **Table S8-3**, while the approximated trace gas constant values of A_x , B_x , a_x and b_x for each analyzer are provided in **Table S8-4**.”

Supplementary Material 10:

“**Supplementary Material 10: Extrapolated source intercept values**

- 45 In Sect. 3.7.2, the extrapolated source intercept values acquired using Keeling analysis showed large standard errors, especially for Experiments 1 and 2 (Table S10-1). This was mostly due to the small mole fraction range (i.e. large inverse mole fraction range) over which the regression line was extrapolated in order to acquire the intercept value.”

50 -----

Reply To Referee #3:

The paper is a well designed experiment that investigate and compare the use, the performance, and the calibration of several instruments that measure N₂O isotopes using laser spectroscopy. Stable isotope measurements of atmospheric N₂O have largely increased in the last years due to the use and spread of these laser isotope analysers (from different manufacturers) in both field and lab conditions. However, it is sometimes unclear how the amount of data produced can be interpreted and compared among studies since several analytical issues has been raised. I believe this paper is timely and brings some light to many of these issues and will become a baseline text for people to get future directions into this fast-growing field. In general, I really enjoyed reading the paper since it is well written and the experimentation results are shown in an order manner. I only have some very minor comments for the authors to consider.

Specific

Referee Comment 1 – I noticed that in some places might be confusing if the authors do not specify that this is of direct application in atmospheric measurements. It is kind of obvious but when general conclusions are discussed like in Page 63 (L10-21), this will not hurt to make their statements clearer to the reader. I can easily think in other applications using laser spectrometers like the stable isotope measurement of dissolved nitrate, which is ultimately, transforms to N₂O for analysis. For instance, these applications have provided some approaches on the dependence of isotopic measurements on N₂O concentration; but as mentioned in the text, these might use standardized gas matrix for injection into the laser analyser.

Authors' response: We thank the Referee for their comment. Indeed, the discussion on P63 L10-21 is more applicable for atmospheric measurement applications, whereas applications like the analysis of $\delta^{15}\text{N}$ and $\delta^{18}\text{O}$ of N₂O derived from dissolved NO₃ are likely to substantially differ in the provided gas volumes and the ways the gases are introduced to the analyzers. The overarching aim of our study was to compare commercially available spectrometers that had not been modified with any additional add-ons. We acknowledge that accessory add-ons such as injection ports (Soto et al., 2015; Wassenaar et al., 2018) will likely be required for such applications, and this is mentioned in Sect. 4.3 Measurement workflow on P63 L24: "For specific applications, such as incubation experiments with He, accessory injection units and setups using TREX, related actions have to be taken.". We agree, however, that this could be made more obvious in the discussion:

*Please note that the following includes corrections implemented as part of our Reply to RC1 Comment 20.

P63 L11: "Researchers should also consider the sample gas volume required for a given measurement application using a specific laser spectrometer. In our experience, ensuring that five laser cavity cell volumes have been flushed prior to measurement is *best practice* to negate any memory effects when these instruments are operated using continuous flow-through configurations (as opposed to discrete sample measurements in a closed laser cavity). By following this procedure and using the operating parameters selected in this study (Table 1), the sample gas volume required for a single 300 s measurement is approximately 80 mL for CRDS II, 150 mL for CRDS I, 600 mL for OA-ICOS I and 1200 mL for QCLAS I. The different sample volumes required for CRDS I and CRDS II is due to the different selected flow rates. By comparison, TREX-QCLAS I requires approximately 5 L of sample gas to allow for N₂O preconcentration. These sample gas volumes represent typical numbers for atmospheric applications; however, instrument parameter settings such as flow rate and cell pressure, which ultimately change the required sample volume, can be optimized depending on the measurement application. This is particularly the case for QCLAS instruments, which can be operated with different user-adjustable settings. For applications requiring discrete sample analysis (e.g. the headspace analysis of $\delta^{15}\text{N}$ and $\delta^{18}\text{O}$ in N₂O derived from dissolved NO₃⁻), high N₂O concentration gas samples with lower volumes can be introduced to these instruments using injection ports and dilution gases (e.g. Soto et al., 2015; Wassenaar

et al., 2018); however we did not test these capabilities in our study. Thus, users should carefully consider the available volume of the sample gas, although the possibility exists to dilute high concentration samples to increase gas volume. Researchers should also ensure that gas samples contain N₂O within the operational ranges of the different laser spectrometers (Table 1).”

Referee Comment 2 – The main text is relative long and I hope the authors can move some details to the Supplementary Information.

Authors’ response: This was an overarching concern of all Referees. We have moved the following sections to the Supplementary Materials:

- Figure 7, 10 and 11 (Ar, CO, H₂O effects)
- Table 8
- Table 9
- Table 10
- P14 L25 (See our reply to RC1)
- P16 L4 (See our reply to RC1)

Technical corrections

Referee Comment 3 – Please explain the coefficients in Figure 1. (e.g. $\times 10^2$).

Authors’ response: The coefficients in Fig. 1 are included to ensure that the absorption lines can be viewed on the same scale within the figure, as not all interfering substances have similar magnitudes of line strength within the wavelength regions of the different spectrometers. We will make the following addition to the Fig.1 caption:

Fig. 1. caption (P8 L3): “N₂O isotopocule absorption line positions in the wavenumber regions selected for A) OA-ICOS; B) CRDS; and C & D) QCLAS techniques. Regions of possible spectral overlap from interfering trace gases such as H₂O, CO₂, CH₄ and CO are shown. The abundance-scaled line strengths of trace gases have been scaled with 10^{-1} to 10^2 (as indicated) because they are mostly weaker than those of the N₂O isotopocules.”

Referee Comment 4 – What is the carrier gas in Figure 2?

Authors’ response: We agree that the identity of the carrier gas may not be clear to the reader. We will therefore change “Carrier Gas” to “Matrix gas” in keeping with Table 2 which outlines their identity, and “S1-C_{90ppm}” to “High N₂O concentration reference gas” in keeping with Table 3. We intended the figure to represent the lab setup more generally, whereas Supplementary Material 2 (now Supplementary Material 3) provided the setup for each individual experiment. We will add the following to the Fig. 2 caption and updated the figure:

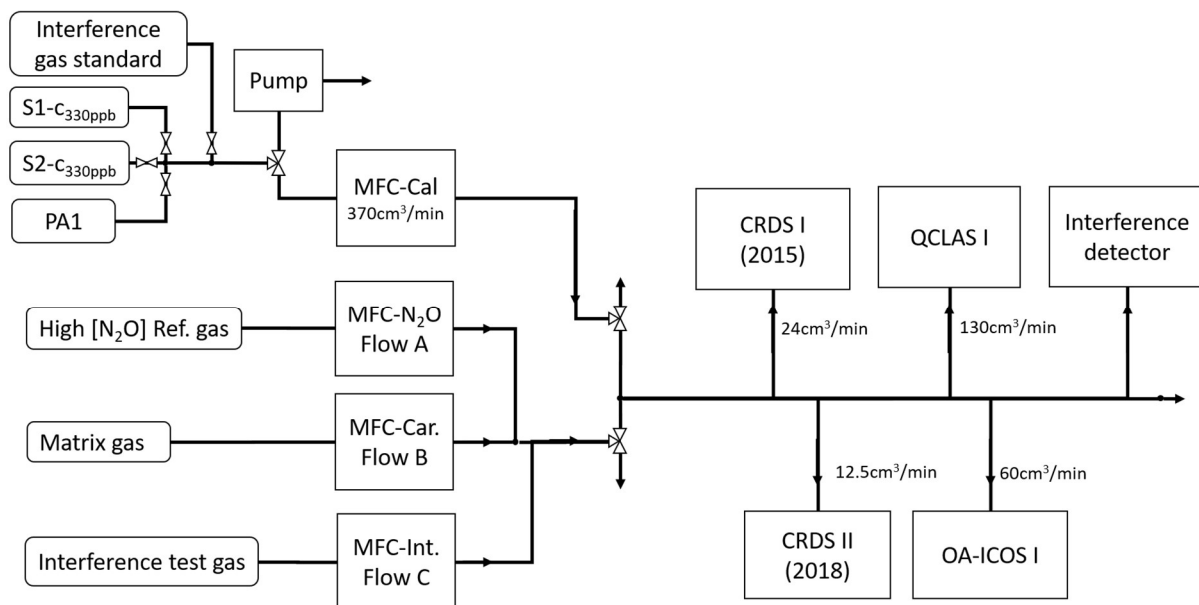


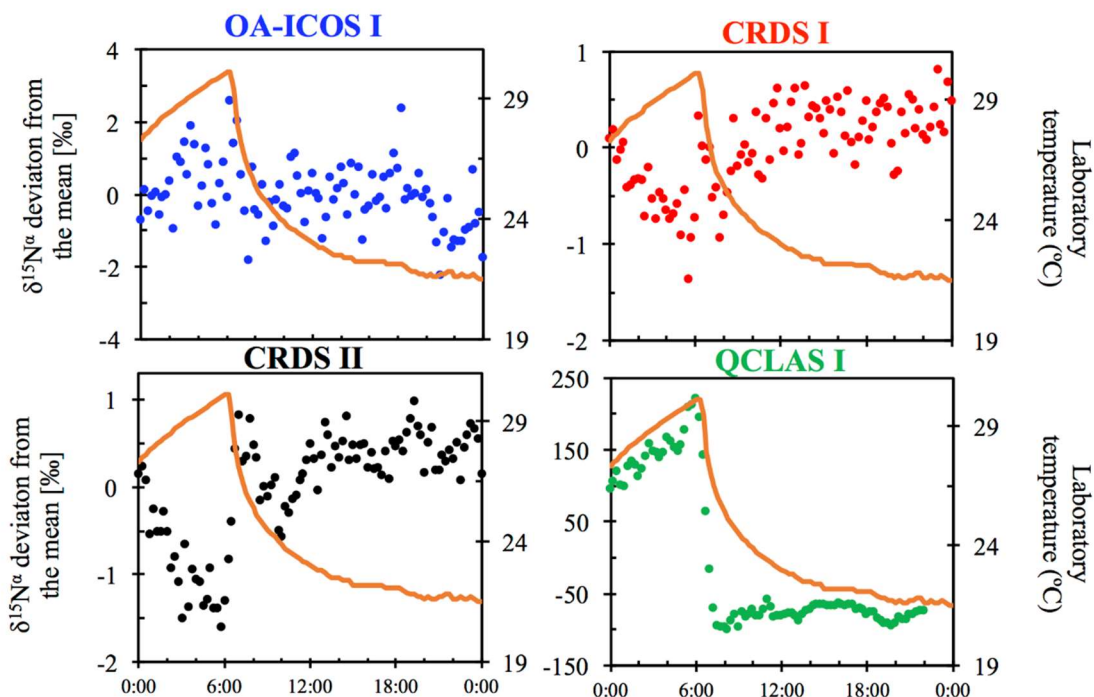
Fig. 2. Caption (P17 L9): “The generalized experimental setup used for all experiments conducted in this study. The gases introduced via MFC flows A, B and C were changed according to the experiments outlined in Sect. 2.4. Table 2 and Table 3 provide the composition of the *matrix gases* (MFC B), *interference test gases* (MFC C) and *high [N₂O] concentration reference gases* (MFC A). Laboratory setups for each individual experiment are provided in Supplementary Material 3.”

Referee Comment 5 – Suggest that the units in Table 6 are specified.

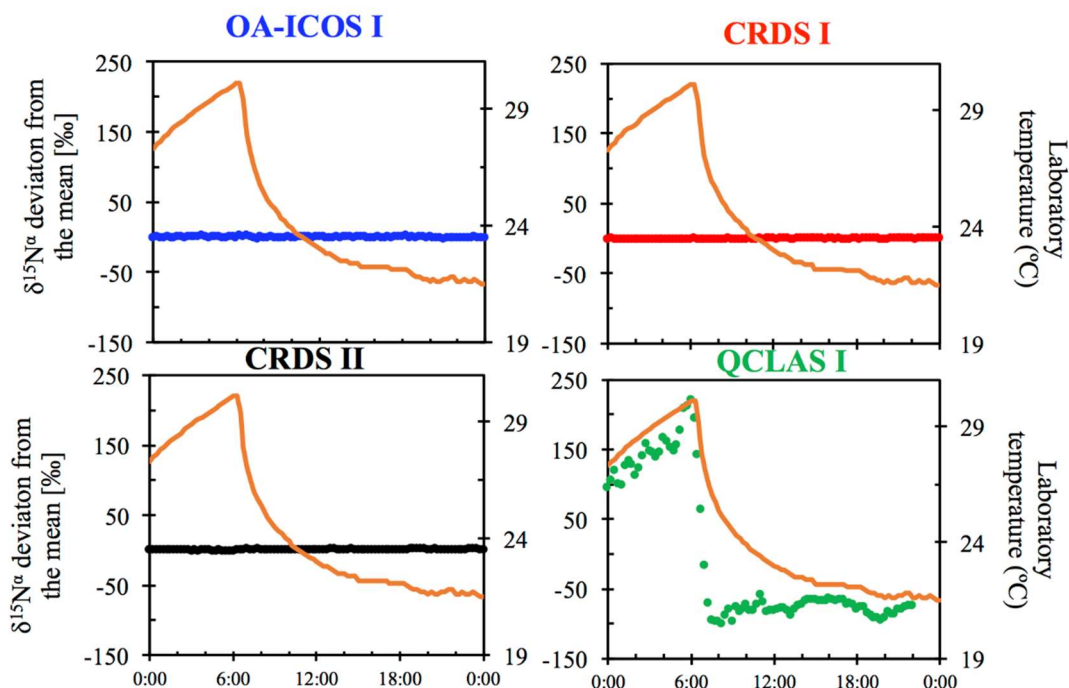
Authors’ response: We thank the referee for highlighting this. We will introduce the units in the first row.

Referee Comment 6 – It would be much easier to compare different laser spectrometers if the same scale is used for each parameter in Figure 4.

Authors’ response: Although we agree that it would be interesting to compare the magnitude of these effects in the figure by using the same scale on the y-axis, the magnitude of the temperature dependence for QCLAS I renders it impossible to discern any of the same dependencies for the OA-ICOS I, CRDS I and CRDS II instruments because they are much smaller. For example, if we consider $\delta^{15}\text{N}^{\alpha}$ for all instruments in the figure below, as is presented in the current manuscript, there is a small, yet important, shift of up to ~2 ‰ for CRDS I and II:



If the y-axis of this figure is then re-scaled to have the same y-axes, these small shifts are indiscernible:



5

Unfortunately, this may prompt the reader into thinking that there is no significant effect, whereas that is not the case. Therefore, we will refrain from changing the y-axis on this figure. However, we will include a row in the new Table 8 (Summary Table as requested by Referee #1 and #2 which compares the various magnitude of temperature effects).

10

*Updated Figure numbering:

- 1 – Isotopocule line positions and interferants
- 2 – Generalized experimental setup (updated)
- 3 – Allan deviation plots (updated)
- 4 – Temperature dependence plots (updated)
- 5 – Mole fraction dependence plots (updated)

15

- 6 – O₂ effects (updated)
- 7 – CO₂ effects (updated)
- 8 – CH₄ effects (updated)
- 9 – OA-ICOS I measured vs expected (updated)
- 5 10 – CRDS I measured vs expected (updated)
- 11 – CRDS II measured vs expected (updated)
- 12 – QCLAS I measured vs expected (updated)
- 13 – TREX-QCLAS I measured vs expected (updated)
- 14 – Source intercepts (updated)
- 10 15 – Measurement workflow (new)

***Updated Table numbering:**

- 1 – Instrument overview
- 2 – Matrix gases and interference test gases
- 15 3 – Reference gas compositions
- 4 – Overview of experiments
- 5 – Gas mixtures introduced for gas matrix and trace gas experiments
- 6 – Allan deviation
- 7 – Long-term repeatability
- 20 8 – Results summary (new)

***Updated Supplementary Materials numbering:**

- 1 – IRMS methodology
- 25 2 – Analysis of high [N₂O] isotope reference gases, ambient reference gasses, PA1 and PA2 (new)
- 3 – Experimental setups
- 4 – Complete datasets (new)
- 5 – Application of an automatic spectral correction method for QCLAS measurements
- 6 – Short-term repeatability
- 30 7 – Scaling of the signal-to-noise ratio
- 8 – Continuity of gas matrix and trace gas corrections at higher N₂O mole fractions
- 9 – Comparison with GC-IRMS
- 10 – Extrapolated source intercept values (new)
- 11 – Lower state energies of probed N₂O isotopocule lines (new)

35

40

N₂O isotopocule measurements using laser spectroscopy: analyzer characterization and intercomparison

Stephen J. Harris^{1,2,*}, Jesper Liisberg^{3,*}, Longlong Xia⁴, Jing Wei⁵, Kerstin Zeyer⁵, Longfei Yu⁵, Matti Barthel⁶, Benjamin Wolf⁴, Bryce F.J. Kelly¹, Dioni I. Cendón², Thomas Blunier³, Johan Six⁶, Joachim Mohn⁵

¹School of Biological, Earth and Environmental Sciences, UNSW Sydney, NSW, Australia

²Australian Nuclear Science and Technology Organisation, Lucas Heights, NSW, Australia

10 ³University of Copenhagen, Niels Bohr Institute, Copenhagen, Denmark

⁴Karlsruhe Institute of Technology, IMK-IFU, Garmisch-Partenkirchen, Germany

⁵Empa, Laboratory for Air Pollution/Environmental Technology, Dübendorf, Switzerland

⁶ETH Zürich, Department of Environmental Systems Science, Zürich, Switzerland

Correspondence to: [Stephen J. Harris \(s.j.harris@unsw.edu.au\)](mailto:s.j.harris@unsw.edu.au) [Joachim Mohn \(email: joachim.mohn@empa.ch\)](mailto:joachim.mohn@empa.ch)

* These authors contributed equally to this work

Abstract. For the past two decades, the measurement of N₂O isotopocules – isotopically substituted molecules ¹⁴N¹⁵N¹⁶O, ¹⁵N¹⁴N¹⁶O and ¹⁴N¹⁴N¹⁸O of the main isotopic species ¹⁴N¹⁴N¹⁶O – has been a promising technique for understanding N₂O production and consumption pathways. The coupling of non-cryogenic and tuneable light sources with different detection schemes, such as direct absorption quantum cascade laser absorption spectroscopy (QCLAS), cavity ring-down spectroscopy (CRDS) and off-axis integrated cavity output spectroscopy (OA-ICOS), has enabled the production of commercially-available and field-deployable N₂O isotopic analyzers. In contrast to traditional isotope-ratio mass-spectrometry (IRMS), these instruments are inherently selective for position-specific ¹⁵N substitution and provide real-time data, with minimal or no sample pretreatment, which is highly attractive for process studies.

Here, we compared the performance of N₂O isotope laser spectrometers with the three most common detection schemes: OA-ICOS (N₂OIA-30e-EP, ABB-Los Gatos Research Inc.), CRDS (G5131-i, Picarro Inc.) and QCLAS (dual QCLAS and preconcentration (TREX)–mini QCLAS, Aerodyne Research Inc.). For each instrument, the precision, drift and repeatability of N₂O mole fraction [N₂O] and isotope data were tested. The analyzers were then characterized for their dependence on [N₂O], gas matrix composition (O₂, Ar) and spectral interferences caused by H₂O, CO₂, CH₄ and CO to develop analyzer-specific correction functions. Subsequently, a simulated two end-member mixing experiment was used to compare the accuracy and repeatability of corrected and calibrated isotope measurements that could be acquired using the different laser spectrometers.

Our results show that N₂O isotope laser spectrometer performance is governed by an interplay between instrumental precision, drift, matrix effects and spectral interferences. To retrieve compatible and accurate results, it is necessary to include appropriate reference materials following the identical treatment (IT)

principle during every measurement. Remaining differences between sample and reference gas compositions have to be corrected by applying analyzer-specific correction algorithms. These matrix and trace gas correction equations vary considerably according to N₂O mole fraction, complicating the procedure further. Thus, researchers should strive to minimize differences in composition between sample and reference gases. In closing, we provide a calibration workflow to guide researchers in the operation of N₂O isotope laser spectrometers in order to acquire accurate N₂O isotope analyses. We anticipate that this workflow will assist in applications where matrix and trace gas compositions vary considerably (e.g. laboratory incubations, N₂O liberated from wastewater or groundwater), as well as extending to future analyzer models and instruments focusing on isotopic species of other molecules.

10 1 Introduction

Nitrous oxide (N₂O) is a long-lived greenhouse gas with a 100-year global warming potential nearly 300 times that of carbon dioxide (CO₂; Forster et al., 2007), and is the largest emission source of ozone-depleting nitrogen oxides in the stratosphere (Ravishankara et al., 2009). In 2019, the globally averaged [N₂O] reached approximately 332 ppb compared to the pre-industrial level of 270 ppb (NOAA/ESRL, 2019). While this increase is known to be linked primarily to increased fertilizer use in agriculture (Bouwman et al., 2002; Mosier et al., 1998; Tian et al., 2015), understanding the underlying microbial processes producing and consuming N₂O has proved more challenging, and individual source contributions from sectors such as agricultural soils, wastewater management and biomass burning to global bottom-up estimates of N₂O emissions have large uncertainties (Denman et al., 2007). Stable isotopes are an effective tool for distinguishing N₂O sources and determining production pathways, which is critical for developing appropriate mitigation strategies (Baggs, 2008; Ostrom and Ostrom, 2011; Toyoda et al., 2017).

The N₂O molecule has an asymmetric linear structure (NNO), with the following most abundant isotopocules: ¹⁴N¹⁵N¹⁶O (¹⁵N^α-N₂O); ¹⁵N¹⁴N¹⁶O (¹⁵N^β-N₂O); ¹⁴N¹⁴N¹⁸O (¹⁸O-N₂O); and ¹⁴N¹⁴N¹⁶O (Yoshida and Toyoda, 2000). The terms ¹⁵N^α and ¹⁵N^β refer to the respective central and terminal positions of nitrogen (N) atoms in the NNO molecule (Toyoda and Yoshida, 1999). Isotopic abundances are reported in δ-notation, where $\delta^{15}\text{N} = R(^{15}\text{N}/^{14}\text{N})_{\text{sample}} / R(^{15}\text{N}/^{14}\text{N})_{\text{reference}} - 1$ denotes the relative difference in per mil (‰) of the sample versus atmospheric N₂ (AIR-N₂). The isotope ratio $R(^{15}\text{N}/^{14}\text{N})$ equals $x(^{15}\text{N})/x(^{14}\text{N})$, with x being the absolute abundance of ¹⁴N and ¹⁵N, respectively. Similarly, Vienna Standard Mean Ocean Water (VSMOW) is the international isotope ratio scale for δ¹⁸O. In practice, the isotope δ value is calculated from measurement of isotopocule ratios of sample and reference gases, with the latter being defined on the AIR-N₂ and VSMOW scales. By extension, δ¹⁵N^α denotes the corresponding relative difference of isotope ratios for ¹⁴N¹⁵N¹⁶O/¹⁴N¹⁴N¹⁶O, and δ¹⁵N^β for

$^{15}\text{N}^{14}\text{N}^{16}\text{O}/^{14}\text{N}^{14}\text{N}^{16}\text{O}$. The site-specific intramolecular distribution of ^{15}N within the N_2O molecule is termed ^{15}N -site preference (SP), and is defined as: $\text{SP} = \delta^{15}\text{N}^\alpha - \delta^{15}\text{N}^\beta$ (Yoshida and Toyoda, 2000). The term $\delta^{15}\text{N}^{\text{bulk}}$ is used to express the average $\delta^{15}\text{N}$ value, and is equivalent to $\delta^{15}\text{N}^{\text{bulk}} = (\delta^{15}\text{N}^\alpha + \delta^{15}\text{N}^\beta)/2$.

5 Extensive evidence has shown that SP, $\delta^{15}\text{N}^{\text{bulk}}$ and $\delta^{18}\text{O}$ can be used to differentiate N_2O source processes and biogeochemical cycling (Decock and Six, 2013; Denk et al., 2017; Heil et al., 2014; Lewicka-Szczebak et al., 2014, 2015; Ostrom et al., 2007; Sutka et al., 2003, 2006; Toyoda et al., 2005, 2017; Wei et al., 2017). Isotopocule abundances have been measured in a wide range of environments, including the troposphere (Harris et al., 2014a; Röckmann and Levin, 2005; Toyoda et al., 2013), agricultural soils
10 (Buchen et al., 2018; Ibraim et al., 2019; Köster et al., 2011; Mohn et al., 2012; Ostrom et al., 2007; Park et al., 2011; Pérez et al., 2001, 2006; Toyoda et al., 2011; Verhoeven et al., 2018, 2019; Well et al., 2008, 2009; Wolf et al., 2015), mixed urban-agricultural environments (Harris et al., 2017), coal and waste combustion (Harris et al., 2014b; Ogawa and Yoshida, 2005), fossil fuel combustion (Toyoda et al., 2008), wastewater treatment (Harris et al., 2015a, b; Wunderlin et al., 2012, 2013), groundwater (Koba et al.,
15 2009; Minamikawa et al., 2011; Nikolenko et al., 2019; Well et al., 2005, 2012), estuaries (Erler et al., 2015), mangrove forests (Murray et al., 2018), stratified water impoundments (Yue et al., 2018), and firn air and ice cores (Bernard et al., 2006; Ishijima et al., 2007; Prokopiou et al., 2017). While some applications like laboratory incubation experiments allow for analysis of the isotopic signature of the pure source, most studies require analysis of the source diluted in ambient air. This specifically applies to
20 terrestrial ecosystem research, since N_2O emitted from soils is immediately mixed with background atmospheric N_2O . To understand the importance of soil emissions for the global N_2O budget, two end-member mixing models commonly interpreted using Keeling or Miller-Tans plots are frequently used to back-calculate the isotopic composition of N_2O emitted from soils (Keeling, 1958; Miller and Tans, 2003).

25

N_2O isotopocules can be analyzed by isotope-ratio mass spectrometry (IRMS) and laser spectroscopic techniques, with currently available commercial spectrometers operating in the mid-infrared (MIR) region to achieve highest sensitivities.~~and mid-infrared (MIR) laser spectroscopic techniques.~~ IRMS analysis of the N_2O intramolecular ^{15}N distribution is based on quantification of the fragmented (NO^+ , m/z 30 and
30 31) and molecular (N_2O^+ , m/z 44, 45 and 46) ions to calculate isotope ratios for the entire molecule ($^{15}\text{N}/^{14}\text{N}$ and $^{18}\text{O}/^{16}\text{O}$) and the central (N^α) and terminal (N^β) N atom (Toyoda and Yoshida, 1999). The analysis of N_2O SP by IRMS is complicated by the rearrangement of N^α and N^β in the ion source, while analysis of $\delta^{15}\text{N}^{\text{bulk}}$ (45/44) involves correction for NN^{17}O (mass 45). IRMS can achieve repeatability as good as 0.1 ‰ for $\delta^{15}\text{N}$, $\delta^{18}\text{O}$, $\delta^{15}\text{N}^\alpha$ and $\delta^{15}\text{N}^\beta$ (Potter et al., 2013; Röckmann and Levin, 2005), but an
35 inter-laboratory comparison study showed substantial deviations in measurements of N_2O isotopic composition, in particular for SP (up to 10 ‰) (Mohn et al., 2014).

The advancement of mid-infrared laser spectroscopic techniques was enabled by the invention and availability of non-cryogenic light sources which have been coupled with different detection schemes, such as direct absorption quantum cascade laser absorption spectroscopy (QCLAS; Aerodyne Research Inc. [ARI]; Wächter et al., 2008), cavity ring-down spectroscopy (CRDS; Picarro Inc.; [Berden et al., 2000](#)) and off-axis integrated-cavity-output spectroscopy (OA-ICOS; ABB Los Gatos Research Inc.; Baer et al., 2002) to realize compact field-deployable analyzers. In short, the emission wavelength of a laser light source is rapidly and repetitively scanned through a spectral region containing the spectral lines of the target N₂O isotopocules. The laser light is coupled into a multi-path cell filled with the sample gas, and the mixing ratios of individual isotopic species are determined from the detected absorption using Beer's Law. The wavelengths of spectral lines of N₂O isotopocules with distinct ¹⁷O, ¹⁸O or position-specific ¹⁵N substitution are unique due to the existence of characteristic rotational-vibrational spectra (Rothman et al., 2005). Thus, unlike IRMS, laser spectroscopy does not require mass-overlap correction. However, the spectral lines may have varying degrees of overlap with those of other gaseous species, which, if unaccounted for, may produce erroneous apparent absorption intensities. One advantage of laser spectroscopy is that instruments can analyze the N₂O isotopic composition in gaseous mixtures (e.g. ambient air) in a flow-through mode, providing real-time data with minimal or no sample pretreatment, which is highly attractive to better resolve the temporal complexity of N₂O production and consumption processes (Decock and Six, 2013; Heil et al., 2014; Köster et al., 2013; Winther et al., 2018). These instruments can analyze the N₂O isotopic composition in gaseous mixtures (e.g. ambient air) in a flow-through mode, providing real-time data with minimal or no sample pretreatment, which is highly attractive to better resolve the temporal complexity of N₂O production and consumption processes (Decock and Six, 2013; Heil et al., 2014; Köster et al., 2013; Winther et al., 2018). Most importantly, MIR laser spectroscopy is selective for ¹⁷O, ¹⁸O and position-specific ¹⁵N substitution due to the existence of characteristic rotational-vibrational spectra (Rothman et al., 2005).

Despite the described inherent benefits of laser spectroscopy for N₂O isotope analysis, applications remain challenging and are still scarce for four main reasons:

- (1) two pure N₂O isotopocule reference materials (USGS51, USGS52) have only recently been made available through the United States Geological Survey (USGS) with provisional values assigned by Tokyo Institute of Technology (Ostrom et al., 2018). The lack of N₂O isotopocule reference materials was identified as a major reason limiting inter-laboratory compatibility (Mohn et al., 2014);
- (2) laser spectrometers are subject to drift effects, in particular under fluctuating environmental conditions, limiting (e.g. due to moving interference fringes), particularly under fluctuating laboratory temperatures, which limits their performance (Werle et al., 1993);

(3) if apparent delta values retrieved from a spectrometer are calculated from raw uncalibrated isotopocule mole fractions, referred to here as a δ -calibration approach, an inverse concentration dependence may be introduced. This can arise if the analyzer measurements of isotopocule mole fractions are linear, yet the relationship between measured and true mole fractions have a non-zero intercept (e.g. Griffith et al., 2012; Griffith, 2018), such as due to baseline structures (e.g. interfering fringes; Tuzson et al. 2008); changes in $[N_2O]$ affect N_2O isotope results when using the δ -calibration approach (Griffith, 2018); and

(4) laser spectroscopic results are affected by mole fraction changes of atmospheric background gases (N_2 , O_2 , and Ar), herein called gas matrix effects, due to the difference of pressure-broadening coefficients (Nara et al., 2012), and potentially by spectral interferences from other atmospheric constituents (H_2O , CO_2 , CH_4 , CO , etc.), herein called trace gas effects, depending on the selected wavelength region. The latter is particularly pronounced for N_2O due to its low atmospheric abundance in comparison to other trace gases.

Several studies have described some of the above effects for CO_2 (Bowling et al., 2003, 2005; Griffiths et al., 2004; Griffith et al., 2012; Friedrichs et al., 2010; Malowany et al., 2015; Pataki et al., 2006; Pang et al., 2016; Rella et al., 2013; Vogel et al., 2013; Wen et al. 2013), CH_4 (Eyer et al., 2016; Griffith et al., 2012; Rella et al., 2013), and recently N_2O isotope laser spectrometers (Erler et al., 2015; Harris et al., 2014; Ibraim et al., 2018; Wächter et al., 2008). However, a comprehensive and comparative characterization of the above effects for commercially-available N_2O isotope analyzers is lacking.

Here, we present an intercomparison study of commercially-available N_2O isotope laser spectrometers with the three most common detection schemes: (1) OA-ICOS (N_2O IA-30e-EP, ABB-Los Gatos Research Inc.); (2) CRDS (G5131-i, Picarro Inc.); (3) QCLAS (dual QCLAS and TREX–mini QCLAS, ARI). Performance characteristics including precision, repeatability, drift and dependence of isotope measurements on $[N_2O]$ were determined. Instruments were tested for gas matrix effects (O_2 , Ar) and spectral interferences from enhanced trace gas mole fractions (CO_2 , CH_4 , CO , H_2O) at various $[N_2O]$ to develop analyzer-specific correction functions. The accuracy of different spectrometer designs was then assessed during a laboratory-controlled mixing experiment designed to simulate two end-member mixing, in which results were compared to calculated expected values, as well as to those acquired using IRMS (δ values) and gas chromatography (GC, N_2O concentration). In closing, we provide a calibration workflow that will assist researchers in the operation of N_2O and other trace gas isotope laser spectrometers in order to acquire accurate isotope analyses.

2 Materials and Methods

2.1 Analytical techniques

Operational details of the laser spectrometers tested in this study, including wavenumber regions, line positions and line strengths of N₂O, are provided in Table 1. In Fig. 1, selected N₂O rotational lines are shown in combination with the absorption lines of the atmospheric most abundant IR-active trace gases (H₂O, CO₂, CH₄, CO and O₃) within the different wavenumber regions used by the analyzers. Fig. 1 can be used to rationalize possible spectral interferences within different wavenumber regions.

Table 1. Overview on the wavelength regions, line positions and line strengths of N₂O isotopocules, and key operating parameters for each laser spectrometer tested in this study.

Detection scheme (model; manufacturer)	N ₂ O range [ppb]	Wavenumber region (cm ⁻¹)	Isotopocules	Line positions (cm ⁻¹) / Flow rate (cm ³ min ⁻¹) Line strength [cm ⁻¹ / (molecule cm ⁻²)]	Cell temperature (°C)	Cell pressure (hPa)	Internal plumbing volume (cm ³)	Effective volume at NTP (cm ³)	Measurement frequency (seconds)	References	
OA-ICOS I (N ₂ OIA-30e-EP; ABB Los Gatos Research Inc.)	300 – 100000	2192.1 – 2192.5	¹⁴ N ¹⁴ N ¹⁶ O ¹⁴ N ¹⁵ N ¹⁶ O ¹⁵ N ¹⁴ N ¹⁶ O ¹⁴ N ¹⁴ N ¹⁸ O	2192.40 / 4.919·10 ⁻²⁰ 2192.44 / 4.919·10 ⁻²⁰ 2192.48 / 3.375·10 ⁻¹⁹ 2192.31 / 3.31·10 ⁻²¹ 2192.33 / 2.968·10 ⁻²¹ 2192.13 / 1.113·10 ⁻²¹	60 43.6	61	930	60.50	1.00	Baer et al. (2002) ABB-Los Gatos Research Inc. (2019)	
CRDS I & II (G5131-i; Picarro Inc.)	300 – 1500	2195.7 – 2196.3	¹⁴ N ¹⁴ N ¹⁶ O ¹⁴ N ¹⁵ N ¹⁶ O ¹⁵ N ¹⁴ N ¹⁶ O ¹⁴ N ¹⁴ N ¹⁸ O	2196.21 / 5.161·10 ⁻²⁰ 2196.24 / 5.161·10 ⁻²⁰ 2195.76 / 2.734·10 ⁻²¹ II) 2195.80 / 2.197·10 ⁻²¹ 2195.95 / 1.431·10 ⁻²¹	25.2 (CRDS I) 40.2 (CRDS II)	100	40	4.22	3.41 (CRDS I) 2.54 (CRDS II)	Picarro Inc. (2019)	
QCLAS I, II & III (CW-QC-TILDAS-SC-D; Aerodyne Research Inc.)	300 – 90000	2187.7 – 2188.15 and 2203.1 – 2203.4	¹⁴ N ¹⁴ N ¹⁶ O ¹⁴ N ¹⁵ N ¹⁶ O ¹⁵ N ¹⁴ N ¹⁶ O ¹⁴ N ¹⁴ N ¹⁸ O	2188.04 / 2.601·10 ⁻²¹ 2187.94 / 3.294·10 ⁻²¹ 2187.85 / 3.274·10 ⁻²¹ 2203.28 / 1.794·10 ⁻²¹	130 ^a	20 ^a	53.3 ^a	2100	104 ^a	1.00 ^a	Nelson (2008) Wächter et al. (2008)
TREX-QCLAS I (Modified CW-QC-TILDAS-76-CS; Aerodyne Research Inc.)	300 – 1500 ^{a,b}	2203.1 – 2203.4 ^a	¹⁴ N ¹⁴ N ¹⁶ O ¹⁴ N ¹⁵ N ¹⁶ O ¹⁵ N ¹⁴ N ¹⁶ O ¹⁴ N ¹⁴ N ¹⁸ O	2203.10 / 2.710·10 ⁻²¹ 2203.11 / 1.435·10 ⁻²¹ 2203.36 / 9.798·10 ⁻²² 2203.20 / 7.016·10 ⁻²² 2203.28 / 1.794·10 ⁻²¹	20 ^a	35.6 ^a	620	20 ^a	1.00 ^a	Ibraim et al. (2018)	

^a) Dual QC-TILDAS and mini QC-TILDAS are flexible spectrometer platforms, which can be used with different parameter settings. The indicated numbers were chosen for the described experiments.

^b) The mini QC-TILDAS spectrometer is used in combination with a preconcentration device (Ibraim et al., 2018), the indicated N₂O concentration range is prior to preconcentration.

^c) The preconcentration – mini QC-TILDAS system is used in a repetitive batch cycle without a continuous sample gas flow (Ibraim et al., 2018, 2019).

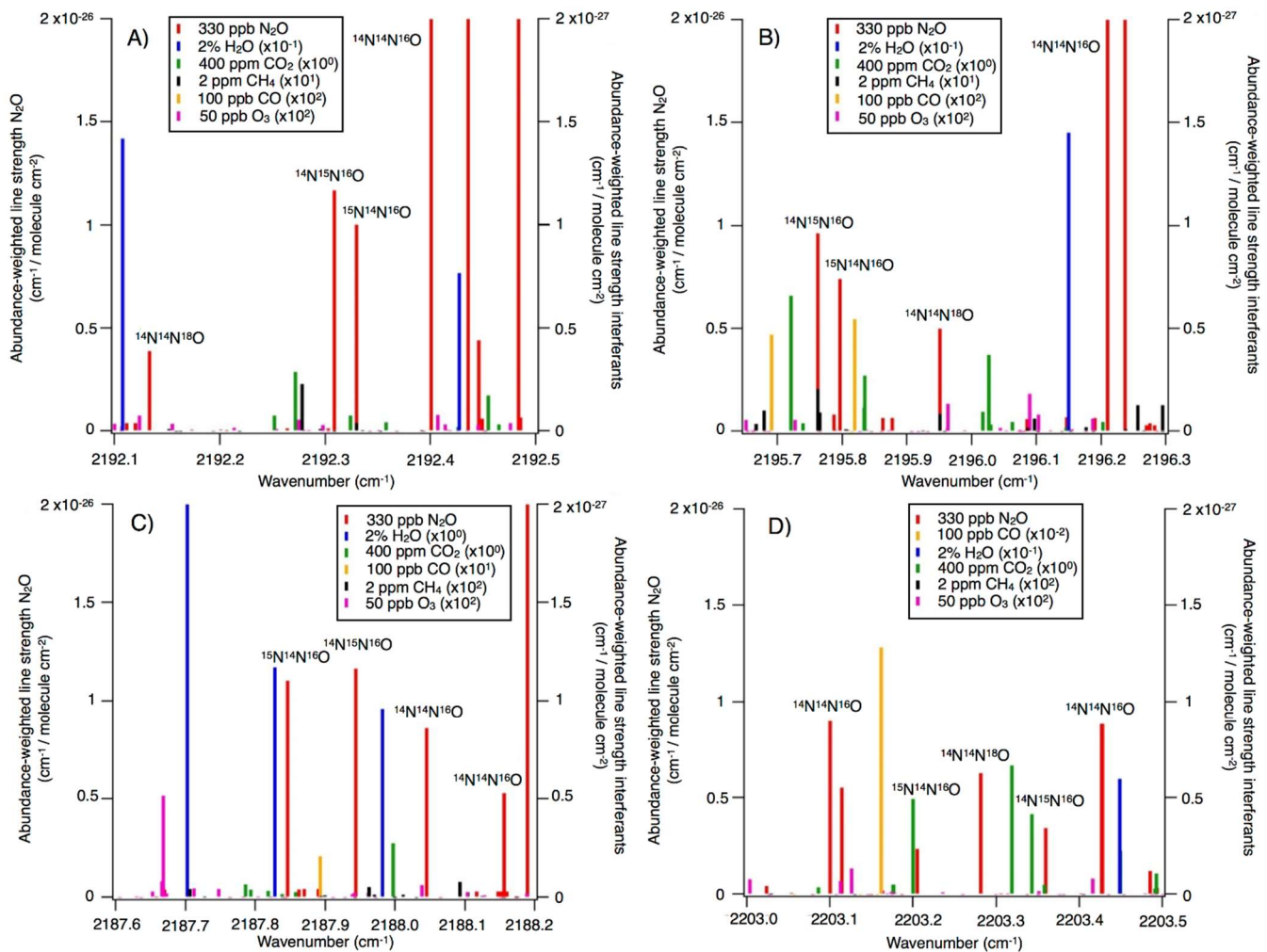


Fig. 1. N₂O isotopocule absorption line positions in the wavenumber regions selected for A) OA-ICOS; B) CRDS; and C & D) QCLAS techniques. Regions of possible spectral overlap from interfering trace gases such as H₂O, CO₂, CH₄ and CO are shown. The abundance-scaled line strengths of trace gases have been scaled with 10⁻¹ to 10² (as indicated) because they are mostly weaker than those of the N₂O isotopocules.

2.1.1 OA-ICOS (ABB-Los Gatos Research Inc.)

The N₂OIA-30e-EP (model 914-0027, [serial number 15-830](#), ABB-Los Gatos Research Inc., USA) tested in this study was provided by the University of New South Wales (UNSW Sydney, Australia), and is herein referred to as OA-ICOS I (Table 1). The instrument employs the OA-ICOS technique integrated with a QCL (Baer et al., 2002). In short, the QCL beam is directed off axis into the cavity cell with highly-reflective mirrors, providing an optical path of several kilometers. For further details on the OA-ICOS technique, the reader is referred to the webpage of ABB-Los Gatos Research Inc. (ABB-Los Gatos Research Inc., 2019) [and Baer et al. \(2002\)](#).

The specific analyzer tested here was manufactured in June 2014, and has had no hardware modifications since then. It is also important to note that a more recent N₂OIA-30e-EP model (model 914-0060) is available, that in addition quantifies δ¹⁷O. We are unaware of any study measuring N₂O isotopocules at natural abundance and ambient mole fractions with the N₂OIA-30e-EP. The only studies published so far

reporting N₂O isotope data apply the N₂OIA-30e-EP either at elevated [N₂O] in a standardized gas matrix or using ¹⁵N labelling, including Soto et al. (2015), Li et al. (2016), Kong et al. (2017), Brase et al. (2017), Wassenaar et al. (2018) and Nikolenko et al. (2019).

2.1.2 CRDS (Picarro Inc.)

- 5 Two G5131-i analyzers (Picarro Inc., USA) were used in this study: a 2015 model (referred to as CRDS I, [serial number 5001-PVU-JDD-S5001](#), delivered September 2015) provided by the Niels Bohr Institute, University of Copenhagen, Denmark; and a 2018 model (referred to as CRDS II, [serial number 5070-DAS-JDD-S5079](#), delivered June 2018) provided by Karlsruhe Institute of Technology, Germany (Table 1). In CRDS, the beam of a single-frequency continuous wave (cw) laser diode enters a three-mirror
- 10 cavity with an effective pathlength of several km to support a continuous traveling light wave. A photodetector measures the decay of light in the cavity after the cw laser diode is shut off to retrieve the mole fraction of N₂O isotopocules. For more details we refer the reader to the webpage of Picarro Inc. (Picarro Inc., 2019) [and Berden et al. \(2000\)](#).
- 15 Importantly, the manufacturer-installed flow-restrictors were replaced in both analyzer models, as we noted reduced flow rates due to clogging during initial reconnaissance testing. In CRDS I, a capillary (inner diameter (ID): 150 µm, length: 81 mm, flow: 25.2 cm³ min⁻¹) was installed, while CRDS II was equipped with a critical orifice (ID: 75 µm, flow: 12.5 cm³ min⁻¹). Both restrictors were tested and confirmed leak-proof. Both analyzers had manufacturer-installed permeation driers located prior to the
- 20 inlet of the cavity, which were not altered for this study. In December 2017, CRDS I received a software and hardware update as per the manufacturer's recommendations. The CRDS II did not receive any software or hardware upgrades as it was acquired immediately prior to testing.

To the best of our knowledge, the work presented in Lee et al. (2017) and Ji and Grundle (2019) are the

25 only published uses of G5131-i models. A prior model (the G5101-i), which employs a different spectral region and does not offer the capability for δ¹⁸O was used by Peng et al. (2014), Erler et al. (2015), Li et al. (2015), Lebegue et al. (2016) and Winther et al. (2018).

2.1.3 QCLAS (Aerodyne Research Inc.)

- Three QCLAS instruments (ARI, USA; CW-QC-TILDAS-SC-D) were used in this study. One instrument
- 30 (QCLAS I, [serial number 046](#)), purchased in 2013, was provided by Karlsruhe Institute of Technology, Germany and two instruments, purchased in 2014 (QCLAS II, [serial number 065](#)) and 2016 (QCLAS III, [serial number 077](#)), were supplied by ETH Zürich, Switzerland (Table 1). [QCLAS I was used in all experiments presented in this study, while QCLAS II and III were only used to assess the reproducibility of drift reported in Sect. 3.1.](#)

All instruments were dual cw QCL spectrometers, equipped with mirror optics guiding the two laser beams through an optical anchor point to assure precise coincidence of the beams at the detector. On the way to the detector, the laser beams are coupled into an astigmatic multipass cell with a volume of approx. 2100 cm³ in which the beams interact with the sample air. The multiple passes through the absorption cell result in an absorption path length of approx. 204 m. The cell pressure can be selected by the user and was set to 53.3 mbar as a trade-off between line separation and sensitivity. This set point is automatically maintained by the TDLWintel software (Version 1.14.89 ARI, MA, USA), which compensates for variations in vacuum pump speed by closing or opening a throttle valve at the outlet of the absorption cell.

QCLAS instruments offer great liberty to the user as the system can also be operated with different parameter settings, such as thee-g. selection of spectral lines for quantification, wavenumber calibration, sample flow rate, and pressure ete. Thereby different applications can be realized, from high flow eddy covariance studies or high mole fraction process studies to high-precision measurements coupled to a customized inlet system. In addition, spectral interferences and gas matrix effects can be taken into consideration by multi-line analysis, inclusion of the respective spectroscopic parameters in the spectral evaluation or adjustment of the pressure broadening coefficients. The spectrometers used in this study (QCLAS I – III) were tested under standard settings but were not optimized for the respective experiments. QCLAS I was operated as a single laser instrument using laser one, to optimize spectral resolution of the frequency sweeps. It is important to note the mixing ratios returned by the instrument are solely based on fundamental spectroscopic constants (Rothman et al., 2005), so that corrections such as the dependence of isotope ratios on [N₂O] have to be implemented by the user in the post processing.

To our knowledge, QCLAS instruments have so far predominately been used for determination of N₂O isotopic composition in combination with preconcentration (see below) or at enhanced mole fractions (Harris et al., 2015; Heil et al. 2014; Köster et al., 2013), except for Yamamoto et al. (2014) who had used a QCLAS (CW-QC-TILDAS-SC-S-N₂OISO; ARI, USA) with one laser (2189 cm⁻¹) in combination with a closed chamber system. To achieve the precision and accuracy levels reported in their study, Yamamoto et al. (2014) corrected their measurements for mixing ratio dependence and minimized instrumental drift by measuring N₂ gas every 1hr for background-correction. These authors also showed that careful temperature control of their instrument in an air-conditioned cabinet was necessary for achieving optimal results. Spectrometer raw data were corrected for drift applying a reference gas every hour and dependence on [N₂O].

2.1.4 TREX-QCLAS

A compact mini QCLAS device (CW-QC-TILDAS-76-CS, [serial number 074](#), ARI, USA) coupled with a preconcentration system, called trace gas extractor (TREX) was provided by Empa, Switzerland. The spectrometer comprises a continuous-wave mid-infrared quantum cascade laser source emitting at 2203 cm^{-1} and an astigmatic multipass absorption cell with a path length of 76 m and a volume of approximately 620 cm^3 (Ibraim et al., 2018) (Table 1). The TREX unit was designed and manufactured at Empa and is used to separate the N_2O from the sample gas prior to QCLAS analysis. Thereby, the initial $[\text{N}_2\text{O}]$ is increased by a factor of 200 – 300, other trace gases are removed and the gas matrix is set to standardized conditions. Before entering the TREX device, CO is oxidized to CO_2 using a metal catalyst (Sofnocat 423, Molecular Products Limited, GB). Water and CO_2 in sample gases were removed by a permeation dryer (PermaPure Inc., USA) in combination with a sodium hydroxide (NaOH) / magnesium perchlorate ($\text{Mg}(\text{ClO}_4)_2$) trap (Ascarite: 6 g, 10–35 mesh, Sigma Aldrich, Switzerland, bracketed by $\text{Mg}(\text{ClO}_4)_2$, $2 \times 1.5 \text{ g}$, Alfa Aesar, Germany). Thereafter, N_2O is adsorbed on a HayeSepD (Sigma Aldrich, Switzerland) filled trap, cooled down to $125.1 \pm 0.1 \text{ K}$ by attaching it to a copper baseplate mounted on a high-power Stirling cryo-cooler (CryoTel GT, Sunpower Inc., USA). N_2O adsorption requires $5.080 \pm 0.011 \text{ L}$ of gas to have passed through the adsorption trap. For N_2O desorption, the trap is decoupled from the copper baseplate, while slowly heating it to 275 K with a heat foil (diameter 62.2 mm, 100 W, HK5549, Minco Products Inc., USA). Desorbed N_2O is purged with $1\text{--}5 \text{ cm}^3 \text{ min}^{-1}$ of synthetic air into the QCLAS cell for analysis. By controlling the flow rate and trapping time, the $[\text{N}_2\text{O}]$ in the QCLAS cell can be adjusted to 60–80 ppm at a cell pressure of $35.6 \pm 0.04 \text{ mbar}$. A custom-written LabVIEW program (Version 18.0.1, National Instruments Corp., USA) allows remote control and automatic operation of the TREX. So far, the TREX-QCLAS system has been successfully applied to determine N_2O emission, as well as N_2O isotopic signatures from various ecosystems (e.g. Mohn et al., 2012; Harris et al., 2014; Wolf et al., 2015; Ibraim et al., 2019).

2.1.5 GC-IRMS

IRMS analyses were conducted at ETH Zürich using a gas preparation unit (Trace Gas, Elementar, Manchester, UK) coupled to an IsoPrime100 IRMS (Elementar, Manchester, UK). $[\text{N}_2\text{O}]$ analysis using gas chromatography was also performed at ETH Zürich (456-GC, Scion Instruments, Livingston, UK). GC-IRMS analyses were conducted as part of experiments described further in Section 2.4.8. Further analytical details are provided in Supplementary Material 1.

2.2 Sample and reference gases

2.2.1 Matrix and interference test gases

Table 2 provides O₂, Ar and trace gas mole fractions of matrix gases and interference test gases used during testing. The four matrix gases comprised: synthetic air (matrix a, Messer Schweiz AG, Switzerland); synthetic air with Ar (matrix b, Carbogas AG, Switzerland); synthetic air with Ar, CO₂, CH₄ and CO at near-ambient mole fractions (matrix c, Carbogas AG, Switzerland); and high purity nitrogen gas (N₂, Messer Schweiz AG, Switzerland). Matrix gases were analyzed in the WMO GAW World Calibration Center at Empa (WCC Empa) for CO₂, CH₄, H₂O (G1301, Picarro Inc., USA), and N₂O and CO (CW-QC-TILDAS-76-CS; ARI, USA) against standards of the National Oceanic and Atmospheric Administration/Earth System Research Laboratory/Global Monitoring Division (NOAA/ESRL/GMD). The [N₂O] in all matrix gases and N₂ were below 0.3 ppb. The three gas mixtures used for testing of spectral interferences contained higher mole fractions of either CO₂, CH₄ or CO in matrix gas b (Carbogas AG, Switzerland), which prevented spectroscopic analysis of other trace substances.

Table 2. O₂, Ar content and trace gas concentrations for matrix and interference test gases. Trace gas concentrations of matrix gases were analyzed by WMO GAW WCC Empa against standards of the NOAA/ESRL/GMD. For trace gas concentrations of interference test gases manufacturer specifications are given. Reported O₂ and Ar contents are according to manufacturer specifications. The given uncertainty is the uncertainty stated by the manufacturer or the standard deviation for analysis of n cylinders of the same specification.

Gas	Abbreviation	O ₂ ^{a)} [%]	Ar ^{a)} [%]	CO ₂ ^{b)} [ppm]	CH ₄ ^{b)} [ppb]	CO ^{b)} [ppb]	N ₂ O ^{b)} [ppb]	n
Matrix gases								
Synthetic air	matrix a	20.5±0.5	-	< 1	< 25	< 200	< 0.25	4
Synthetic air + Ar	matrix b	20.95±0.2	0.95±0.01	< 0.5	< 15	< 150	< 0.15	3
Synthetic air + Ar + CO ₂ + CH ₄ + CO	matrix c	20.95±0.4	0.95±0.02	397±3	2004±20	195±3	< 0.15	9
Nitrogen (6.0)	N ₂	< 0.00003	< 0.0001	< 0.2	< 1	< 1	< 0.05	2
		O ₂ ^{a)} [%]	Ar ^{a)} [%]	CO ₂ ^{a)} [%]	CH ₄ ^{a)} [ppm]	CO ^{a)} [ppm]	N ₂ O ^{a)} [ppb]	n
Interference test gases								
CO ₂ in synthetic air + Ar	CO ₂ in matrix b	21.06±0.2	0.94±0.01	4.02±0.04	n.a.	n.a.	n.a.	-
CH ₄ in synthetic air + Ar	CH ₄ in matrix b	20.79±0.4	0.96±0.02	n.a.	199±4	n.a.	n.a.	-
CO in synthetic air + Ar	CO in matrix b	20.95±0.4	0.95±0.02	n.a.	n.a.	20.6±0.4	n.a.	-

^{a)} manufacturer specifications

^{b)} analyzed at WMO GAW WCC Empa

n.a. not analyzed due to very high concentration of one trace substance, which affects spectroscopic analysis of other species

2.2.2 Reference gases (S1, S2) and pressurized air (PA1, PA2)

Preparation of pure and diluted reference gases

Two reference gases (S1, S2) with different N₂O isotopic composition were used in this study. Pure N₂O reference gases were produced from high purity N₂O (Linde, Germany) decanted into evacuated Luxfer aluminum cylinders (S1: P3333N, S2: P3338N) with ROTAREX valves (Matar, Italy) to a final pressure of maximum 45 bar to avoid condensation. Reference gas 1 (S1) was high purity N₂O only. For reference gas 2 (S2), high purity N₂O was supplemented with defined amounts of isotopically pure (>98%) ¹⁴N¹⁵NO (NLM-1045-PK), ¹⁵N¹⁴NO (NLM-1044-PK) (Cambridge Isotope Laboratories, USA) and NN¹⁸O using a ten-port two-position valve (EH2C10WEPH with 20 mL sample loop, Valco Instruments Inc., Switzerland). Since NN¹⁸O was not commercially available, it was synthesized using the following procedure: (1) ¹⁸O exchange of HNO₃ (1.8 mL, Sigma Aldrich) with 97% H₂¹⁸O (5 mL, Medical Isotopes Inc.) under reflux for 24 hours; (2) condensation of NH₃ and reaction controlled by LN₂; and (3) thermal decomposition of NH₄NO₃ in batches of 1 g in 150 mL glass bulbs with breakseal (Glasbläserei Möller AG, Switzerland) to produce NN¹⁸O. The isotopic enrichment was analyzed after dilution in N₂ (99.9999 %, Messer Schweiz AG) with a Vision 1000C quadrupole mass spectrometer (QMS) equipped with a customized ambient pressure inlet (MKS Instruments, UK). Triplicate analysis provided the following composition: 36.25 ± 0.10 % of NN¹⁶O and 63.75 ± 0.76 % of NN¹⁸O.

High [N₂O] reference gases (S1-a_{90ppm}, S1-b_{90ppm}, S1-c_{90ppm}, S2-a_{90ppm}) with a target mole fraction of 90 ppm were prepared in different matrix gases (a, b, c) using a two-step procedure. First, defined volumes of S1 and S2 were dosed into Luxfer aluminum cylinders (ROTAREX valve, Matar, Italy) filled with matrix gas (a, b and c) to ambient pressure using N₂O calibrated MFCs (Vögtlin Instruments GmbH, Switzerland). Second, the N₂O was gravimetrically diluted (ICS429, Mettler Toledo GmbH, Switzerland) with matrix gas to the target mole fraction. Ambient [N₂O] reference gases (S1-c_{330ppb}, S2-c_{330ppb}) with a target mole fraction of 330 ppb were prepared by dosing S1-c_{90ppm} or S2-c_{90ppm} into evacuated cylinders with a calibrated MFC, followed by gravimetric dilution with matrix c.

25

Analysis of reference gases and pressurized air

Table 3 details the trace gas mole fractions and N₂O isotopic composition of high and ambient [N₂O] reference gases, as well as commercial pressurized air (PA1 and PA2) used during testing. Trace gas mole fractions of high [N₂O] reference gases were acquired from the trace gas levels in the respective matrix gases (Table 2), while ambient [N₂O] reference gases and target as well as background gases were analyzed by WCC Empa. The isotopic composition of high [N₂O] isotope reference gases in synthetic air (S1-a_{90ppm}, S2-a_{90ppm}) was analyzed in relation to N₂O isotope standards (Cal1 – Cal3) in an identical matrix gas (matrix a) using laser spectroscopy (CW-QC-TILDAS-200; ARI, Billerica, USA). The composition of Cal1 – Cal3 are outlined in Supplementary Material 2.(for S1-a_{90ppm}: Cal1 and Cal2; for S2-a_{90ppm}: Cal3 and Cal2) in an identical gas matrix (matrix a) by laser spectroscopy (CW-QC-TILDAS-200; ARI, Billerica, USA). The applied standards (Cal1 – 3) have previously been measured by Sakae

35

Toyoda at Tokyo Institute of Technology: Cal1 ($\delta^{15}\text{N}^{\alpha} = 2.06 \pm 0.05 \text{ ‰}$, $\delta^{15}\text{N}^{\beta} = 1.98 \pm 0.20 \text{ ‰}$, $\delta^{18}\text{O} = 36.12 \pm 0.32 \text{ ‰}$); Cal2 ($\delta^{15}\text{N}^{\alpha} = -48.59 \pm 0.25 \text{ ‰}$, $\delta^{15}\text{N}^{\beta} = -46.11 \pm 0.43 \text{ ‰}$, $\delta^{18}\text{O} = 27.37 \pm 0.11 \text{ ‰}$); and Cal3 ($\delta^{15}\text{N}^{\alpha} = 25.73 \pm 0.24 \text{ ‰}$, $\delta^{15}\text{N}^{\beta} = 25.44 \pm 0.36 \text{ ‰}$, $\delta^{18}\text{O} = 35.86 \pm 0.22 \text{ ‰}$).

- 5 **Table 3.** Trace gas concentrations and N₂O isotopic composition of high and ambient N₂O concentration reference gases, and pressurized air. Trace gas concentrations of high concentration reference gases were retrieved from the composition of matrix gases used for their production (see Table 24), trace gas concentrations in ambient concentration reference gases and pressurized air were analyzed by WMO GAW WCC Empa against standards of the NOAA/ESRL/GMD. The N₂O isotopic composition was quantified by laser spectroscopy (QCLAS) and preconcentration - laser spectroscopy (TREX-QCLAS) against reference gases previously analyzed by Tokyo Institute of Technology.

Gas	CO ₂ [ppm]	CH ₄ [ppb]	CO [ppb]	N ₂ O [ppb]	$\delta^{15}\text{N}^{\alpha}$ vs AIR-N ₂ [‰]	$\delta^{15}\text{N}^{\beta}$ vs AIR-N ₂ [‰]	$\delta^{18}\text{O}$ vs VSMOW [‰]
High N ₂ O concentration reference gases							
S1-a _{90ppm}	< 1	< 25	< 200	~90000	0.54±0.17	1.15±0.06	39.46±0.01
S1-b _{90ppm}	< 0.5	< 15	< 150	~90000	0.54±0.17	1.15±0.06	39.46±0.01
S1-c _{90ppm}	397±3	2004±20	195±3	~90000	0.54±0.17	1.15±0.06	39.46±0.01
S2-a _{90ppm}	< 1	< 25	< 200	~90000	51.43±0.06	55.14±0.09	100.09±0.03
S2-c _{90ppm}	397±3	2004±20	195±3	~90000	51.43±0.06	55.14±0.09	100.09±0.03
Ambient N ₂ O concentration reference gases							
S1-c _{330ppb}	399.78±0.04	2022±0.2	195±0.3	327.45±0.06	0.92±0.39	1.44±0.25	39.12±0.18
S2-c _{330ppb}	398.62±0.04	2020±0.2	193±0.3	323.97±0.06	52.38±0.10	55.61±0.12	99.59±0.03
High N ₂ O concentration source gas (SG) for two-end member mixing experiments (Sect. 2.4.8)							
SG1-a _{90ppm}	< 1	< 25	< 200	~90000	-	-	31.79±0.12
					24.35±0.32	22.94±0.33	
SG2-a _{90ppm}	< 1	< 25	< 200	~90000	51.43±0.06	55.14±0.09	100.09±0.03
Pressurized air							
Pressurized air (PA1)	200.55±0.07	2582±0.2	187±0.2	326.51±0.06	15.83±0.03	-3.39±0.14	44.66±0.02
Pressurized air (PA2)	437.99±0.36	2957±0.3	275±0.4	333.50±0.09	15.81±0.07	-	44.72±0.04
						3.31±0.004	

- For high mole fraction reference gases in matrix b and c (S1-b_{90ppm}, S1-c_{90ppm}, S2-c_{90ppm}), the δ values acquired for S1-a_{90ppm} and S2-a_{90ppm} were assigned, since all S1 and S2 reference gases (irrespective of gas matrix) were generated from the same source of pure N₂O gas. Direct analysis of S1-b_{90ppm}, S1-c_{90ppm} and S2-c_{90ppm} by QCLAS was not feasible as no N₂O isotope standards in matrix b and c were available.~~applied.~~ The absence of significant difference (< 1 ‰) in N₂O isotopic composition between S1-b_{90ppm} and S1-c_{90ppm} in relation to S1-a_{90ppm} (and S2-c_{90ppm} to S2-a_{90ppm}) was assured by first statically diluting S1-b_{90ppm}, S1-c_{90ppm} and S2-c_{90ppm} to ambient N₂O mole fractions with synthetic air. This was followed by analysis using TREX-QCLAS (as described in Sect. 2.1.4) against the same standards used for S1-a_{90ppm}, S2-a_{90ppm} isotope analysis.

Ambient mole fraction N₂O isotope reference gases (S1-c_{330ppb}, S2-c_{330ppb}) and PA1 and PA2 were analyzed by TREX-QCLAS (Sect. 2.1.4) using N₂O isotope standards (Cal1 – Cal5) as outlined in

~~Supplementary Material 2. The following N₂O isotope standards (values assigned by Tokyo Institute of Technology) were used: Cal1 and Cal2 for S1- $\epsilon_{330\text{ppm}}$; Cal3 and Cal2 for S2- $\epsilon_{330\text{ppm}}$; Cal4 ($\delta^{15}\text{N}^{\alpha} = -16.29 \pm 0.07 \text{‰}$, $\delta^{15}\text{N}^{\beta} = -2.59 \pm 0.06 \text{‰}$, $\delta^{18}\text{O} = 39.37 \pm 0.04 \text{‰}$) and Cal5 ($\delta^{15}\text{N}^{\alpha} = -51.09 \pm 0.07 \text{‰}$, $\delta^{15}\text{N}^{\beta} = -48.12 \pm 0.04 \text{‰}$, $\delta^{18}\text{O} = 30.81 \pm 0.03 \text{‰}$) for PA1 and PA2.~~

5 2.3 Laboratory setup, measurement procedures and data processing

2.3.1 Laboratory setup

All experiments were performed at the Laboratory for Air Pollution / Environmental Technology, Empa, Switzerland during June 2018 and February 2019. The laboratory was air conditioned to 295 K (± 1 K), with ± 0.5 K diel variations (Saveris 2, Testo AG, Switzerland), with the exception of a short period (7th to 8th July 2018), where the air conditioning was deactivated to test the temperature dependence of analyzers. Experiments were performed simultaneously for all analyzers, with the exception of the TREX-QCLAS, which requires an extensive measurement protocol and additional time to trap and measure N₂O (Ibraim et al., 2018) and thus could not be integrated concurrently with the other analyzers.

Fig. 2 shows a generalized experimental setup used for all experiments. Additional information for specific experiments is given in Section 2.4, and individual experimental setups are depicted in Supplementary Material [32](#). Gas flows were controlled using a set of mass flow controllers (MFC, model high-performance, Vögtlin Instruments GmbH, Switzerland) integrated into a MFC control unit (Contrec AG, Switzerland). All MFCs were calibrated by the manufacturer for whole air, which according to Vögtlin Instruments is valid for pure N₂ and pure O₂ as well. Operational ranges of applied MFCs ranged from 0–25 cm³ min⁻¹ to 0–5000 cm³ min⁻¹, and had reported uncertainties of 0.3 % of their maximum flow and 0.5 % of actual flow. To reduce the uncertainty of the flow regulation, the MFC with the smallest maximum flow range available was selected. The sum of dosed gas flows was always higher than the sum of gas consumption by analyzers, with the overflow exhausted to room air. Gas lines between gas cylinders and MFCs, as well as between MFCs and analyzers, were 1/8" stainless steel tubing (type 304, Supelco, Sigma-Aldrich Chemie GmbH, Switzerland). Manual two-way (SS-1RS4 or SS-6H-MM, Swagelok, Switzerland) or three-way valves (SS-42GXS6MM, Swagelok, Switzerland) were used to separate or combine gas flows.

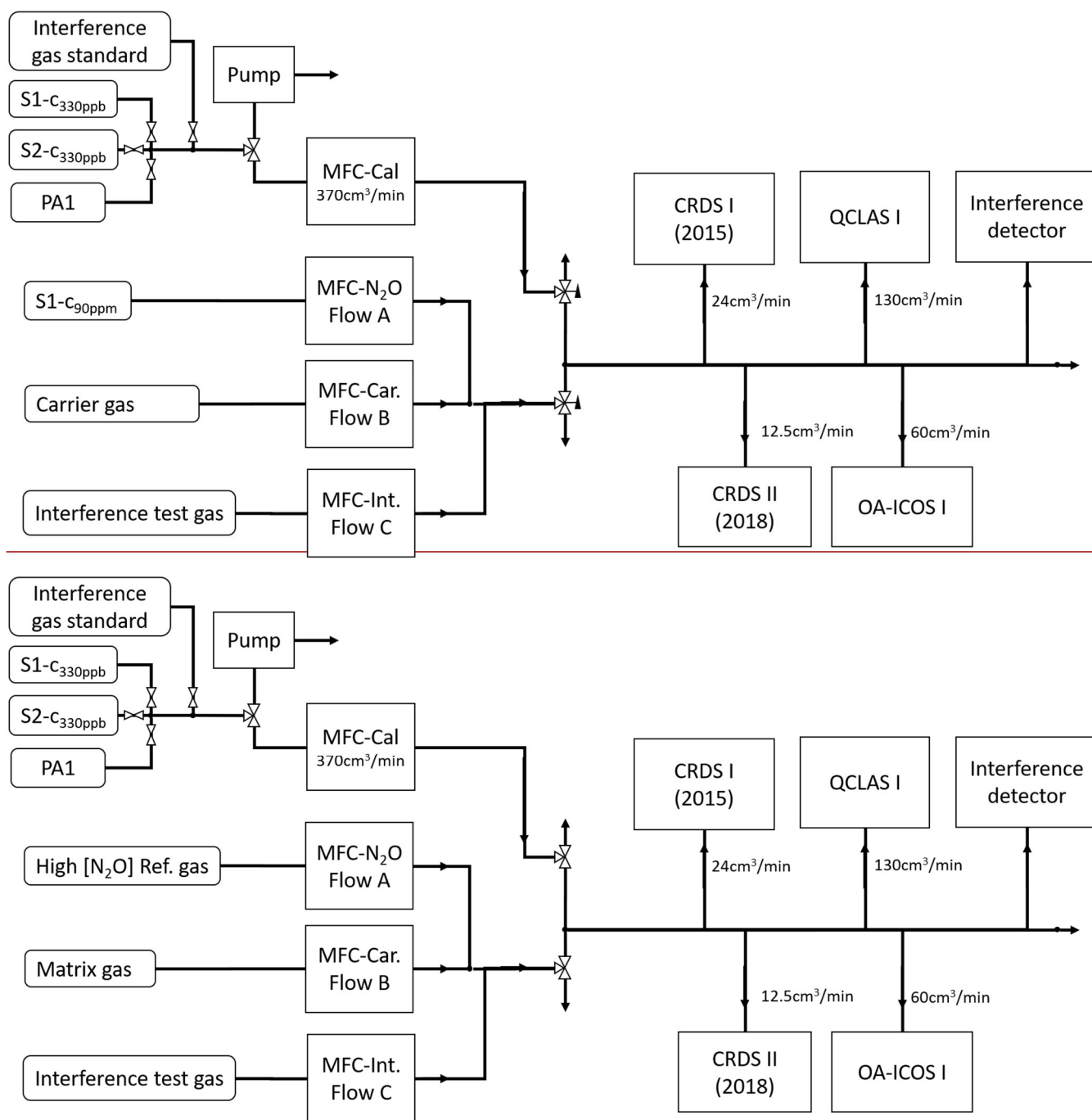


Fig. 2. The generalized experimental setup used for all experiments conducted in this study. The gases introduced via MFC flows A, B and C were changed according to the experiments outlined in Sect. 2.4. Table 2 and Table 3 provide the composition of the *matrix gases* (MFC B), *interference test gases* (MFC C) and *high [N₂O] concentration reference gases* (MFC A). Laboratory setups for each individual experiment are provided in Supplementary Material 3.

2.3.2 Measurement procedures, data processing and calibration

With the exception of Allan variance experiments performed in Sect. 2.4.1, all gas mixtures analyzed during this study were measured by the laser spectrometers for a period of 15 minutes, with the last 5 minutes used for data processing. Customized R-scripts (R Core Team, 2017) were used to extract the 5 min averaged data for each analyzer. Whilst the OA-ICOS and QCLAS instruments provide individual $^{14}\text{N}^{14}\text{N}^{16}\text{O}$, $^{14}\text{N}^{15}\text{N}^{16}\text{O}$, $^{15}\text{N}^{14}\text{N}^{16}\text{O}$ and $^{14}\text{N}^{14}\text{N}^{18}\text{O}$ mole fractions, the default data output generated by the

CRDS analyzers are δ values, with underlying calculation schemes inaccessible to the user. Therefore, to remain consistent across analyzers, uncalibrated δ values were calculated for OA-ICOS and QCLAS instruments first, using literature values for the $^{15}\text{N}/^{14}\text{N}$ (0.0036782) and $^{18}\text{O}/^{16}\text{O}$ (0.0020052) isotope ratios of AIR-N2 and VSMOW (Werner and Brand, 2001).

5

Each experiment was performed over the course of one day, and consisted of three phases: (1) an initial calibration phase; (2) an experimental phase; and (3) a final calibration phase. During phases (1) and (3), reference gases S1-c_{330ppb} and S2-c_{330ppb} were analyzed. On each occasion (i.e. twice a day), this was followed by the analysis of PA1, which was used to determine the long-term (day-to-day) repeatability of the analyzers. Phase (2) experiments are outlined in Sect. 2.4. Throughout all three phases, all measurements were systematically alternated with an Anchor gas measurement, the purpose of which was twofold: (1) to enable drift correction; and (2) as a means of quantifying deviations of the measured $[\text{N}_2\text{O}]$ and δ values caused by increasing $[\text{N}_2\text{O}]$ (Sect. 2.4.4), the removal of matrix gases (O_2 and Ar in Sect. 2.4.5) or addition of trace gases (CO_2 , CH_4 and CO in Sect 2.4.6). Accordingly, the composition of the Anchor gas varied across experiments (see Sect. 2.4), but remained consistent throughout each experiment. A drift correction was applied to the data if a linear or non-linear model fitted to the Anchor gas measurement over the course of an experiment was statistically significant at $p < 0.05$. Otherwise, no drift correction was applied.

20 In Sects. 2.4.3 (repeatability experiments) and 2.4.8 (two end-member mixing experiments), trace gas effects were corrected according to Eqs. (1), (2) and (3) using derived analyzer-specific correction functions because the CO_2 , CH_4 and CO composition of PA1 in Sect. 2.4.3 and the gas mixtures in Sect. 2.4.8 varied from those of the calibration gases S1-c_{330ppb} (S1) and S2-c_{330ppb} (S2):

$$[\text{N}_2\text{O}]_{tc,G} = [\text{N}_2\text{O}]_{meas,G} - \sum_x \left(\Delta[\text{N}_2\text{O}] (\Delta[x]_G, [\text{N}_2\text{O}]_{meas,G}) \right) \quad (1)$$

$$25 \quad \delta_{tc,G} = \delta_{meas,G} - \sum_x \left(\Delta\delta (\Delta[x]_G, \delta_{meas,G}) \right) \quad (2)$$

and,

$$\Delta[x]_G = [x]_G - \frac{[x]_{S1} + [x]_{S2}}{2} \quad (3)$$

where $[\text{N}_2\text{O}]_{tc,G}$ and $\delta_{tc,G}$ refer to the trace gas-corrected $[\text{N}_2\text{O}]$ and δ values ($\delta^{15}\text{N}^\alpha$, $\delta^{15}\text{N}^\beta$ or $\delta^{18}\text{O}$) of sample gas G, respectively; $[\text{N}_2\text{O}]_{meas,G}$ and $\delta_{meas,G}$ are the raw uncorrected $[\text{N}_2\text{O}]$ and δ values measured by the analyzer for sample gas G, respectively; $\Delta[\text{N}_2\text{O}]$ and $\Delta\delta$ refer to the offset on the $[\text{N}_2\text{O}]$ or δ values, respectively, resulting from the difference in trace gas mole fraction between sample gas G and reference gases, denoted $\Delta[x]_G$; $[x]_G$ is the mole fraction of trace gas x (CO_2 , CH_4 or CO) in sample gas G; and $[x]_{S1}$ and $[x]_{S2}$ are the mole fractions of trace gas x in reference gases S1-c_{330ppb} and S2-c_{330ppb}. It is

important to note that the differences in CO₂ and CH₄ mole fractions in S1-c₃₃₀ppb and S2-c₃₃₀ppb are two orders of magnitude smaller than the differences to PA1.

Thereafter, δ values of trace gas-corrected, mole fraction-corrected (Sect.2.4.8 only) and drift-corrected measurements from the analyzers were normalized to δ values on the international isotope ratio scales using a two-point linear calibration procedure derived from values of S1-c₃₃₀ppb (S1) and S2-c₃₃₀ppb (S2) calculated using Eq. (4) (Gröning, 2018):

$$\delta_{cal,G} = \frac{\delta_{reftrue,S1} - \delta_{reftrue,S2}}{\delta_{corrmeas,S1} - \delta_{corrmeas,S2}} * (\delta_{corruneat,G} - \delta_{corrmeas,S1}) + \delta_{reftrue,S1} \quad (4)$$

where $\delta_{cal,G}$ is the calibrated δ value for sample gas G normalized to international isotope ratio scales; $\delta_{reftrue,S1}$ and $\delta_{reftrue,S2}$ are the respective δ values assigned to reference gases S1-c₃₃₀ppb and S2-c₃₃₀ppb; $\delta_{corrmeas,S1}$ and $\delta_{corrmeas,S2}$ are the respective δ values measured for the of reference gases S1-c₃₃₀ppb and S2-c₃₃₀ppb measured by the analyzer which, if required, were drift-corrected; and $\delta_{corruneat,G}$ is the trace gas-corrected, mole fraction-corrected (Sect.2.4.8 only) and drift-corrected (if required) δ value measured for the sample gas G. ~~is the trace gas-corrected, mole fraction-corrected (Sect.2.4.8 only) and drift-corrected measurement of sample gas G acquired by the analyzer. In Eq. (4), the calibration span is given by the difference in δ values between S1 and S2.~~

2.4 Testing of instruments

An overview of all experiments performed in this study, including applied corrections and instruments tested, is provided in Table 4.

Table 4. Overview of the experiments performed in this study.

Experiment	Sections	Aims	Corrections applied	Instruments tested	Comments
Instrumental precision (Allan deviation)	2.4.1 3.1	Short-term precision, optimal integration time/maximum precision and drift	None	OA-ICOS I CRDS I & II QCLAS I QCLAS II & III (ambient only) TREX-QCLAS I	Conducted at N ₂ O concentrations ~326, 1000, 10000 ppb
Temperature effects	2.4.2 3.2	Temperature effects on [N ₂ O] and isotope deltas	None	OA-ICOS I CRDS I & II QCLAS I	
Repeatability (short-term, ~2 hour)	2.4.3 3.3	Repeatability	Drift	OA-ICOS I CRDS I & II QCLAS I TREX-QCLAS I	Conducted at N ₂ O concentrations ~326, 1000, 10000 ppb
Repeatability (long-term, ~2 week)	2.4.3 3.3	Repeatability	Drift, delta calibration, trace gas effect ^{a)}	OA-ICOS I CRDS I & II QCLAS I TREX-QCLAS I	Conducted at ~326 ppb N ₂ O using PA1
N ₂ O mole fraction effects	2.4.4 3.4	[N ₂ O] effects on isotope deltas, and derive correction functions	Drift	OA-ICOS I CRDS I & II QCLAS I	CRDS: 300 to 1500 ppb N ₂ O, OA-ICOS, QCLAS: 300 to 90000 ppb
Gas matrix effects (N ₂ , O ₂ and Ar)	2.4.5 3.5	Gas matrix effects on [N ₂ O] and isotope deltas, and derive correction functions	Drift	OA-ICOS I CRDS I & II QCLAS I TREX-QCLAS I	Conducted at N ₂ O concentrations ~330, 660, 990 ppb
Trace gas effects (H ₂ O, CO ₂ , CH ₄ , CO)	2.4.6 3.6	Trace gas effects on [N ₂ O] and isotope deltas, and derive correction functions	Drift	OA-ICOS I CRDS I & II QCLAS I TREX-QCLAS I (except H ₂ O)	Conducted at N ₂ O concentrations ~330, 660, 990 ppb
CO ₂ and CO removal	2.4.7 3.6	Effects of removal of CO ₂ (Ascarite) and CO (Sofnocat) on [N ₂ O] and isotope deltas	Drift	OA-ICOS I CRDS I & II QCLAS I	Conducted at N ₂ O concentrations ~330 ppb
Two end-member mixing	2.4.8 3.7	Test the ability of the instruments to extrapolate a N ₂ O source using a Keeling plot approach	Drift, 3-point concentration dependence, delta calibration, trace gas effect ^{a)} , and scaled with N ₂ O ^{b)}	OA-ICOS I (exp. 1-6) CRDS I & II (exp. 1-4) QCLAS I (exp. 1-6) TREX-QCLAS I (exp. 1-2) GC [N ₂ O], IRMS [δ] (exp. 1-6)	The workflow provided in Sect. 4.3 was applied

^{a)} Derived from trace gas effect determined in Sections 3.6.

^{b)} Derived from scaling effects described in Section 3.6.2.

2.4.1 Allan precision

- The precision of the laser spectrometers was determined using the Allan variance technique (Allan, 1966; Werle et al., 1993). Experiments were conducted at different [N₂O]: ambient, 1000 ppb, and 10000 ppb. For the Allan variance testing conducted at ambient [N₂O], a continuous flow of PA1 was measured continuously for 30 h. For testing conducted at 1000 and 10000 ppb [N₂O], S1-c_{90ppm} was dynamically

diluted to 1000 or 10000 ppb [N₂O] with matrix gas c for 10 h. CRDS I and II were disconnected for the 10000 ppb measurement because [N₂O] exceeded the specified measurement range. Daily drifts were estimated using the slope of the linear regression over the measurement period normalized to 24 h (i.e. ppb d⁻¹ and ‰ d⁻¹).

5 2.4.2 Temperature effects

To investigate instrumental sensitivities to variations in ambient temperature, PA1 was simultaneously and continuously measured by all analyzers in flow-through mode for a period of 24 h while the air conditioning of the laboratory was turned off for over 10 h. This led to a rise in temperature from 21°C to 30°C, equating to an increase in temperature of approximately 0.9°C per hour. The increase in laboratory room temperature was detectable shortly after the air conditioning was turned off due to considerable heat being released from several other instruments located in the laboratory. Thereafter, the air conditioning was restarted and the laboratory temperature returned to 21°C over the course of 16 h, equating to a decrease of roughly 0.6°C per hour, with most pronounced effects observable shortly after restart of air conditioning when temperature changes were highest~~30 h, which led to a rise in room temperature from 21 °C to 30 °C. Thereafter, the air conditioning was restarted and the laboratory temperature returned to 21°C.~~

2.4.3 Repeatability

Measurements of PA1 were taken twice daily over ~2 weeks prior to and following the experimental measurement period to test the long-term repeatability of the analyzers. Measurements were sequentially corrected for differences in trace gas concentrations (Eqs. 1 – 3), drift (if required), and then δ -calibrated (Eq. 4). No matrix gas corrections were applied because the N₂, O₂ and Ar composition of PA1 was identical to that of S1-c_{330ppb} and S2-c_{330ppb}. TREX-QCLAS I measurements for long-term repeatability were collected separately from other instruments over a period of six-months. Repeatability over shorter time periods (2.5 h) was also tested for each analyzer by acquiring 10 repeated 15 min measurements at different N₂O mole fractions: ambient (PA1), 1000 ppb and 10000 ppb N₂O.

2.4.4 N₂O mole fraction dependence

To determine the effect of changing [N₂O] on the measured δ values, S1-c_{90ppm} was dynamically diluted with matrix c to various [N₂O] spanning the operational ranges of the instruments. For both CRDS analyzers mole fractions between 300 to 1500 ppb were tested, while for the OA-ICOS I and QCLAS I mixing ratios ranged from 300 to 90000 ppb. Between each [N₂O] step change, the dilution ratio was systematically set to 330 ppb N₂O to perform an Anchor gas measurement. For each instrument, the effect of increasing [N₂O] on δ values was quantified by comparing the measured δ values at each step change

to the mean measured δ values of the Anchor gas, and was denoted $\Delta\delta$ such that $\Delta\delta = \delta_{\text{measured}} - \delta_{\text{Anchor}}$ and $\Delta\delta_{\text{Anchor}} = 0$. The experiment was repeated on three consecutive days to test day-to-day variability.

2.4.5 Gas matrix effects (O₂ and Ar)

Gas matrix effects were investigated by determining the dependence of [N₂O] and isotope δ values on the O₂ or Ar mixing ratio of a gas mixture. For O₂ testing, Gas 1, 2 and 3 (N₂) were mixed to incrementally change mixing ratios of O₂ (0–20.5 % O₂) while maintaining a consistent [N₂O] of 330 ppb. As an Anchor gas, Gas 1 (S1-a90ppm) was dynamically diluted with Gas 2 (matrix a) to produce 330 ppb N₂O in matrix a (Table 5). O₂ mole fractions in the various gas mixtures were analyzed with a paramagnetic O₂ analyzer (Servomex, UK) and agreed with expected values to within 0.3 % (relative). For Ar testing, Gas 1 (S1-b90ppm) was dynamically diluted with Gas 2 (matrix b) to produce an Anchor gas with ~330 ppb N₂O in matrix b. Gas 1, 2 and 3 (N₂ + O₂) were then mixed to incrementally change mixing ratios of Ar (0.003–0.95 % Ar), while a consistent [N₂O] of 330 ppb was maintained. Ar compositional differences were estimated based on gas cylinder manufacturer specifications and selected gas flows. The effects of decreasing O₂ and Ar on [N₂O] and δ values were quantified by comparing the measured [N₂O] and δ values at each step change to the mean measured [N₂O] and δ values of the Anchor gas, and were denoted $\Delta[\text{N}_2\text{O}]$ and $\Delta\delta$, similar to Sect. 2.4.4. Deviations in O₂ and Ar mixing ratios were quantified by comparing the [O₂] and [Ar] at each step change to the mean [O₂] and [Ar] of the Anchor gas, and were denoted ΔO_2 and ΔAr such that, for example, $\Delta\text{O}_2 = \text{O}_2_{\text{measured}} - \text{O}_2_{\text{Anchor}}$ and $\Delta\text{O}_2_{\text{Anchor}} = 0$. Both O₂ and Ar experiments were triplicated.

In addition, O₂ and Ar effects were derived for N₂O mole fractions of ~660 ppb and ~990 ppb. These experiments were undertaken in a way similar to those described above, except Anchor gas measurements were conducted once (not triplicated).

Table 5. Gas mixtures used to test effects of gas matrix (O₂, Ar) or trace gases (CO₂, CH₄, CO) on [N₂O] and isotope deltas. Gas 1 was dynamically diluted with Gas 2 to make up an Anchor gas with [N₂O] of ~330 ppb which was systematically measured throughout the experiments to (1) enable drift correction, and (2) quantify deviations of the measured [N₂O] and δ values caused by the removal of matrix gases (O₂ and Ar in Sect. 2.4.5) or addition of trace gases (CO₂, CH₄ and CO in Sect 2.4.6). Gas 1, 2 and 3 were combined in different fractions to make up sample gas with identical [N₂O] but varying mixing ratio of the target compound.

Target compound	Gas 1	Gas 2	Gas 3	Mixing range
O ₂	S1-a90ppm (N ₂ O + N ₂ + O ₂)	N ₂ + O ₂ ^a	N ₂	0-20.5 % O ₂
Ar	S1-b90ppm (N ₂ O + N ₂ + O ₂ + Ar)	N ₂ + O ₂ + Ar ^b	N ₂ + O ₂ ^a	0.003-0.95 % Ar
CO ₂	S1-b90ppm (N ₂ O + N ₂ + O ₂ + Ar)	N ₂ + O ₂ + Ar ^b	CO ₂ in N ₂ + O ₂ + Ar ^b	1.72-2030 ppm CO ₂
CH ₄	S1-b90ppm (N ₂ O + N ₂ + O ₂ + Ar)	N ₂ + O ₂ + Ar ^b	CH ₄ in N ₂ + O ₂ + Ar ^b	0.014-10.25 ppm CH ₄
CO	S1-b90ppm (N ₂ O + N ₂ + O ₂ + Ar)	N ₂ + O ₂ + Ar ^b	CO in N ₂ + O ₂ + Ar ^b	0.14-2.13 ppm CO

^a) matrix a: 20.5 % O₂ in N₂

^b) matrix b: 20.95 % O₂, 0.95 % Ar in N₂

2.4.6 Trace gas effects (CO₂, CH₄, CO and H₂O)

The sensitivity of [N₂O] and δ values on changing trace gas concentrations was tested in a similar way to those described in Sect. 2.4.5. In short, Gas 1 (S1-b_{90ppm}) was dynamically diluted with Gas 2 (matrix b) to create an Anchor gas with 330 ppb N₂O in matrix b. Gas 1, 2 and 3 (either CO₂, CH₄ or CO in matrix gas b) were mixed to incrementally change the mixing ratios of the target substances (1.7 – 2030 ppm CO₂, 0.01 – 10.25 ppm CH₄ and 0.14 – 2.14 ppm CO) while maintaining a consistent gas matrix and [N₂O] of 330 ppb (Table 5). Trace gas mole fractions in the produced gas mixtures were analyzed with a Picarro G2401 (Picarro Inc., USA) and agreed with predictions within better than 2–3 % (relative). Similar to Sect. 2.4.4, the effects of increasing CO₂, CH₄ and CO on [N₂O] and δ values were quantified by comparing the measured [N₂O] and δ values at each step change to the mean measured [N₂O] and δ values of the Anchor gas, and were denoted Δ [N₂O] and $\Delta\delta$. Similar to Sect. 2.4.5, deviations in CO₂, CH₄ and CO mixing ratios were quantified by comparing the measured [CO₂], [CH₄] and [CO] at each step change to the mean measured [CO₂], [CH₄] and [CO] of the Anchor gas. Each experiment was triplicated. The interference effects were also tested at ~660 ppb and ~990 ppb N₂O.

15

The sensitivity of the analyzers to water vapor was tested by firstly diluting Gas 1 (S1-c_{90ppm}) with Gas 2 (matrix c) to produce an Anchor gas with 330 ppb N₂O. This mixture was then combined with Gas 3 (also matrix c) which had been passed through a humidifier (customized setup by Glasbläserei Möller, Switzerland) set to 15°C (F20 Julabo GmbH, Germany) dew point. By varying the flows of Gas 2 and 3, different mixing ratios of water vapor ranging from 0 – 13800 ppm were produced and measured using a dewpoint meter (model 973, MBW, Switzerland). H₂O effects were quantified as described above, but [N₂O] results were additionally corrected for dilution effects caused by the addition of water vapor into the gas stream. Water vapor dependence testing was not performed on the TREX-QCLAS I as the instrument is equipped with a permeation dryer at the inlet.

25 2.4.7 CO₂ and CO removal using NaOH (Ascarite) and Sofnocat

The efficiency of NaOH and Sofnocat for removing spectral effects caused by CO₂ and CO was assessed by repeating CO₂ and CO interference tests (Sect. 2.4.6), but with the respective traps connected in-line. These experiments were triplicated but only undertaken at ~330 ppb N₂O. NaOH traps were prepared using stainless steel tubing (OD 2.54 cm, length 20 cm) filled with 14 g Ascarite (0-30 mesh, Sigma Aldrich, Switzerland) bracketed by 3g Mg(ClO₄)₂ (Alfa Aesar, Germany) each separated by glass wool. The Sofnocat trap was prepared similarly using stainless steel tubing (OD 2.54 cm, length 20 cm) filled with 50 g Sofnocat (Sofnocat 423, Molecular Products Limited, GB) and capped on each side with glass wool.

30

2.4.8 Two end-member mixing

The ability of the instruments to accurately extrapolate N₂O source compositions was tested using a simulated two end-member mixing scenario in which a gas with high N₂O concentration, considered to be a N₂O *source* gas (SG), was dynamically diluted into a gas with ambient N₂O concentration (PA2), considered to be *background* air. N₂O mole fractions were raised above ambient levels (denoted as Δ N₂O) in three different scenarios ranging from: (1) 0–30 ppb; (2) 0–700 ppb and (3) 0–10000 ppb. In each scenario, two isotopically different *source* gases with high N₂O concentration were used; one *source* gas (SG1-a_{90ppm}) ¹⁵N depleted compared to PA2; and a second *source* gas (SG2-a_{90ppm}) ¹⁵N enriched compared to PA2 (Table 3). The three different mixing scenarios and two different *source* gases resulted in a total of six mixing scenarios (referred to as Exp. 1–6). During each experiment, PA2 was alternated with PA2 + SG in four different mixing ratios to give a span of N₂O concentrations and isotopic compositions required for Keeling plot analysis. Each experiment was triplicated. OA-ICOS I and QCLAS I were used in all experiments (Exp. 1–6), CRDS was used for Δ N₂O 0–30 ppb and 0–700 ppb (Exp. 1–4) and TREX-QCLAS was only used for Δ N₂O 0–30 ppb (Exp. 1–2).

15

To test the robustness of trace gas correction equations derived for each analyzer in Sect. 3.6, NaOH and Sofnocat traps were placed in-line between the PA2 + SG mixtures and the analyzers such that we could ensure a difference in CO₂ and CO mole fractions between the measured gas mixture and reference gases (S1-c_{330ppb}, S2-c_{330ppb}). The experiments were also bracketed by two calibration phases (S1-c_{330ppb}, S2-c_{330ppb}) to allow for δ calibration, followed by two phases where the N₂O concentration dependence was determined.

20

Gas samples for GC-IRMS analysis were taken in the same phase (last five min of 15 min interval) used during the minute prior to the final five minutes used for averaging by the laser-based analyzers. The gas was collected at the common overflow port of the laser spectrometers using a 60 mL syringe connected via a Luer lock three-way valve to needle and port. 200 mL samples were taken at each concentration step. 180 mL of gas sample was stored in pre-evacuated 110 mL serum crimp vials for isotopic analysis using IRMS. IRMS analyses were conducted at ETH Zürich using a gas preparation unit (Trace Gas, Elementar, Manchester, UK) coupled to an IsoPrime100 IRMS (Elementar, Manchester, UK). The remaining 20 mL were injected in a pre-evacuated 12 mL Labco exetainer for [N₂O] analysis using gas chromatography equipped with Electron Capture Detector (ECD) performed at ETH Zürich (Bruker, 456-GC, Scion Instruments, Livingston, UK). After injection, samples were separated on HayeSep D packed columns with a 5% CH₄ in Ar mixture (P5) as carrier and make-up gas. The GC was calibrated using a suite of calibration gases at N₂O concentrations of 0.393 (Carbagas AG, Switzerland), 1.02 (PanGas AG,

30

Switzerland) and 3.17 ppm (Carbagas AG, Switzerland). For further analytical details see Verhoeven et al. (2019) and Supplementary Material 1.

For the laser-based analyzers, data was processed as described in Sect. 2.3.2 using the following sequential order: (1) analyzer-specific correction functions, determined in Sect 3.6, were applied to correct for differences in trace gas concentrations (CO_2 , CO) between sample gas and calibration gases; (2) the effect of $[\text{N}_2\text{O}]$ changes was corrected using a three-point correction; (3) a drift-correction based on repeated measurements of PA2 was applied if necessary; and (4) ~~a δ -calibration~~ values standardized to international scales (Eq. 4) using S1-c_{330ppb} and S2-c_{330ppb} ~~was applied~~.

10 3 Results

Note: due to the large number of results acquired in this Section, only selected results are shown in Figs. 3 to 14. The complete datasets (including $[\text{N}_2\text{O}]$, $\delta^{15}\text{N}^\alpha$, $\delta^{15}\text{N}^\beta$ and $\delta^{18}\text{O}$ acquired by all instruments tested) are provided in Supplementary Material 4.

15 3.1 Allan precision

Allan deviations (square root of Allan variance) for 5 min and 10 min averaging times, often reported in manufacturer specifications, at ~327 ppb, 1000 ppb and 10000 ppb $[\text{N}_2\text{O}]$ are shown in Table 6.

At near-atmospheric N_2O mole fractions of ~326.5 ppb, both CRDS analyzers showed the ~~greatest~~ best precision and stability for the measurement of $\delta^{15}\text{N}^\alpha$, $\delta^{15}\text{N}^\beta$ and $\delta^{18}\text{O}$ (0.32 – 0.41 ‰, 0.41 – 0.45 ‰, 0.41 – 0.46 ‰ at 300 s averaging time, respectively), while for the precision of $[\text{N}_2\text{O}]$, the OA-ICOS I and the CRDS II showed best performance ($1.7 \cdot 10^{-2}$ ppb at 300 s averaging time) (Figs. 3 and S4-1; Table 6). The Allan precision of CRDS and OA-ICOS analyzers further improved with increasing averaging times and optimal averaging times typically exceeded 1.5-3 h. The precision and daily drift of the OA-ICOS I and both CRDS analyzers were in agreement with manufacturer specifications (ABB-Los Gatos Research Inc., 2019; Picarro Inc., 2019). The CRDS II outperformed the CRDS I for precision, presumably due to manufacturer upgrades/improvements in the newer model. The QCLAS spectrometers exhibited significant differences between instruments, which might be due to differences in the instrument hardware / design, as instruments were manufactured between 2012 – 2016, or in the parameter setting (such as cell pressure and tuning parameters) of different analyzers.

Generally, short-term (approx. up to 100 s) precision of QCLAS instruments was compatible or superior to CRDS or OA-ICOS, but data quality was decreased for longer averaging times due to drift effects.

Nonetheless, the performance of QCLAS I, II and III generally agrees with Allan precision measurements executed by Yamamoto et al. (2014), who reported 1.9 – 2.6 ‰ precision for δ values at ambient N₂O mole fractions and 0.4 – 0.7 ‰ at 1000 ppb N₂O. QCLAS I, which was tested further in Sects. 3.2 – 3.7, displayed the poorest performance of all QCLAS analyzers, in particular for $\delta^{15}\text{N}^{\beta}$. The primary cause of the observed excess drift in QCLAS I was fluctuating spectral baseline structure (pers. comm. ARI), which can be significantly reduced by applying an automatic spectral correction method developed by ARI. This methodology is currently in trial phase and, thus, not yet implemented in the software that controls the QCLAS instruments. A brief overview of the methodology is provided in Supplementary Material 53, and corrected results for QCLAS I provided in Table 6. This methodology is not discussed in detail here as it is beyond the scope of this work. Nonetheless, QCLAS I achieved Allan deviations of ~0.4 ‰ at 300 s averaging time for $\delta^{15}\text{N}^{\alpha}$ and $\delta^{15}\text{N}^{\beta}$ at ambient N₂O mole fractions when this correction method was applied by ARI.

At [N₂O] of 1000 ppb, the precision of δ values measured by all analyzers, except CRDS I, significantly improved due to greater signal-to-noise ratios. Whilst the performance of OA-ICOS I was similar to that of CRDS II for $\delta^{15}\text{N}^{\alpha}$ and $\delta^{15}\text{N}^{\beta}$ (0.24‰ and 0.24‰ for CRDS II; 0.28‰ and 0.37‰ for OA-ICOS I at 300 s averaging time), CRDS II displayed the best precision for $\delta^{18}\text{O}$ (0.21‰ at 300 s averaging time). Also notable was the improved performance of the 2018 model (CRDS II) compared to the 2015 model (CRDS I). QCLAS analyzers showed the best 1 s precision for δ values, but beyond 100 s, δ -measurements were still heavily affected by instrumental drift resulting in lower precision, especially for QCLAS I. When the spectral correction method described in Supplementary Material 53 was applied, QCLAS I achieved Allan deviations of ~0.2 ‰ at 300 s averaging time for $\delta^{15}\text{N}^{\alpha}$ and $\delta^{15}\text{N}^{\beta}$ at 1000 ppb N₂O.

At [N₂O] of 10000 ppb all analyzers showed excellent precision, with QCLAS I, II and III outperforming OA-ICOS I for precision of $\delta^{15}\text{N}^{\alpha}$ and $\delta^{15}\text{N}^{\beta}$ (collectively better than 0.10 ‰ at 300 s averaging time for both $\delta^{15}\text{N}^{\alpha}$ and $\delta^{15}\text{N}^{\beta}$). QCLAS II had the best precision for [N₂O] (1.2 ppb at 300 s averaging time). OA-ICOS I and QCLAS III were the only analyzers tested in this study that could be used to measure $\delta^{18}\text{O}$ at 10000 ppb N₂O. OA-ICOS I attained a precision of 0.17 ‰, while QCLAS III attained a precision of 0.48 ‰, both with 300 s averaging time. QCLAS I achieved Allan deviations of ~0.02 – 0.03 ‰ at 300 s averaging time for $\delta^{15}\text{N}^{\alpha}$ and $\delta^{15}\text{N}^{\beta}$ at 10000 ppb N₂O when the spectral correction method (Supplementary Material 53) was applied.

The precision of instruments on [N₂O] measurements at 1000 and 10000 ppb N₂O might not be representative because of small fluctuations in the final gas mixture produced by the MFCs, which were likely amplified due to the small dilution ratios. Therefore, the indicated [N₂O] precisions should be

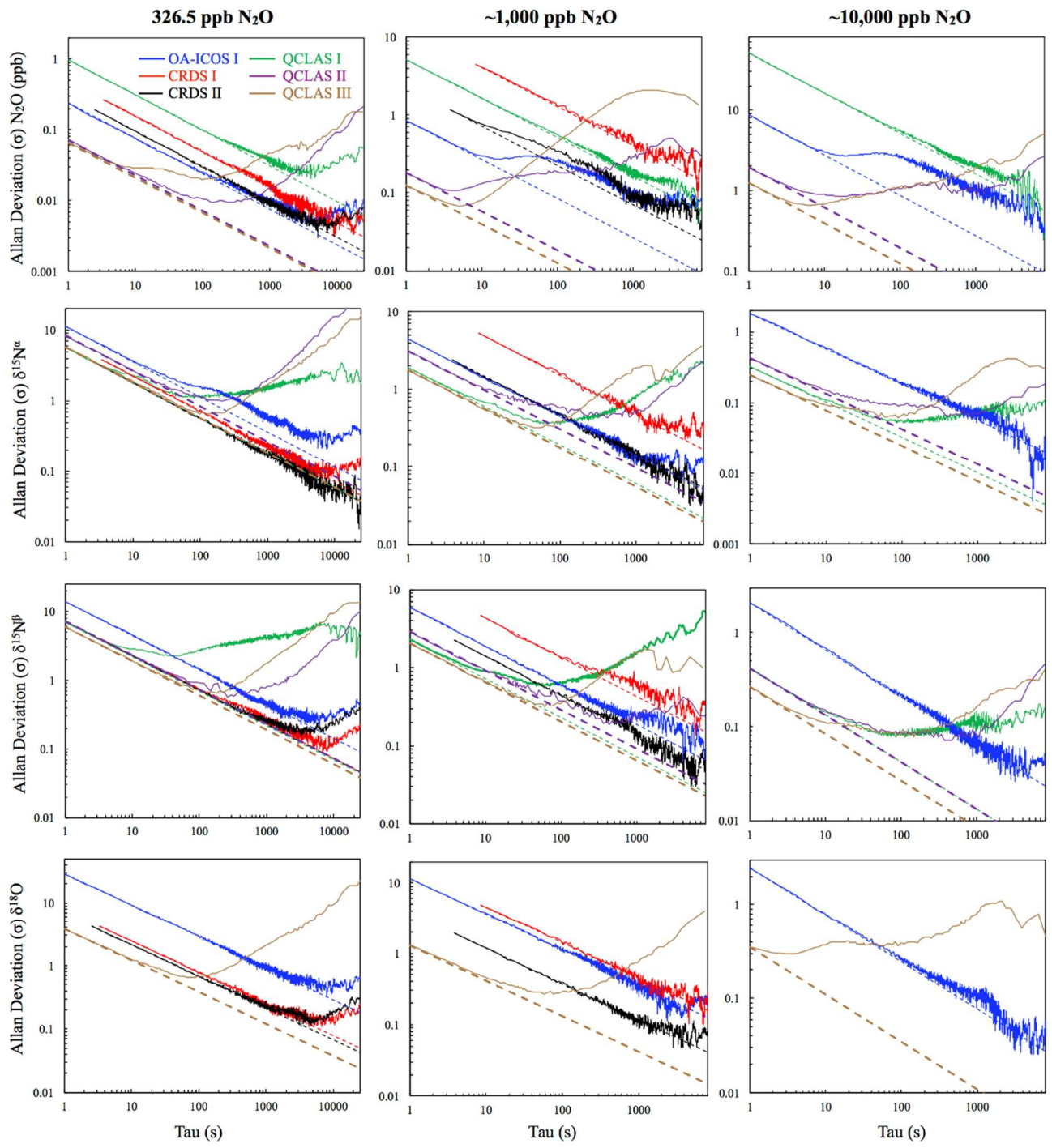
considered as a pessimistic estimate. This was most apparent for the QCLAS and the OA-ICOS analyzers, which showed the highest short-term precision, although this likely applies to all analyzers. Accordingly, the deviation of the Allan variance of mole fraction measurements by QCLAS II and III as well as OA-ICOS I at elevated $[\text{N}_2\text{O}]$ from instrumental white (Gaussian) noise was likely due to uncertainty contributions from MFCs. Therefore, it is likely that the precision of all analyzers for $[\text{N}_2\text{O}]$ measurements is better than shown in Fig. 3 and Table 6. Nonetheless, at 1000 ppb N_2O , QCLAS III showed the best precision for $[\text{N}_2\text{O}]$ ($1.0 \cdot 10^{-1}$ ppb at 300 s averaging time), which was almost one order of magnitude greater than at atmospheric N_2O mole fractions.

Table 6. Key parameters for instrument stability retrieved from Allan variance experiments for $[\text{N}_2\text{O}]$, $\delta^{15}\text{N}^a$, $\delta^{15}\text{N}^b$ and $\delta^{18}\text{O}$: precision (1σ) at 300s and 600s averaging times, and daily drift at various N_2O concentrations. 1σ data refers to Allan deviation (square root of Allan variance).

Instrument	$1\sigma \text{ N}_2\text{O}$ [ppb] (300 s)	$1\sigma \text{ N}_2\text{O}$ [ppb] (600 s)	N_2O drift [(ppb day ⁻¹)]	1σ $\delta^{15}\text{N}^a$ [‰] (300s)	1σ $\delta^{15}\text{N}^a$ [‰] (600s)	$\delta^{15}\text{N}^a$ drift [(‰ day ⁻¹)]	1σ $\delta^{15}\text{N}^b$ [‰] (300s)	1σ $\delta^{15}\text{N}^b$ [‰] (600s)	$\delta^{15}\text{N}^b$ drift [(‰ day ⁻¹)]	$1\sigma \delta^{18}\text{O}$ [‰] (300s)	$1\sigma \delta^{18}\text{O}$ [‰] (600s)	$\delta^{18}\text{O}$ drift [(‰ day ⁻¹)]
326.5 ppb N_2O												
CRDS I	$3.0 \cdot 10^{-2}$	$2.3 \cdot 10^{-2}$	$2.0 \cdot 10^{-2}$	0.41	0.27	0.22	0.45	0.38	0.18	0.46	0.34	0.03
CRDS II	$1.7 \cdot 10^{-2}$	$1.2 \cdot 10^{-2}$	$3.2 \cdot 10^{-2}$	0.32	0.23	$3.5 \cdot 10^{-3}$	0.41	0.31	0.14	0.41	0.28	0.10
OA-ICOS I	$1.7 \cdot 10^{-2}$	$1.3 \cdot 10^{-2}$	$1.5 \cdot 10^{-2}$	1.08	0.82	0.07	0.79	0.52	0.50	1.69	1.14	2.34
QCLAS I	$6.3 \cdot 10^{-2}$	$4.6 \cdot 10^{-2}$	$3.7 \cdot 10^{-2}$	1.24	1.41	6.80	3.45	4.22	15.81	n.d.	n.d.	n.d.
QCLAS I ^a	$2.1 \cdot 10^{-2}$	$2.4 \cdot 10^{-2}$	0.12	0.39	0.37	0.71	0.42	0.55	4.83	n.d.	n.d.	n.d.
QCLAS II	$9.5 \cdot 10^{-3}$	$1.1 \cdot 10^{-2}$	1.00	1.08	1.44	0.20	0.60	0.72	0.05	n.d.	n.d.	n.d.
QCLAS III	$2.5 \cdot 10^{-2}$	$3.6 \cdot 10^{-2}$	0.75	0.81	1.23	0.09	0.78	1.22	0.04	0.97	1.51	0.13
~1000 ppb N_2O												
CRDS I	$7.7 \cdot 10^{-1}$	$6.0 \cdot 10^{-1}$	0.29	0.88	0.67	0.67	0.89	0.73	1.39	0.81	0.67	0.32
CRDS II	$2.1 \cdot 10^{-1}$	$1.3 \cdot 10^{-1}$	0.54	0.24	0.20	0.36	0.24	0.18	0.23	0.21	0.13	0.86
OA-ICOS I	$1.7 \cdot 10^{-1}$	$1.2 \cdot 10^{-1}$	1.02	0.28	0.23	0.93	0.37	0.25	0.54	0.67	0.44	0.15
QCLAS I	$3.3 \cdot 10^{-1}$	$2.4 \cdot 10^{-1}$	1.03	0.47	0.61	7.25	0.83	1.11	8.01	n.d.	n.d.	n.d.
QCLAS I ^a	$1.4 \cdot 10^{-1}$	$1.0 \cdot 10^{-1}$	$1.2 \cdot 10^{-3}$	0.19	0.23	0.61	0.20	0.22	0.11	n.d.	n.d.	n.d.
QCLAS II	$2.0 \cdot 10^{-1}$	$2.4 \cdot 10^{-1}$	4.11	0.52	0.49	0.04	0.22	0.19	$4.3 \cdot 10^{-3}$	n.d.	n.d.	n.d.
QCLAS III	$1.0 \cdot 10^{-1}$	$1.6 \cdot 10^0$	1.61	0.81	1.37	0.06	0.72	1.18	0.03	0.38	0.54	0.05
~10000 ppb N_2O												
OA-ICOS I	$1.7 \cdot 10^0$	$1.3 \cdot 10^{-3}$	1.30	0.12	0.10	0.12	0.15	0.09	0.54	0.17	0.12	0.35
QCLAS I	$3.3 \cdot 10^0$	$2.3 \cdot 10^0$	3.74	0.06	0.07	1.09	0.09	0.11	0.82	n.d.	n.d.	n.d.
QCLAS I ^a	$4.6 \cdot 10^{-1}$	$3.8 \cdot 10^{-1}$	0.10	0.03	0.03	0.02	0.02	0.03	0.10	n.d.	n.d.	n.d.
QCLAS II	$1.2 \cdot 10^0$	$9.9 \cdot 10^{-1}$	35.1	0.09	0.07	$2.9 \cdot 10^{-3}$	0.09	0.08	$7.0 \cdot 10^{-3}$	n.d.	n.d.	n.d.
QCLAS III	$1.3 \cdot 10^0$	$1.6 \cdot 10^0$	66.1	0.10	0.17	$3.4 \cdot 10^{-3}$	0.10	0.13	$5.8 \cdot 10^{-3}$	0.48	0.65	$2.8 \cdot 10^{-3}$

^{a)} Data re-processed by Aerodyne Research Inc. technicians using an automatic spectral correction method. This method corrects data that was influenced by changing baseline structure. Further information on this method is provided in Supplementary Material [S3](#).

n.d. not determined



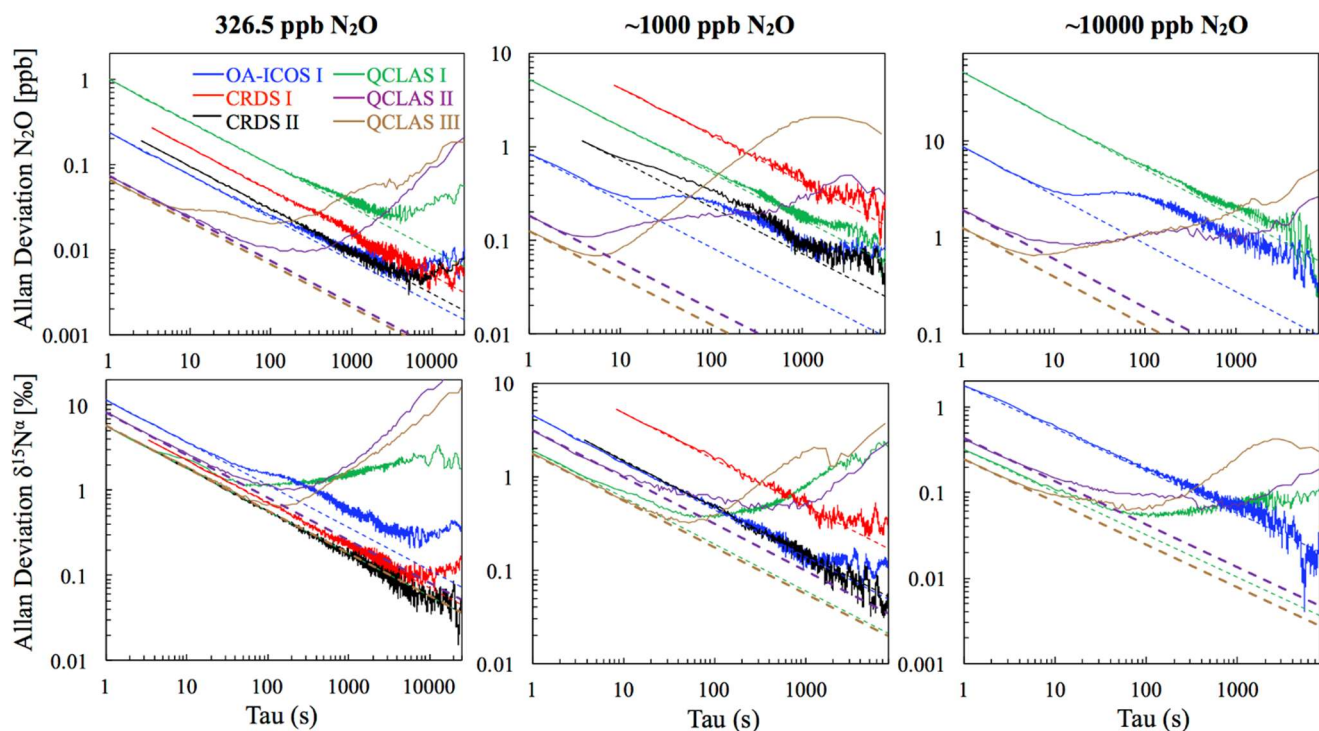
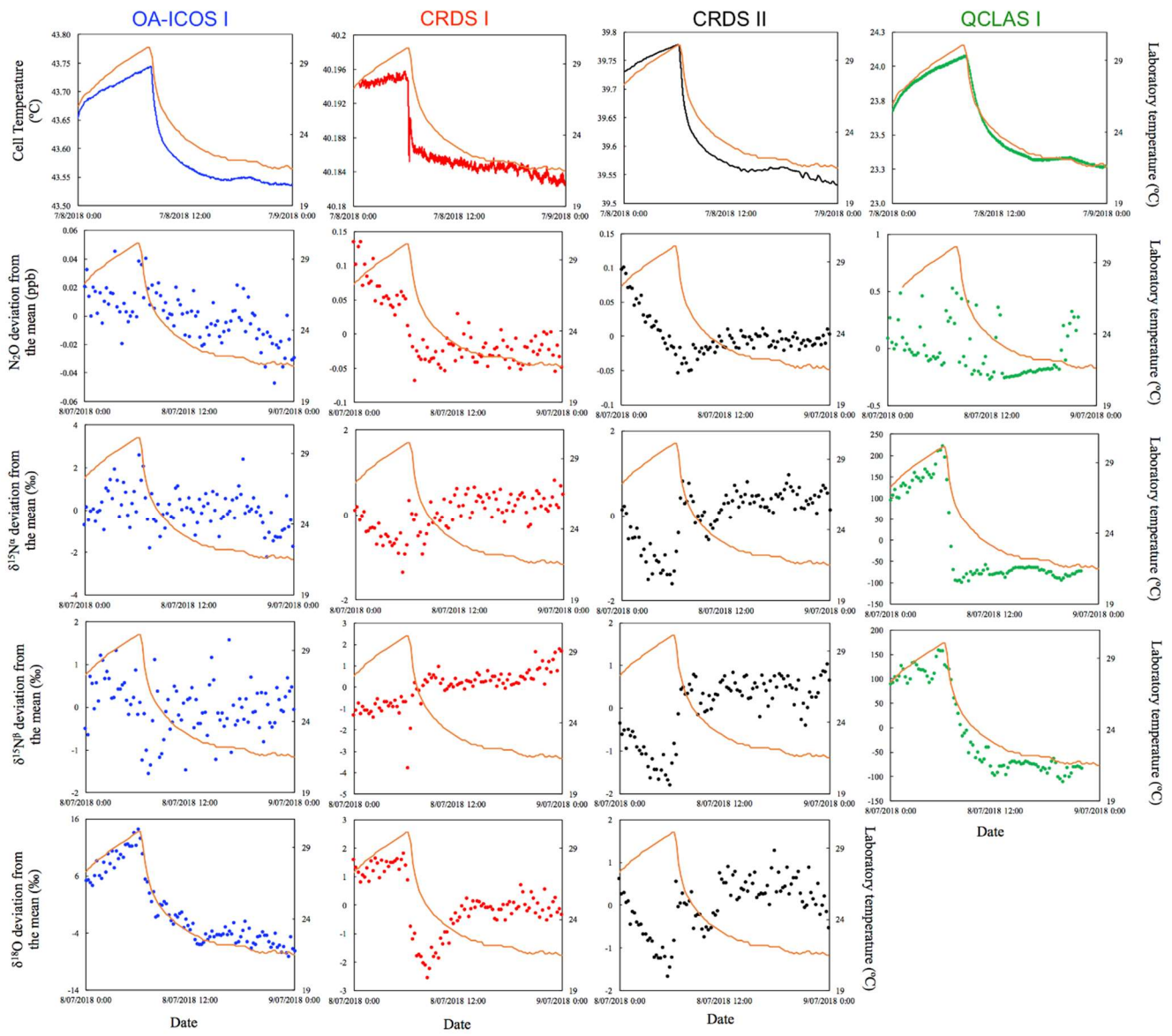


Fig. 3. Allan deviation (square root of Allan Variance) plots for the OA-ICOS I (blue), CRDS I (red), CRDS II (black), QCLAS I (green), QCLAS II (purple) and QCLAS III (brown) at different N_2O mole fractions (~327, 1000 and 10000 ppb). The dashed lines represent a slope of -0.5 (log-log scale) and indicate the expected behavior for Gaussian white noise in each analyzer. The Allan deviations of all analyzers tested were reproducible on three separate occasions prior to the test results presented here. Allan deviation plots for $\delta^{15}\text{N}^\beta$ and $\delta^{18}\text{O}$ are provided in Supplementary Material 4 (Fig. S4-1).

3.2 Temperature effects

All instruments tested showed significant effects, albeit to varying degrees, on their measurements due to the change in laboratory temperature (Figs. 4 and S4-2). The OA-ICOS I displayed no clear temperature effects for $[\text{N}_2\text{O}]$, $\delta^{15}\text{N}^\alpha$ and $\delta^{15}\text{N}^\beta$, but displayed a moderate temperature dependence for $\delta^{18}\text{O}$ measurements (up to 14‰ deviation from the mean), with measurement drift closely paralleling the laboratory temperature ($r^2 = 0.78$). Both CRDS instruments displayed smaller shifts in $[\text{N}_2\text{O}]$ (up to 0.14 ppb deviation from the mean), $\delta^{15}\text{N}^\alpha$, $\delta^{15}\text{N}^\beta$ and $\delta^{18}\text{O}$ that occurred particularly when the laboratory temperature had an acute change. QCLAS I showed a strong temperature dependence on $\delta^{15}\text{N}^\alpha$ ($r^2 = 0.85$) and $\delta^{15}\text{N}^\beta$ ($r^2 = 0.96$).



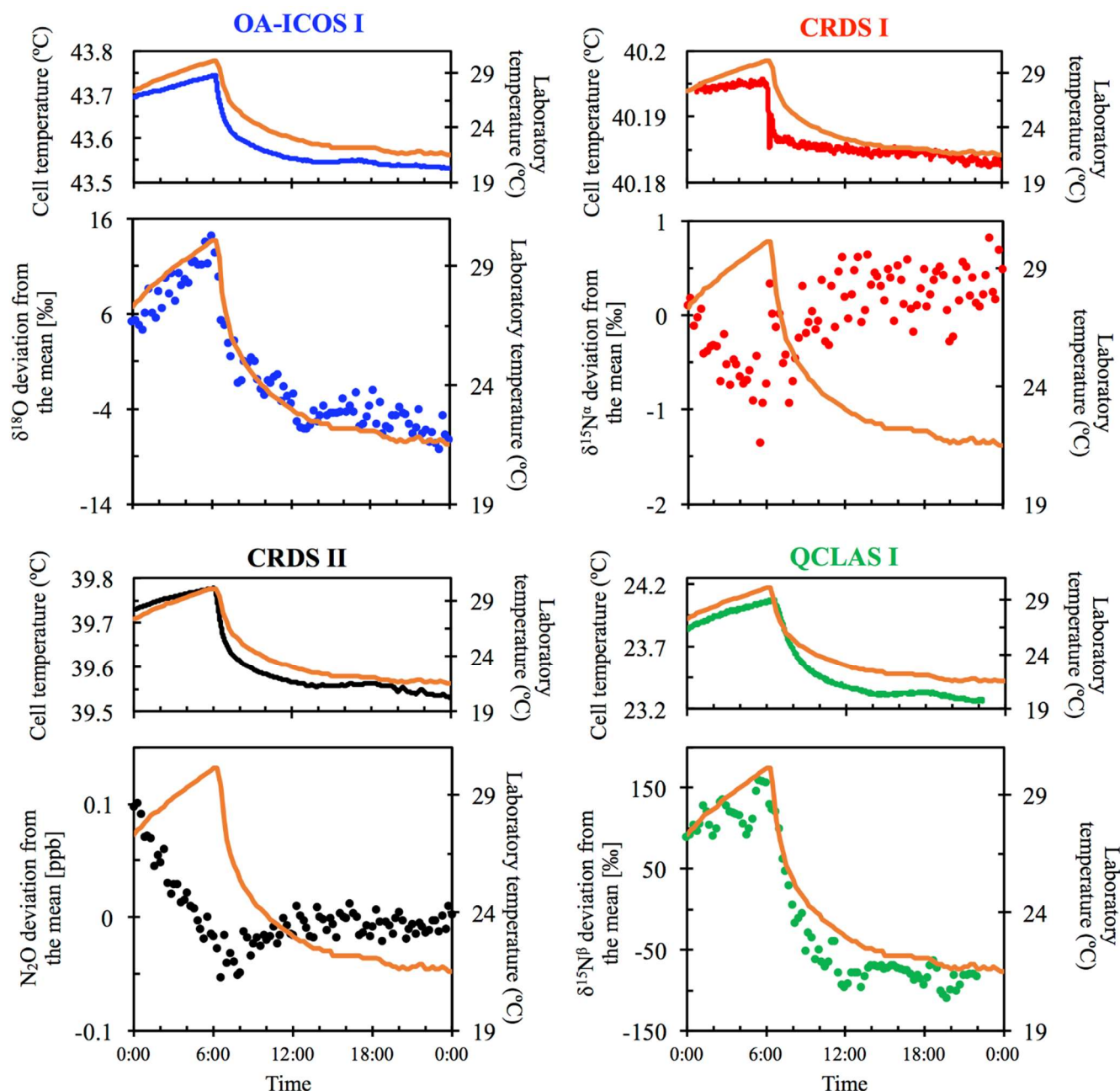


Fig. 4. Examples of the dependency of different measurements on laboratory temperature (°C) for OA-ICOS I (blue), CRDS I (red), CRDS II (black) and QCLAS I (green). The complete dataset is provided in Supplementary Material 4 (Fig. S4-2). Dependency of the measured [N₂O], $\delta^{15}\text{N}^{\alpha}$, $\delta^{15}\text{N}^{\beta}$ and $\delta^{18}\text{O}$ values on laboratory temperature (°C) for OA-ICOS I (blue), CRDS I (red), CRDS II (black) and QCLAS I (green). The laboratory temperature is indicated by a solid orange line and was allowed to vary over time. Cell temperatures for each instrument are also plotted for comparison. The analyzers began acquiring measurements at 00:00 on 8/07/2018, capturing the end of the rising limb of the laboratory temperature. Cell temperatures for each instrument are also plotted for comparison. Results are plotted as the deviation from the mean, without any anchoring to reference gases.

3.3 Repeatability

The best long-term repeatability for δ values was achieved by TREX-QCLAS I with 0.60 ‰ for $\delta^{15}\text{N}^{\alpha}$, 0.37 ‰ for $\delta^{15}\text{N}^{\beta}$ and 0.46 ‰ for $\delta^{18}\text{O}$, even though measurements were taken over a six-month period (Table 7). The best repeatability without preconcentration was achieved by CRDS analyzers with 0.52 –

0.75 ‰ for CRDS II and 0.79 – 0.83 ‰ for CRDS I for all δ values. OA-ICOS I achieved repeatability between 1 – 2 ‰ (1.47, 1.19 and 2.17 ‰ for $\delta^{15}\text{N}^{\alpha}$, $\delta^{15}\text{N}^{\beta}$ and $\delta^{18}\text{O}$, respectively). QCLAS I isotopic measurements attained repeatability of 5.4 and 8.6 ‰ for $\delta^{15}\text{N}^{\alpha}$ and $\delta^{15}\text{N}^{\beta}$, respectively. Short-term repeatability results for 10 repeated 15 min measurements periods over 2.5 h are provided in

5 Supplementary Material [64](#).

Table 7. Summary of the measured $[\text{N}_2\text{O}]$, $\delta^{15}\text{N}^{\alpha}$, $\delta^{15}\text{N}^{\beta}$ and $\delta^{18}\text{O}$ and associated 1σ at 300s averaging times based on repeated measurements of PA1.

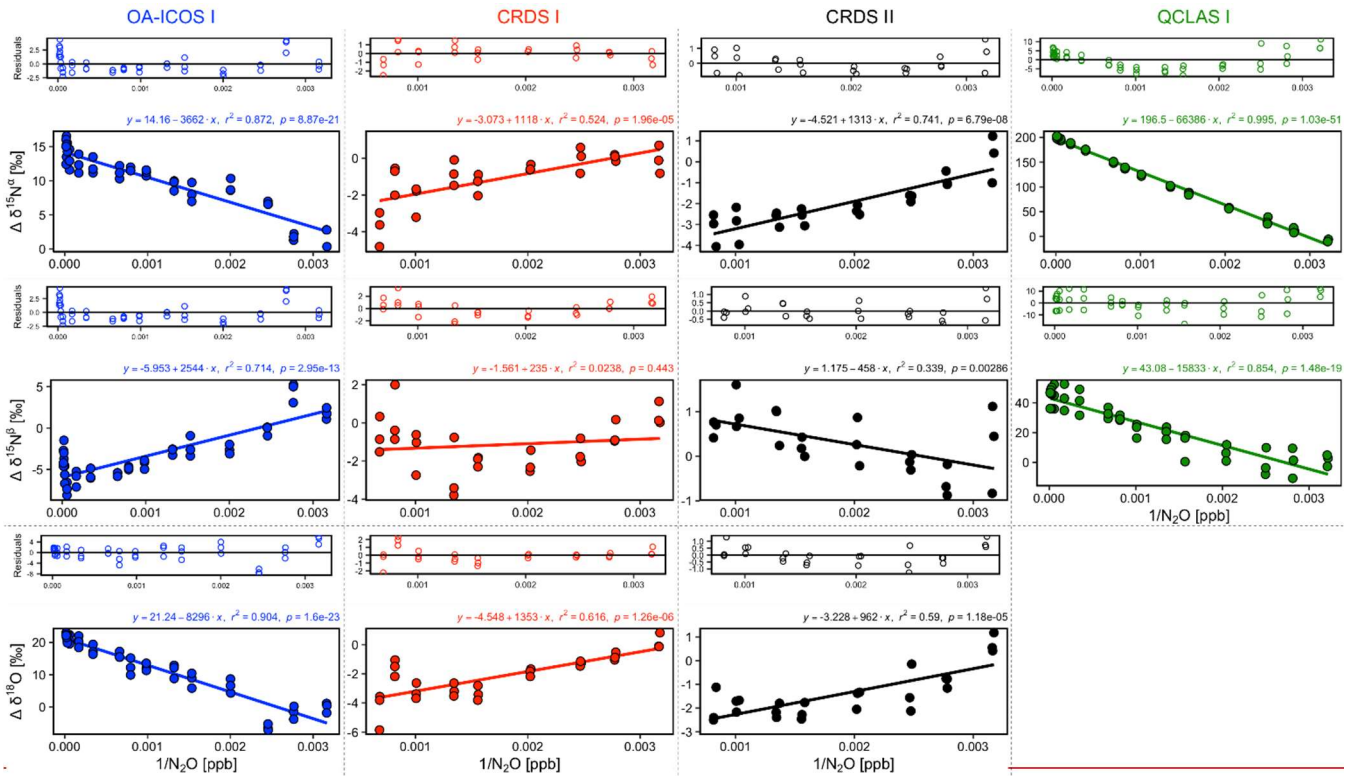
Instrument	n	N_2O [ppb]	1σ N_2O [ppb]	$\delta^{15}\text{N}^{\alpha}$ [‰]	1σ $\delta^{15}\text{N}^{\alpha}$ [‰]	$\delta^{15}\text{N}^{\beta}$ [‰]	1σ $\delta^{15}\text{N}^{\beta}$ [‰]	$\delta^{18}\text{O}$ [‰]	1σ $\delta^{18}\text{O}$ [‰]
CRDS I	22	326.66	0.30	15.86	0.79	-2.30	0.83	44.48	0.81
CRDS II	22	326.72	0.26	15.71	0.52	-2.86	0.64	44.40	0.75
OA-ICOS I	22	326.49	0.07	15.29	1.47	-2.11	1.19	44.01	2.17
QCLAS I	22	326.82	0.16	13.92	5.35	-2.97	8.57	-	-
TREX-QCLAS I	28	326.70	1.29	15.72	0.60	-2.82	0.37	44.31	0.46
Empa-assigned values	3	326.51	0.06	15.81	0.07	-3.31	0.004	44.72	0.04

3.4 Dependence of isotopic measurements on N_2O mole fraction

10 There was an offset in measured δ values resulting from the change in $[\text{N}_2\text{O}]$ introduced to the analyzers (Figs. 5 and [S4-3](#)). A linear relationship between $\Delta\delta^{15}\text{N}^{\alpha,\beta}$ and $\Delta\delta^{18}\text{O}$ values with $[1/\text{N}_2\text{O}]$ was observed across all analyzers tested, ~~which is characteristic of optical analyzers calibrated using a δ calibration scheme (Griffith et al., 2012; Griffith, 2018).~~ However, examination of the residuals from the linear regression revealed varying degrees of residual curvature, highlighting that further non-linear terms

15 would be required to adequately describe, and correct for, this mole fraction dependence ~~(see Griffith et al., 2012).~~ Repeated analysis of $[\text{N}_2\text{O}]$ dependencies on consecutive days showed similar trends, indicating that the structure of non-linear effects might be stable over short periods of time. Nevertheless, there were small variabilities in δ values at a given N_2O mole fraction, which could be due to the inherent uncertainty of the measurement and/or day-to-day variations in the mole fraction dependence. The

20 standard deviation of individual 5 min averages of $\delta^{15}\text{N}^{\alpha,\beta}$ and $\delta^{18}\text{O}$ also varied according to the $[\text{N}_2\text{O}]$ measured by each analyzer due to variations in the signal:noise ratio (Supplementary Material [75](#)).



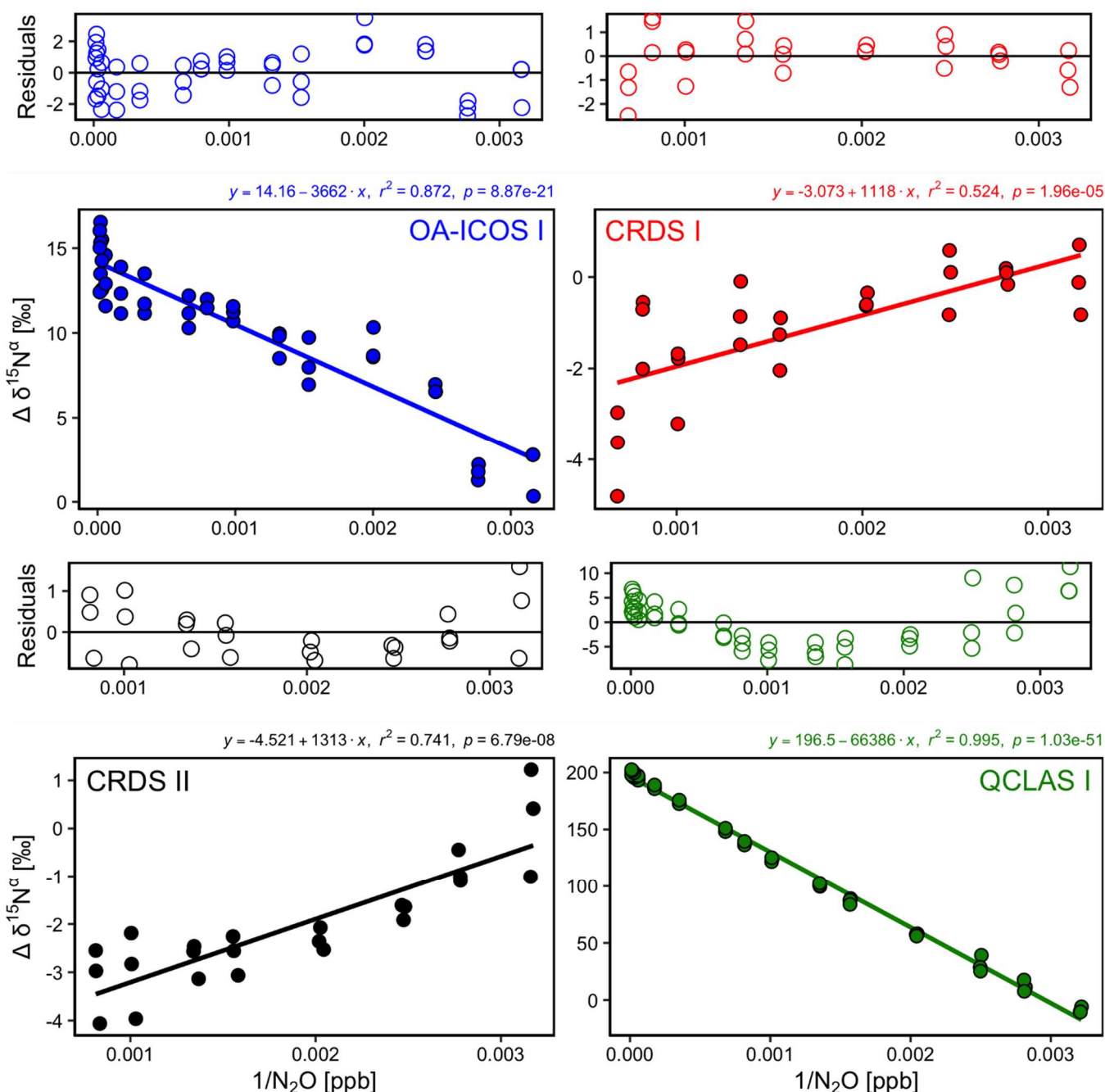


Fig. 5. Deviations of the measured $\delta^{15}\text{N}^\alpha$, $\delta^{15}\text{N}^\beta$ and $\delta^{18}\text{O}$ values according to $1/[\text{N}_2\text{O}]$ for the OA-ICOS I (blue), CRDS I (red), CRDS II (black) and QCLAS I (green). Measurements span the manufacturer-specified operational ranges of the analyzers. The experiment was repeated on three separate days. A linear regression is indicated by the solid line, and a residual plot is provided above each plot. Individual linear equations, coefficients of determination (r^2) and p -values are indicated above each plot. The remaining plots for $\delta^{15}\text{N}^\beta$ and $\delta^{18}\text{O}$ are provided in Supplementary Material 4 (Fig. S4-3).

3.5 Gas matrix effects (O_2 and Ar)

10 3.5.1 Gas matrix effects at ambient N_2O mole fractions

With the exception of TREX-QCLAS I, all instruments displayed strong O_2 dependencies for $[\text{N}_2\text{O}]$ and δ values (Figs. 6 and S4-4). For these instruments, linear regressions best described the offset of measured $[\text{N}_2\text{O}]$ and δ values resulting from the change in O_2 composition of the matrix gas. Importantly, CRDS I

and II displayed different degrees of O₂ interference on [N₂O] and δ values, suggesting that these dependencies were either analyzer-specific or differences were due to hardware/software modifications between different production years. Preconcentration prior to analysis, as performed in TREX-QCLAS I, eliminated O₂ dependencies as the gas matrix was normalized to synthetic air (20.5 % O₂).

5

The change in Ar composition of the matrix gas caused minor, yet measurable, interferences on [N₂O] and δ measurements (~~Fig. 7~~Fig. S4-5). The range investigated was between approximately 0 % and 0.95 % Ar, as anticipated for an N₂O in synthetic air (no Ar) reference gas versus a whole air (with Ar) sample gas. The effects observed for 0.95 % change in [Ar] were significantly smaller than that observed for O₂, but might extend to a similar range for sample and reference gases with higher differences in [Ar]., and as such the effects were significantly smaller than that observed for O₂. The interference effects were found to be best described by second-order polynomial functions, though we expect that a linear fit would serve equally well if a larger change in [Ar] wider range of effects were was investigated. ~~Whilst Although~~ most functions to describe the dependence on Ar across all instruments were statistically significant ($p < 0.05$), maximum effects ~~were typically only one-tenth of maximum O₂ effects, and~~ did not transgress the repeatability (1σ) of the Anchor gas measurements. TREX-QCLAS I measurements were not impaired by gas matrix effects.

10

15

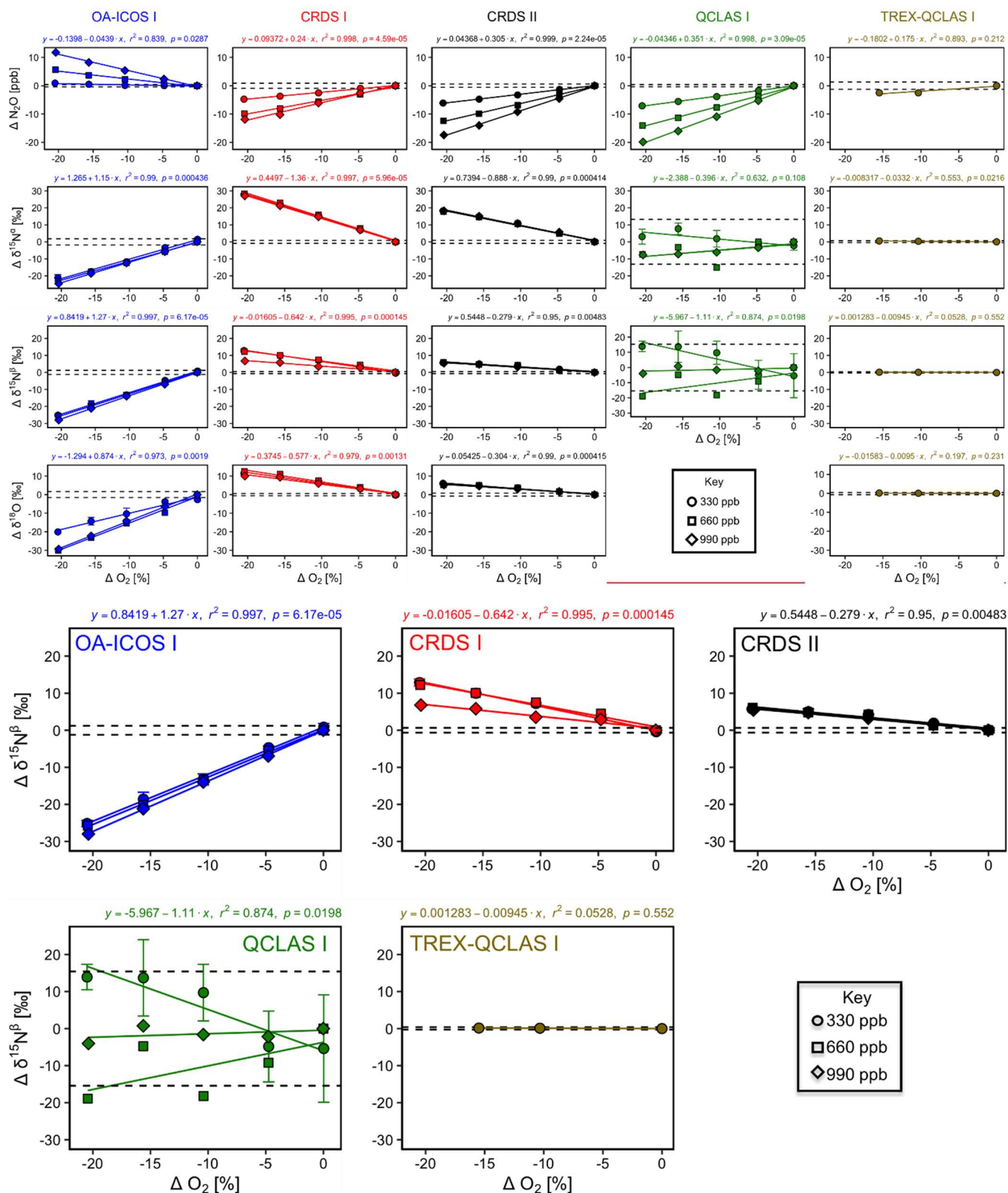


Fig. 6. Deviations of the measured $[\text{N}_2\text{O}]$, $\delta^{15}\text{N}^\alpha$, $\delta^{15}\text{N}^\beta$ and $\delta^{18}\text{O}$ values according to ΔO_2 (%) at different N_2O mole fractions (330, 660 and 990 ppb) for the OA-ICOS I (blue), CRDS I (red), CRDS II (black), QCLAS I (green) and TREX-QCLAS I (brown). The remaining plots for $[\text{N}_2\text{O}]$, $\delta^{15}\text{N}^\alpha$ and $\delta^{18}\text{O}$ are provided in Supplementary Material 4 (Fig. S4-4). The standard deviation of the Anchor gas ($\pm 1\sigma$) is indicated by dashed lines. Data points represent the mean and standard deviation (1σ) of triplicate measurements. Dependencies are best-described using linear regression, which are indicated by a solid line. Individual equations, coefficients of determination (r^2) and p -values are indicated above each plot for the 330 ppb N_2O data only.

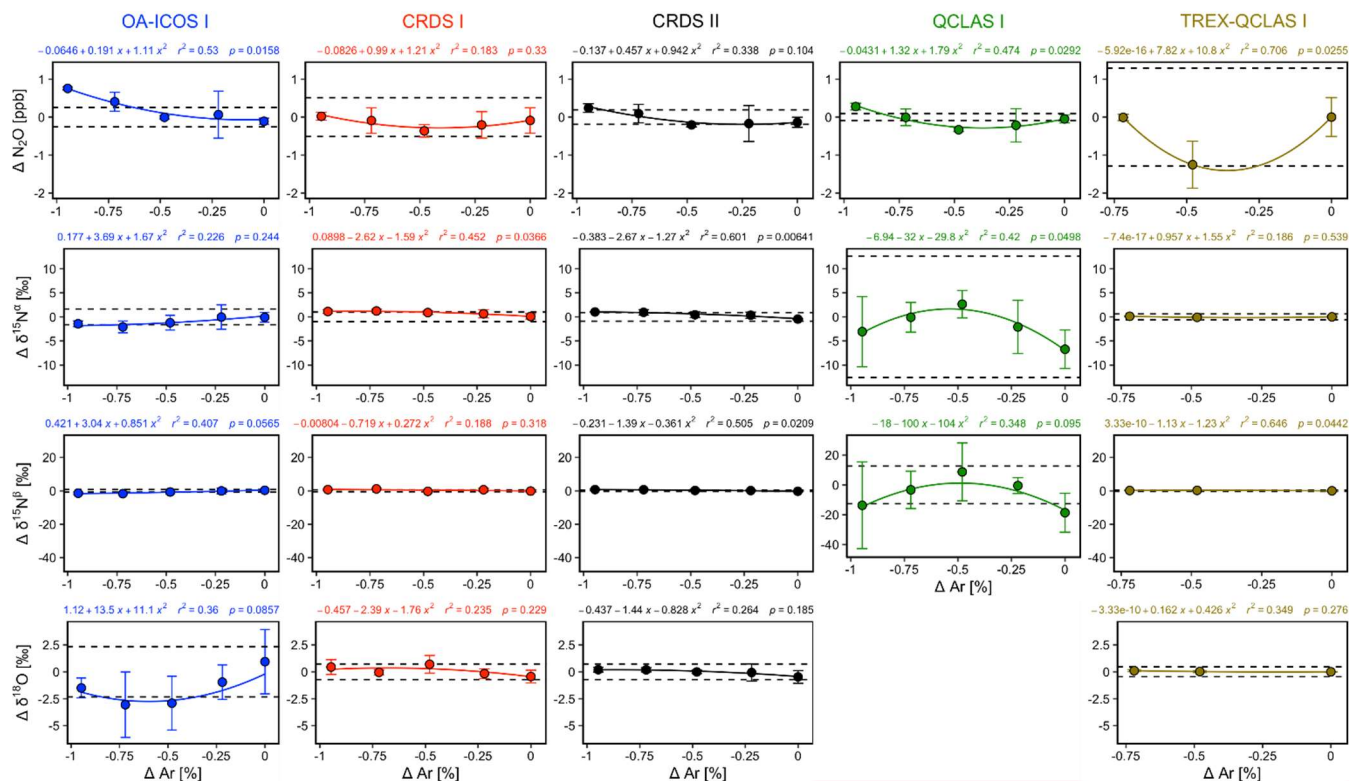


Fig. 7. Deviations of the measured $[\text{N}_2\text{O}]$, $\delta^{15}\text{N}^\alpha$, $\delta^{15}\text{N}^\beta$ and $\delta^{18}\text{O}$ values according to ΔAr (%) for the OA-ICOS I (blue), CRDS I (red), CRDS II (black), QCLAS I (green) and TREX-QCLAS I (brown). Data points represent the mean and standard deviation (1σ) of triplicate measurements. Dependencies are best described by polynomial fits, which are indicated by solid lines. Individual equations, coefficients of determination (r^2) and p -values are indicated above each plot.

3.5.2 Continuity of gas matrix corrections at higher N_2O mole fractions

When mole fractions of 660 and 990 ppb N_2O were measured by the laser spectrometers, O_2 interference effects on $[\text{N}_2\text{O}]$ and δ values were well-described using linear regression, albeit with different slopes to those obtained for 330 ppb N_2O (Figs. 6 and S4-4; [Supplementary Material 8 Table 8](#)).

Table 8. Summary of regression slopes and coefficients of determination (r^2) for O_2 interferences performed at different N_2O mole fractions (330, 660 and 990 ppb) for OA-ICOS I, CRDS I and II, and QCLAS I.

ΔO_2 [%]	Co-measured N_2O [ppb]	OA-ICOS I		CRDS I		CRDS II		QCLAS I	
		Slope	r^2	Slope	r^2	Slope	r^2	Slope	r^2
N_2O [ppb]	330	-0.044	0.84	0.24	1.00	0.305	1.00	0.351	1.00
	660	-0.273	0.98	0.478	0.99	0.608	1.00	0.690	1.00
	990	-0.570	0.99	0.61	0.99	0.859	1.00	0.979	1.00
$\delta^{15}\text{N}^\alpha$ [‰]	330	1.146	0.99	-1.364	1.00	-0.888	0.99	n.s.	n.s.

	660	1.116	1.00	-1.387	1.00	-0.874	0.99	n.s.	n.s.
	990	1.204	1.00	-1.326	1.00	-0.891	0.99	0.374	0.90
$\delta^{15}\text{N}[\text{‰}]$	330	1.270	1.00	-0.642	1.00	-0.279	0.95	-1.111	0.87
	660	1.282	1.00	-0.580	0.98	-0.303	0.96	n.s.	n.s.
	990	1.361	1.00	-0.319	0.96	-0.273	0.99	n.s.	n.s.
$\delta^{18}\text{O}[\text{‰}]$	330	0.874	0.97	-0.577	0.98	-0.304	0.99	n.d.	n.d.
	660	1.419	0.99	-0.621	0.98	-0.267	0.94	n.d.	n.d.
	990	1.446	1.00	-0.507	0.97	-0.256	0.98	n.d.	n.d.

n.d. not determined

n.s. not statistically significant at $p < 0.05$

We could not adequately predict the nature in which the slopes of the interference effects scaled with N_2O mole fractions. Overall, this suggests that interference effects were analyzer-specific and varied according to instrumental-specific parameters, rather than due to *bona fide* scaling of the pressure broadening effect. Therefore, to account for combined effects of $[\text{O}_2]$ and $[\text{N}_2\text{O}]$ changes on measurements, a user would be required to perform a series of laboratory tests across the range of expected $[\text{O}_2]$ and $[\text{N}_2\text{O}]$. In an exemplary approach, we applied a series of empirical equations (Eqs. 5 – 6) to predict the offset of measured $[\text{N}_2\text{O}]$ and δ values caused by changes in $[\text{O}_2]$ as a function of $[\text{N}_2\text{O}]$ introduced to the analyzers in this study:

$$\Delta[\text{N}_2\text{O}]_{\text{meas,mix}}(\Delta[\text{O}_2]_A, [\text{N}_2\text{O}]_{\text{exp,mix}}) = (A \cdot [\text{N}_2\text{O}]_{\text{exp,mix}}^2 + B \cdot [\text{N}_2\text{O}]_{\text{exp,mix}}) \cdot \Delta[\text{O}_2]_A \quad (5)$$

$$\Delta\delta_{\text{meas,mix}}(\Delta[\text{O}_2]_A, [\text{N}_2\text{O}]_{\text{exp,mix}}) = (a \cdot [\text{N}_2\text{O}]_{\text{exp,mix}}^2 + b \cdot [\text{N}_2\text{O}]_{\text{exp,mix}} + c) \cdot \Delta[\text{O}_2]_A \quad (6)$$

where $\Delta[\text{N}_2\text{O}]_{\text{meas,mix}}$ and $\Delta\delta_{\text{meas,mix}}$ are the measured offsets on $[\text{N}_2\text{O}]$ and δ values for the gas mixtures introduced to the analyzers as reported in Sect. 3.5.1, respectively; $\Delta[\text{O}_2]_A$ is the difference in O_2 mole fraction between the gas mixture and Anchor gas as reported in Sect. 3.5.1; $[\text{N}_2\text{O}]_{\text{exp,mix}}$ is the expected $[\text{N}_2\text{O}]$ of gas mixtures introduced to the analyzer, calculated based on gas flows and cylinder compositions of Gases 1, 2 and 3 as reported in Sect. 2.4.5; A and B, and a, b and c are analyzer-specific constants.

Using Eqs. (5) and (6) to fit values for the constants A and B for $\Delta[\text{N}_2\text{O}]_{\text{meas,mix}}$, and a, b and c for $\Delta\delta_{\text{meas,mix}}$ resulted in a total of 11 analyzer-specific values (Supplementary Material [86](#)). With gas-specific constants established, interferences on $[\text{N}_2\text{O}]$ and δ measurements for a sample gas G for a given analyzer can be corrected using Eqs. (7–8):

$$[\text{N}_2\text{O}]_{\text{mc,G}} = \frac{-(1+B\Delta[\text{O}_2]_G) + \sqrt{(1+B\Delta[\text{O}_2]_G)^2 + 4 \cdot A \cdot \Delta[\text{O}_2]_G \cdot [\text{N}_2\text{O}]_{\text{meas,G}}}}{2 \cdot A \cdot \Delta[\text{O}_2]_G} \quad (7)$$

$$\delta_{\text{mc,G}} = \delta_{\text{meas,G}} - (a \cdot [\text{N}_2\text{O}]_{\text{mc,G}}^2 + b \cdot [\text{N}_2\text{O}]_{\text{mc,G}} + c) \cdot \Delta[\text{O}_2]_G \quad (8)$$

where $[N_2O]_{mc,G}$ and $\delta_{mc,G}$ are the matrix-corrected $[N_2O]$ and δ values of sample gas G, respectively; $\Delta[O_2]_G$ is the difference in O_2 mole fraction between sample gas G and reference gases. Correction using Eqs. (7–8) removes the O_2 effect to a degree that corrected measurements from Sect. 3.5.1 are typically within the uncertainty bounds of the anchor (Supplementary Material [86](#)).

5

Although Ar effects seemingly scaled with increased N_2O mole fractions (~~not shown in Fig. 7 for clarity~~), we did not derive scaling coefficients for Ar because the derived Ar correction equations at 330, 660 and 990 ppb N_2O were typically not statistically significant at $p < 0.05$. These interferences also did not always exceed the repeatability of Anchor gas measurements. ~~Although we could have tested for effects for [Ar] changes greater than 0.95%, we limited our experiments to [Ar] expected in tropospheric samples. While the effects could be more fully investigated with higher levels of Ar, we limited the investigated to Ar levels close to ambient conditions.~~

10

3.6 Trace gas effects (H_2O , CO_2 , CH_4 and CO)

3.6.1 Trace gas effects at ambient N_2O mole fractions

15

The apparent offset of $[N_2O]$ and δ values resulting from the change in CO_2 composition of the matrix gas were best described by linear functions (Figs. [7](#) and [S4-68](#)). OA-ICOS I exhibited discrete and well-defined linear interference effects of CO_2 on $[N_2O]$, $\delta^{15}N^{\alpha}$, $\delta^{15}N^{\beta}$ and $\delta^{18}O$ (all $r^2 > 0.95$), likely due to crosstalk between CO_2 absorption lines situated near 2192.46 cm^{-1} and 2192.33 cm^{-1} . Both CRDS instruments showed CO_2 interference effects of smaller magnitude for $[N_2O]$, $\delta^{15}N^{\alpha}$ and $\delta^{18}O$, presumably due to CO_2 absorption lines at 2196.21 cm^{-1} , 2195.72 cm^{-1} and 2196.02 cm^{-1} . QCLAS I displayed less well-defined CO_2 interference effects for $\delta^{15}N^{\beta}$, which was possibly due to several overlapping absorption lines of CO_2 located near 2187.85 cm^{-1} . All linear functions derived for the TREX-QCLAS I were not statistically significant at $p < 0.05$. As shown in Figs. [7](#) and [S4-68](#), the NaOH trap was effective in removing the CO_2 effect (if present) across the mole fraction ranges tested for all instruments.

20

25

Similarly, CH_4 effects on apparent $[N_2O]$ and δ values were well-described by linear functions (Figs. [8](#) and [S4-7-9](#)). The largest effects were for CRDS I and II, which both displayed strong CH_4 dependencies for $\delta^{15}N^{\alpha}$ and $\delta^{18}O$ of similar magnitude. This might be due to crosstalk of $^{14}N^{15}N^{16}O$ and $^{14}N^{14}N^{18}O$ absorption lines with the respective CH_4 lines located at 2195.76 cm^{-1} and 2195.95 cm^{-1} . For OA-ICOS I, minor CH_4 effects were observed for $\delta^{15}N^{\beta}$, due to absorption line overlap at 2192.33 cm^{-1} . QCLAS I did not display any CH_4 interference effect over the tested $[CH_4]$ range. Linear functions derived for the TREX-QCLAS I were not statistically significant at $p < 0.05$. The similarity between the $[N_2O]$ dependencies on CH_4 mole fractions for OA-ICOS I, CRDS I, II and QCLAS I suggests that the apparent

30

effects may be due to small fluctuations in the gas mixtures produced by the MFCs, rather than a discrete spectral interference effect.

The CRDS analyzers showed minor interference effects for $\delta^{15}\text{N}^{\alpha}$ and $\delta^{15}\text{N}^{\beta}$ on [CO] (0.14 – 2.14 ppm) (Fig. [S4-8](#)), likely due to crosstalk with CO absorption lines located at 2195.69 cm^{-1} and 2195.83 cm^{-1} . The magnitude of these effects was similar for both models. QCLAS I displayed interference effects for $\delta^{15}\text{N}^{\alpha}$ and $\delta^{15}\text{N}^{\beta}$ caused by a CO absorption line located near 2187.9 cm^{-1} , although this effect did not exceed the repeatability of the Anchor gas (containing no CO) over the measurement range. The effects of [CO] on δ values acquired using OA-ICOS I and TREX-QCLAS I were not statistically significant at $p < 0.05$. Similar to CH_4 , the resemblance of [CO] effects on $[\text{N}_2\text{O}]$ measurements for OA-ICOS I, CRDS I, II and QCLAS I suggests that the apparent effects may be due to inaccuracies in the dynamic dilution process, rather than a discrete spectral interference effect. ~~As shown in Fig. 10,~~ the Sofnocat trap was effective in removing CO (if present) across the mole fraction ranges tested for all instruments.

OA-ICOS I exhibited large effects of $[\text{H}_2\text{O}]$ (0 – 13800 ppm) on $\delta^{15}\text{N}^{\beta}$ (up to -10 ‰) and $\delta^{18}\text{O}$ (up to -15 ‰), and minor dependencies for $\delta^{15}\text{N}^{\alpha}$ (up to 4 ‰) and $[\text{N}_2\text{O}]$ (up to 1 ppb) across the range tested (Fig. [S4-9-11](#)). For QCLAS I, the H_2O effect was largest for $\delta^{15}\text{N}^{\alpha}$ (up to 20 ‰), whilst minor effects for $[\text{N}_2\text{O}]$ (up to 2 ppb) were observed in relation to the Anchor gas (no H_2O). In contrast, both CRDS instruments showed no significant effects across the range tested, which is attributable to the installation of permeation dryers inside the analyzers by the manufacturer.

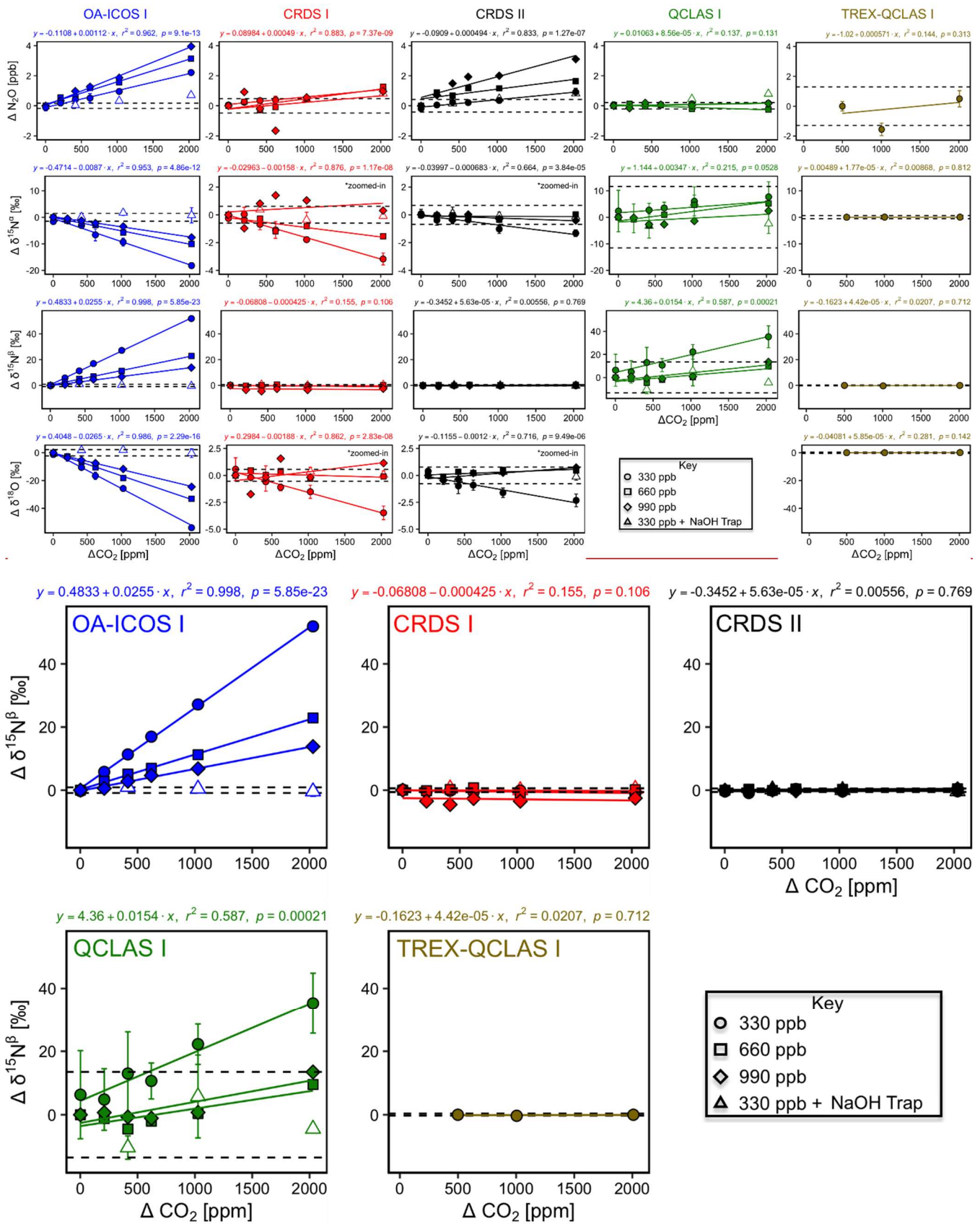
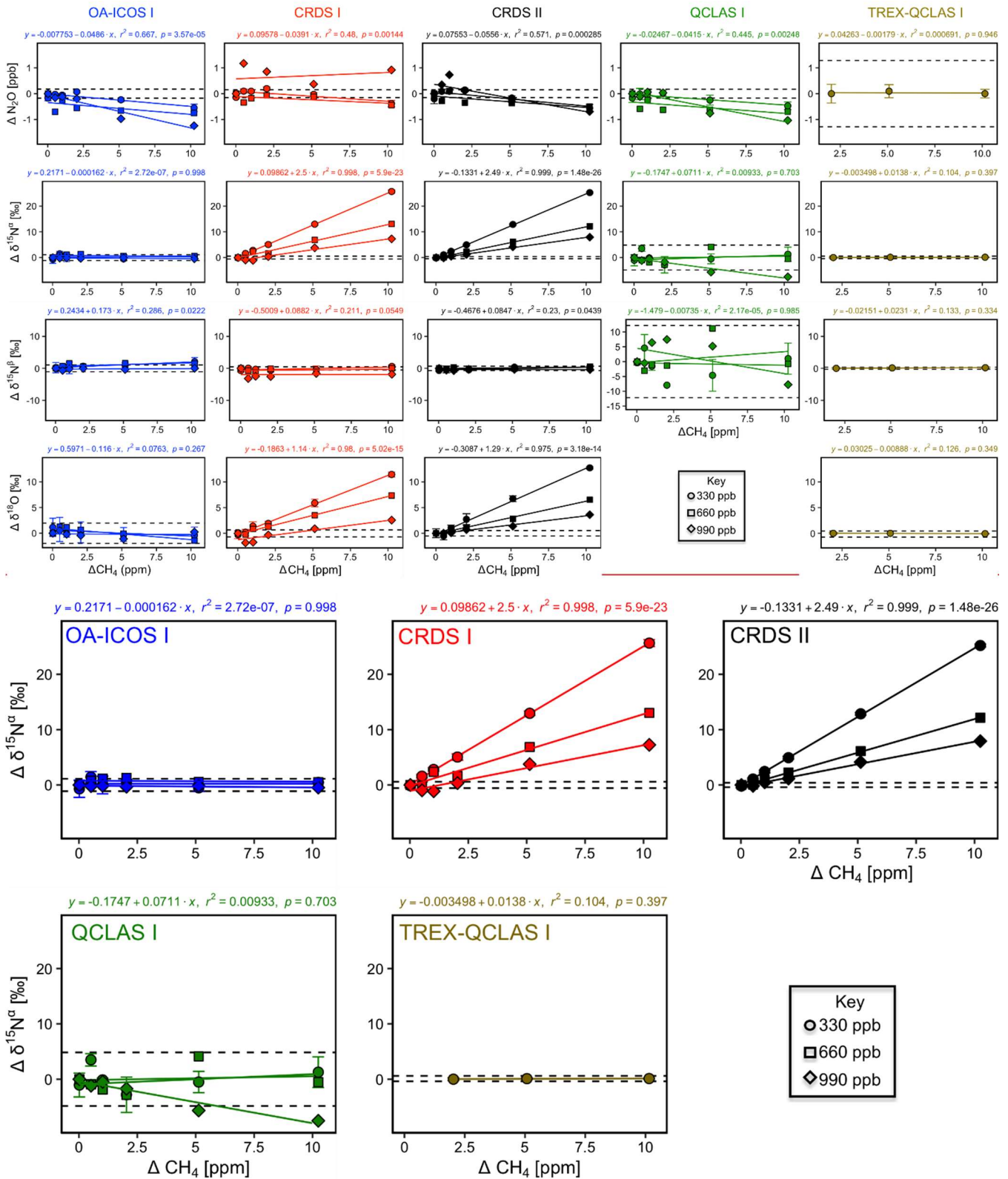


Fig. 78. Deviations of the measured $[\text{N}_2\text{O}]$, $\delta^{15}\text{N}^\alpha$, $\delta^{15}\text{N}^\beta$ and $\delta^{18}\text{O}$ values according to ΔCO_2 (ppm) at different N_2O mole fractions (330, 660 and 990 ppb) for the OA-ICOS I (blue), CRDS I (red), CRDS II (black), QCLAS I (green) and TREX-QCLAS I (brown). The remaining plots for $[\text{N}_2\text{O}]$, $\delta^{15}\text{N}^\alpha$ and $\delta^{18}\text{O}$ are provided in Supplementary Material 4 (Fig. S4-6). The standard deviation of the Anchor gas ($\pm 1\sigma$) is indicated by dashed lines. Data points represent the mean and standard deviation (1σ) of triplicate measurements. Dependencies are best-described by linear fits, which are indicated by solid lines.

Individual equations, coefficients of determination (r^2) and p -values are indicated above each plot for the 330 ppb N₂O data only.



5 **Fig. 89.** Deviations of the measured [N₂O], $\delta^{15}\text{N}^\alpha$, $\delta^{15}\text{N}^\beta$ and $\delta^{18}\text{O}$ values according to ΔCH_4 (ppm) at different N₂O mole fractions (330, 660 and 990 ppb) for the OA-ICOS I (blue), CRDS I (red), CRDS II (black), QCLAS I (green) and TREX-QCLAS I (brown). The remaining plots for [N₂O], $\delta^{15}\text{N}^\beta$ and $\delta^{18}\text{O}$ are provided in Supplementary Material 4 (Fig. S4-7). Data points represent the mean and standard deviation (1σ) of triplicate measurements. Dependencies are best-described by linear fits, which are indicated by solid lines. Individual equations, coefficients of determination (r^2) and p -values are indicated above each plot for the 330 ppb N₂O data only.

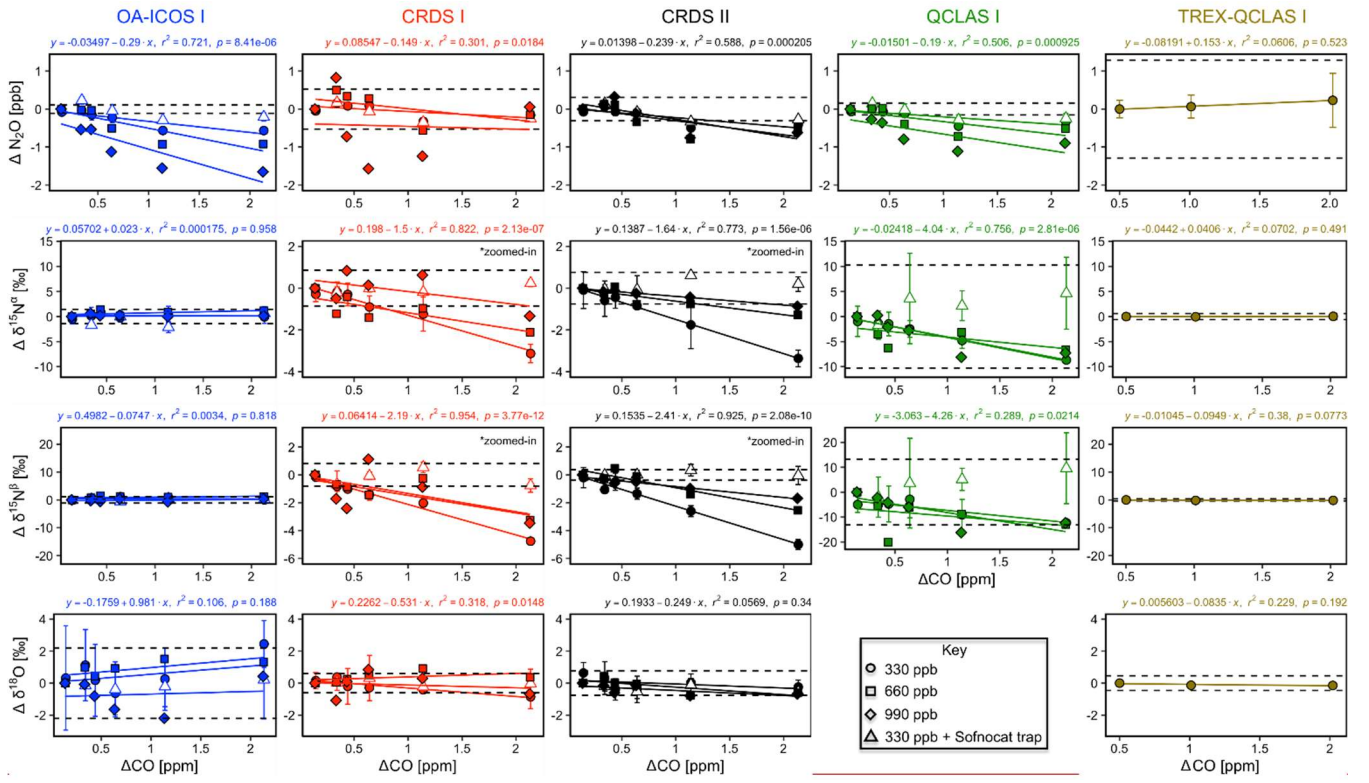


Fig. 10. Deviations of the measured $[N_2O]$, $\delta^{15}N^{\alpha}$, $\delta^{15}N^{\beta}$ and $\delta^{18}O$ values according to ΔCO (ppm) at different N_2O mole fractions (330, 660 and 990 ppb) for OA-ICOS I (blue), CRDS I (red), CRDS II (black), QCLAS I (green) and TREX-QCLAS I (brown). The standard deviation of the Anchor gas ($\pm 1\sigma$) is indicated by dashed lines. Data points represent the mean and standard deviation (1σ) of triplicate measurements. Dependencies are best described by linear fits, which are indicated by solid lines. Individual equations, coefficients of determination (r^2) and p -values are indicated above each plot for the 330 ppb N_2O data only.

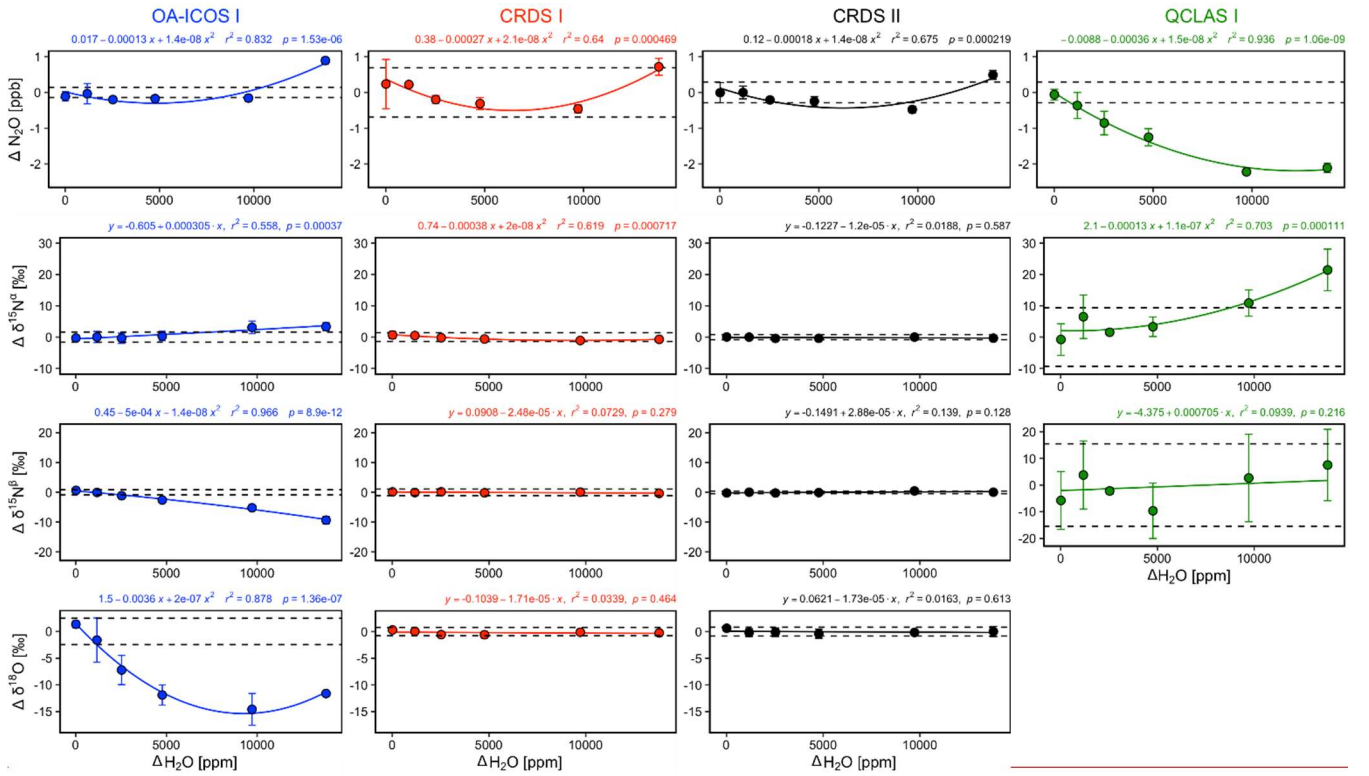


Fig. 11. Deviations of the measured $[N_2O]$, $\delta^{15}N^a$, $\delta^{15}N^b$ and $\delta^{18}O$ values according to ΔH_2O (ppm) for OA ICOS I (blue), CRDS I (red), CRDS II (black) and QCLAS I (green). The standard deviation of the Anchor gas ($\pm 1\sigma$) is indicated by dashed lines. Data points represent the mean and standard deviation (1σ) of triplicate measurements. Dependencies are best described by either linear or polynomial fits, which are indicated by solid lines. Individual equations, coefficients of determination (r^2) and p -values are indicated above each plot.

3.6.2 Continuity of trace gas corrections at higher N_2O mole fractions

Interference effects from CO_2 , CH_4 and CO on apparent δ values, where significant, inversely scaled with increasing $[N_2O]$ (Figs. 7, 8, S4-8 and Supplementary Material 88, 9 and 10; Table 9). The scaling of trace gas effects can be explained by simple spectral overlap of the $^{14}N^{15}N^{16}O$, $^{15}N^{14}N^{16}O$ and $^{14}N^{14}N^{18}O$ lines with those of the trace gas, which results in the interference effects being inversely proportional to the mixing ratio of N_2O . However, there may be additional spectral overlap between the trace gas and the $^{14}N^{14}N^{16}O$ peak resulting in an offset for the measured $[N_2O]$, which introduces a further shift in the δ values (as shown in Sect. 3.4). The effect on the apparent $[N_2O]$ was less clear and was possibly confounded by inaccuracies during dynamic gas mixing. In this study, the scaling of interference effects from trace gases as a function of the $[N_2O]$ introduced to the analyzers could be described using Eqs. (9) and (10):

$$\Delta[N_2O]_{meas,mix}(\Delta[x]_A, [N_2O]_{exp,mix}) = \left(A_x \frac{1}{[N_2O]_{exp,mix}} + B_x \right) \cdot \Delta[x]_A \quad (9)$$

$$\Delta\delta_{meas,mix}(\Delta[x]_A, [N_2O]_{exp,mi}) = \left(a_x * \frac{1}{[N_2O]_{exp,mix}} + b_x \right) \cdot \Delta[x]_A \quad (10)$$

where $\Delta[N_2O]_{meas,mix}$ and $\Delta\delta_{meas,mix}$ are the measured offsets on $[N_2O]$ and δ values for the gas mixtures introduced to the analyzers as reported in Sect. 3.6.1, respectively; $\Delta[x]_A$ is the difference in trace gas mole fraction between the gas mixture and Anchor gas as reported in Sect. 3.6.1; and A_x , B_x , a_x and b_x are constants that are trace gas and instrument specific. The constant b_x only occurs when there is spectral overlap from the trace gas and $^{14}N^{14}N^{16}O$ absorption lines.

For a sample gas G, the effect can then be corrected by using Eq. (11) and Eq. (12):

$$[N_2O]_{tc,G} = [N_2O]_{meas,G} - \sum_x \left(\left(A_x \frac{1}{[N_2O]_{meas,G}} + B_x \right) \cdot \Delta[x]_G \right) \quad (11)$$

$$\delta_{tc,G} = \delta_{meas,G} - \sum_x \left(\left(a_x \frac{1}{[N_2O]_{meas,G}} + b_x \right) \cdot \Delta[x]_G \right) \quad (12)$$

In Eqs. (11–12), the sum of the effect of all interfering gases with overlapping absorption lines is taken into account. Similar to Section 3.5.2, correction using Eqs. (11–12) removes the trace gas interference effects to the extent that corrected measurements from Sect. 3.6.1 are within the repeatability bounds of the Anchor gas (Supplementary Material 86). Similar inverse relationships have been described by Malowany et al. (2015) for H_2S interferences on $\delta^{13}C-CO_2$.

Table 9. Summary of regression slopes and coefficients of determination (r^2) for trace gas interferences (CO_2 , CH_4 and CO) performed at different N_2O mole fractions (330, 660 and 990 ppb) for OA-ICOS I, CRDS I and II, and QCLAS I.

		OA-ICOS I		CRDS I		CRDS II		QCLAS I	
ΔCO_2 [ppm]	Co-measured N_2O [ppb]	Slope	r^2	Slope	r^2	Slope	r^2	Slope	r^2
N_2O [ppb]	330	$1.12 \cdot 10^{-3}$	0.96	$4.90 \cdot 10^{-4}$	0.88	$4.94 \cdot 10^{-4}$	0.83	n.s.	n.s.
	660	$1.50 \cdot 10^{-3}$	0.99	$6.57 \cdot 10^{-4}$	0.75	$6.45 \cdot 10^{-4}$	0.73	$-1.64 \cdot 10^{-4}$	0.70
	990	$1.92 \cdot 10^{-3}$	0.99	n.s.	n.s.	$1.37 \cdot 10^{-3}$	0.87	n.s.	n.s.
$\delta^{15}\text{N}^\alpha$ [‰]	330	$-8.70 \cdot 10^{-3}$	0.95	$-1.58 \cdot 10^{-3}$	0.88	$-6.83 \cdot 10^{-4}$	0.66	n.s.	n.s.
	660	$-5.01 \cdot 10^{-3}$	0.99	$-6.95 \cdot 10^{-4}$	0.76	n.s.	n.s.	n.s.	n.s.
	990	$-3.80 \cdot 10^{-3}$	1.00	n.s.	n.s.	n.s.	n.s.	n.s.	n.s.
$\delta^{15}\text{N}^\beta$ [‰]	330	$2.55 \cdot 10^{-2}$	1.00	n.s.	n.s.	n.s.	n.s.	$1.54 \cdot 10^{-2}$	0.59
	660	$1.11 \cdot 10^{-2}$	1.00	n.s.	n.s.	n.s.	n.s.	$5.50 \cdot 10^{-3}$	0.70
	990	$6.94 \cdot 10^{-3}$	0.99	n.s.	n.s.	n.s.	n.s.	$6.64 \cdot 10^{-3}$	0.76
$\delta^{18}\text{O}$ [‰]	330	$-2.65 \cdot 10^{-2}$	0.99	$-1.88 \cdot 10^{-3}$	0.86	$-1.20 \cdot 10^{-3}$	0.72	n.d.	n.d.
	660	$-1.66 \cdot 10^{-2}$	1.00	n.s.	n.s.	n.s.	n.s.	n.d.	n.d.
	990	$-1.18 \cdot 10^{-2}$	1.00	n.s.	n.s.	$5.09 \cdot 10^{-4}$	0.72	n.d.	n.d.
ΔCH_4 [ppm]									
N_2O [ppb]	330	$-4.86 \cdot 10^{-2}$	0.67	$-3.91 \cdot 10^{-2}$	0.48	$-5.56 \cdot 10^{-2}$	0.57	$-4.15 \cdot 10^{-2}$	0.45
	660	n.s.	n.s.	n.s.	n.s.	n.s.	n.s.	n.s.	n.s.
	990	$-1.28 \cdot 10^{-1}$	0.92	n.s.	n.s.	$-1.06 \cdot 10^{-1}$	0.69	$-1.14 \cdot 10^{-1}$	0.88
$\delta^{15}\text{N}^\alpha$ [‰]	330	n.s.	n.s.	$2.50 \cdot 10^0$	1.00	$2.49 \cdot 10^0$	1.00	n.s.	n.s.
	660	n.s.	n.s.	$1.29 \cdot 10^0$	0.98	$1.22 \cdot 10^0$	1.00	n.s.	n.s.
	990	n.s.	n.s.	$8.26 \cdot 10^{-1}$	0.95	$8.13 \cdot 10^{-1}$	0.99	$-7.59 \cdot 10^{-1}$	0.93
$\delta^{15}\text{N}^\beta$ [‰]	330	$1.73 \cdot 10^{-1}$	0.29	n.s.	n.s.	$8.47 \cdot 10^{-2}$	0.23	n.s.	n.s.
	660	n.s.	n.s.	n.s.	n.s.	n.s.	n.s.	n.s.	n.s.

	990	n.s.	n.s.	n.s.	n.s.	n.s.	n.s.	n.s.	n.s.
	330	n.s.	n.s.	$1.14 \cdot 10^0$	0.98	$1.29 \cdot 10^{-1}$	0.97	n.d.	n.d.
$\delta^{18}\text{O}$ [‰]	660	$-2.21 \cdot 10^{-1}$	0.74	$7.34 \cdot 10^{-1}$	0.99	$6.36 \cdot 10^{-1}$	0.99	n.d.	n.d.
	990	n.s.	n.s.	$3.76 \cdot 10^{-1}$	0.79	$3.55 \cdot 10^{-1}$	0.98	n.d.	n.d.
<hr/> ΔCO [ppm] <hr/>									
	330	$-2.90 \cdot 10^{-1}$	0.72	$-1.49 \cdot 10^{-1}$	0.30	$-2.39 \cdot 10^{-1}$	0.59	$-1.90 \cdot 10^{-1}$	0.51
N_2O [ppb]	660	$-5.29 \cdot 10^{-1}$	0.76	n.s.	n.s.	n.s.	n.s.	n.s.	n.s.
	990	$-7.72 \cdot 10^{-1}$	0.76	n.s.	n.s.	n.s.	n.s.	n.s.	n.s.
	330	n.s.	n.s.	$-1.50 \cdot 10^0$	0.82	$-1.64 \cdot 10^0$	0.77	$-4.04 \cdot 10^0$	0.76
$\delta^{15}\text{N}^{\alpha}$ [‰]	660	n.s.	n.s.	n.s.	n.s.	$-6.49 \cdot 10^{-1}$	0.81	n.s.	n.s.
	990	n.s.	n.s.	n.s.	n.s.	$-4.16 \cdot 10^{-1}$	0.98	$-4.17 \cdot 10^0$	0.73
	330	n.s.	n.s.	$-2.19 \cdot 10^0$	0.95	$-2.41 \cdot 10^0$	0.92	$-4.26 \cdot 10^0$	0.29
$\delta^{15}\text{N}^{\beta}$ [‰]	660	n.s.	n.s.	$-1.31 \cdot 10^0$	0.67	$-1.44 \cdot 10^0$	0.89	n.s.	n.s.
	990	n.s.	n.s.	n.s.	n.s.	$-7.86 \cdot 10^{-1}$	0.95	n.s.	n.s.
	330	n.s.	n.s.	$-5.31 \cdot 10^{-1}$	0.32		n.s.	n.d.	n.d.
$\delta^{18}\text{O}$ [‰]	660	n.s.	n.s.	n.s.	n.s.	n.s.	n.s.	n.d.	n.d.
	990	n.s.	n.s.	n.s.	n.s.	n.s.	n.s.	n.d.	n.d.

n.d. not determined

n.s. not statistically significant at $p < 0.05$

3.7 Two end-member mixing

Results for the two end-member mixing experiment were evaluated in two different ways. First, results for individual gas mixtures acquired by laser spectroscopy and GC-IRMS were compared to expected $[\text{N}_2\text{O}]$ and δ values calculated from N_2O mole fractions and isotopic composition of end-members and mixing fractions. Second, source values were extrapolated using a weighted total least squares regression analysis, known as Keeling plot analysis (Keeling, 1958), and compared to assigned δ values of the *source* gas used in each experiment.

3.7.1 Comparison with expected $[\text{N}_2\text{O}]$ and δ values

Triplicate measurements (mean $\pm 1\sigma$) obtained using the laser spectrometers and GC-IRMS were plotted against expected $[\text{N}_2\text{O}]$ and δ values calculated using MFC flow rates, N_2O mole fractions and isotopic composition of *background* and *source* gases (Figs. 12-15). Comparisons between individual laser spectrometer measurements and GC-IRMS are plotted in Supplementary Material 97, and are discussed only briefly below.

OA-ICOS I

Generally, there was good agreement of $[\text{N}_2\text{O}]$ between the OA-ICOS I and expected values, although the analyzer over-estimated mole fractions at higher $\Delta\text{N}_2\text{O}$ during experiments 5 and 6 (~~Fig. 12~~). There was excellent agreement between the OA-ICOS I and calculated expected δ values (all $r^2 > 0.95$; [Figs. 9 and S4-10](#)). Measurements for $\delta^{15}\text{N}^a$ were mostly within ± 2.4 ‰ of expected values, while $\delta^{15}\text{N}^b$, $\delta^{15}\text{N}^{\text{bulk}}$ and SP were all within ± 2 ‰ of expected values. $\delta^{18}\text{O}$ measurements were the poorest performing, but were typically within ± 3.6 ‰ of expected values. Similarly, there was excellent agreement between OA-ICOS I and IRMS isotope values (all $r^2 > 0.95$), which agreed within 1.7–2.4 ‰ ([Fig. S96-2](#)). The standard deviations of triplicate isotope measurements decreased dramatically with increasing $\Delta\text{N}_2\text{O}$, improving from 1 – 2 ‰ during experiments 1 and 2 to typically better than 0.1 ‰ during experiments 5 and 6. Conversely, the standard deviations of triplicate sample measurements for $[\text{N}_2\text{O}]$ increased with increasing $\Delta\text{N}_2\text{O}$, rising from < 0.1 ppb during experiments 1 through 4, to > 1 ppb during experiments 5 and 6. Nonetheless, all OA-ICOS I $[\text{N}_2\text{O}]$ measurements had better 1σ repeatability than those acquired using GC. The repeatability of the triplicate isotope measurements with OA-ICOS I was typically better than IRMS exclusively at higher $\Delta\text{N}_2\text{O}$ (> 700 ppb).

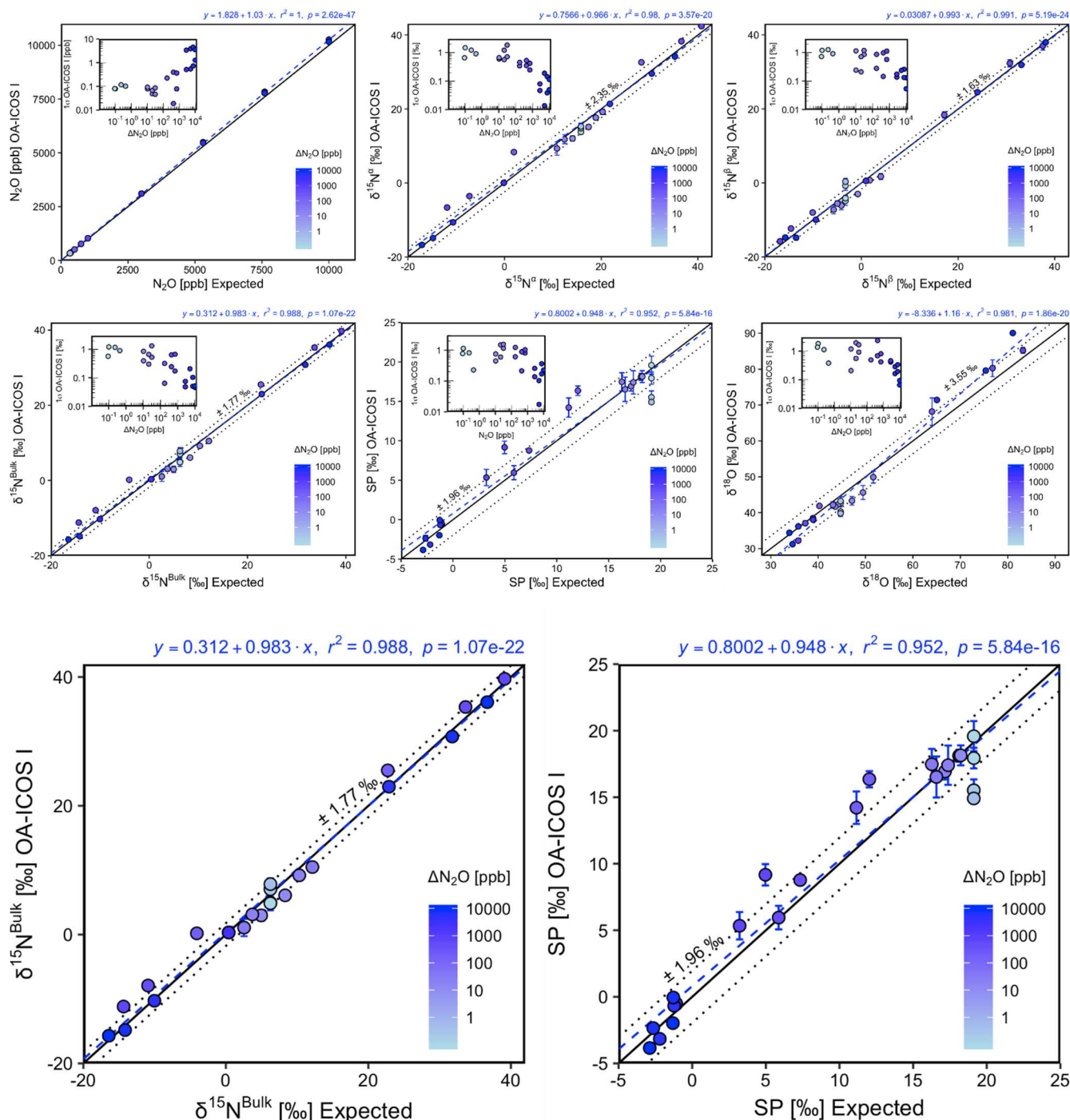


Fig. 912. Correlation diagrams for $\delta^{15}\text{N}^{\text{bulk}}$ and SP measurements at various $\Delta\text{N}_2\text{O}$ mole fractions analyzed by OA-ICOS I plotted against expected values. The remaining plots for $[\text{N}_2\text{O}]$, $\delta^{15}\text{N}^{\text{a}}$, $\delta^{15}\text{N}^{\text{b}}$ and $\delta^{18}\text{O}$ are provided in Supplementary Material 4 (Fig. S4-10). $[\text{N}_2\text{O}]$, $\delta^{15}\text{N}^{\text{a}}$, $\delta^{15}\text{N}^{\text{b}}$, $\delta^{15}\text{N}^{\text{bulk}}$, SP and $\delta^{18}\text{O}$ measurements at various $\Delta\text{N}_2\text{O}$ mole fractions analyzed by the OA-ICOS I plotted against expected values. The solid black line denotes the 1:1 line, while the dotted line indicates $\pm 1\sigma$ of the residuals from the 1:1 line. The dashed blue line represents a linear fit to the data. Individual equations, coefficients of determination (r^2) and p -values are indicated above each plot. Each data point represents the mean and standard deviation (1σ) of triplicate measurements. The inset plots indicate the standard deviation (1σ) of the triplicate measurements achieved at different $\Delta\text{N}_2\text{O}$ mole fractions, and the 1:1 line is similarly a solid line.

CRDS I

$[\text{N}_2\text{O}]$ acquired by CRDS I were in good agreement with expected values, although the analyzer slightly under-estimated mole fractions at higher $\Delta\text{N}_2\text{O}$ during experiments 3 and 4 (Fig. 13). There was excellent

agreement between the CRDS I and calculated expected isotope values (all $r^2 > 0.95$; [Figs. 10 and S4-11](#)). Measurements for $\delta^{15}\text{N}^{\alpha}$ and $\delta^{15}\text{N}^{\beta}$ were mostly better than ± 1.1 ‰ of expected values, while $\delta^{15}\text{N}^{\text{bulk}}$ was within ± 0.5 ‰ of expected values. SP and $\delta^{18}\text{O}$ measurements were typically within ± 1.5 ‰ of expected values. There was excellent agreement between CRDS I and IRMS isotope values (all $r^2 > 0.93$), which agreed to within 0.5 – 1.9 ‰ (Fig. [S96-3](#)). In general, the standard deviations of triplicate isotope measurements increased as a function of $\Delta\text{N}_2\text{O}$, with the lowest deviations of 0.1–1 ‰ occurring when $\Delta\text{N}_2\text{O} < 100$ ppb. However, two triplicated measurements for $\delta^{15}\text{N}^{\text{bulk}}$ had standard deviations better than 0.1 ‰. The standard deviations of triplicate measurements for $[\text{N}_2\text{O}]$ also increased with increasing $\Delta\text{N}_2\text{O}$ mole fractions, rising from 0.03–0.07 ppb when $\Delta\text{N}_2\text{O} = \sim 0$ ppb (i.e. ambient conditions) to ~ 1 ppb when $\Delta\text{N}_2\text{O} = \sim 700$ ppb. With the exception of one triplicate measurement, all CRDS I $[\text{N}_2\text{O}]$ measurements had better 1σ repeatability than those acquired using GC. Overall, IRMS had slightly better repeatability (most ranging from 0.1 – 1 ‰) than CRDS I (most ranging from 0.1 – 2 ‰) for isotopic measurements.

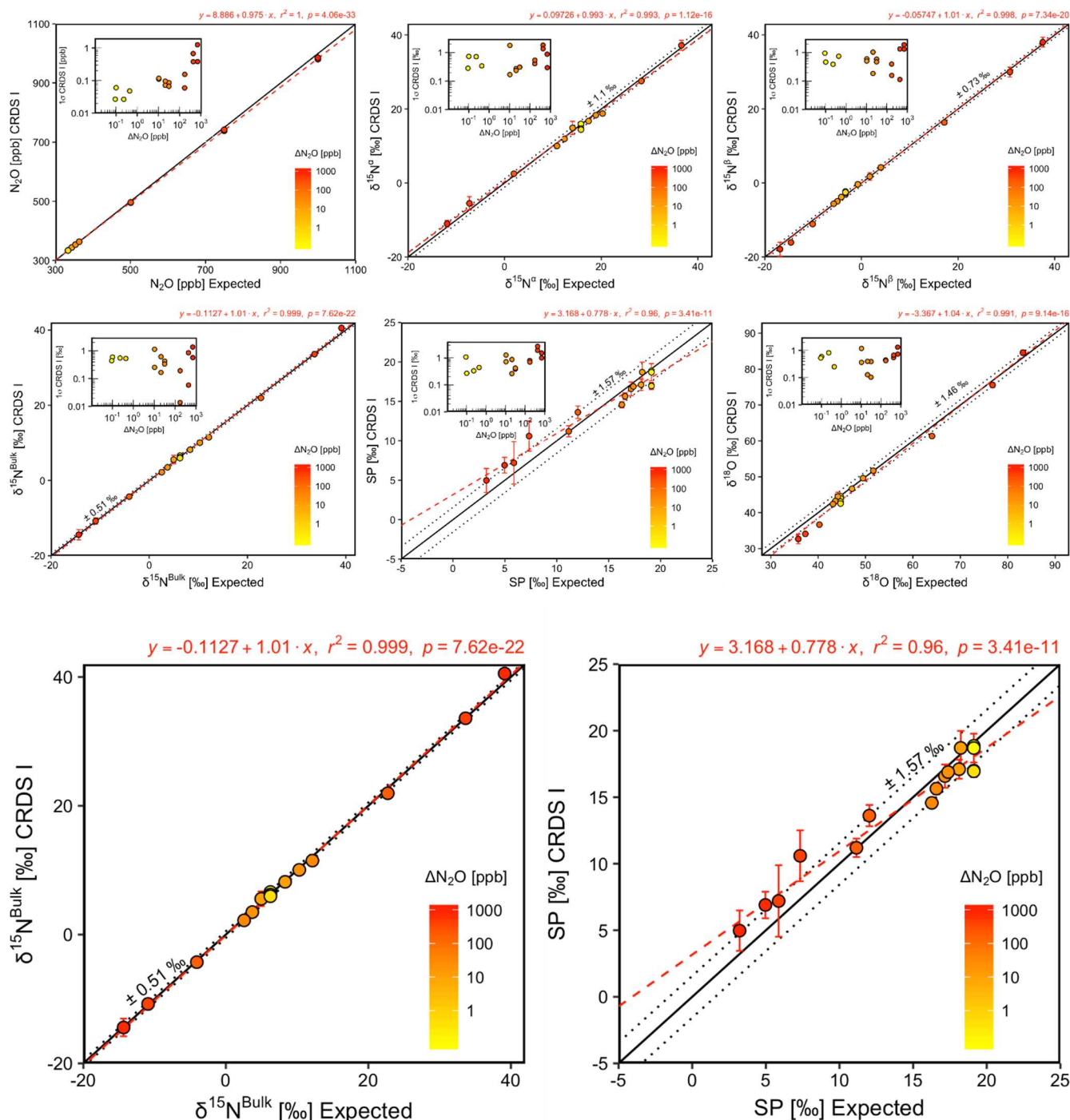


Fig. 103. Correlation diagrams for $\delta^{15}\text{N}^{\text{bulk}}$ and SP measurements at various $\Delta\text{N}_2\text{O}$ mole fractions analyzed by CRDS I plotted against expected values. The remaining plots for $[\text{N}_2\text{O}]$, $\delta^{15}\text{N}^{\text{a}}$, $\delta^{15}\text{N}^{\text{b}}$ and $\delta^{18}\text{O}$ are provided in Supplementary Material 4 (Fig. S4-11). $[\text{N}_2\text{O}]$, $\delta^{15}\text{N}^{\text{a}}$, $\delta^{15}\text{N}^{\text{b}}$, $\delta^{15}\text{N}^{\text{bulk}}$, SP and $\delta^{18}\text{O}$ measurements at various $\Delta\text{N}_2\text{O}$ mole fractions analyzed by the CRDS I plotted against expected values. The solid black line denotes the 1:1 line, while the dotted line indicates $\pm 1\sigma$ of the residuals from the 1:1 line. The dashed red line represents a linear fit to the data. Individual equations, coefficients of determination (r^2) and p -values are indicated above each plot. Each data point represents the mean and standard deviation (1σ) of triplicate measurements. The inset plots indicate the standard deviation (1σ) of the triplicate measurements achieved at different $\Delta\text{N}_2\text{O}$ mole fractions, and the 1:1 line is similarly a solid line.

Similar to results for CRDS I, $[\text{N}_2\text{O}]$ acquired by CRDS II were in good agreement with expected values but slightly under-estimated mole fractions at higher $\Delta\text{N}_2\text{O}$ during experiments 3 and 4 (~~Fig-14~~). There was excellent agreement between the CRDS II and calculated expected isotope values (all $r^2 > 0.99$; [Figs. 11 and S4-12](#)). Measurements for $\delta^{15}\text{N}^{\alpha}$ and SP were typically better than ± 0.8 ‰ of expected values, while $\delta^{15}\text{N}^{\beta}$, $\delta^{15}\text{N}^{\text{bulk}}$ measurements were all within ± 0.4 ‰ of expected values. $\delta^{18}\text{O}$ measurements were within ± 1.0 ‰ of expected values. There was excellent agreement between CRDS II and IRMS isotope values (all $r^2 > 0.98$), which agreed within ± 0.6 – 1.4 ‰ (Fig. [S96-4](#)). The standard deviations of triplicate isotope measurements typically decreased as a function of $\Delta\text{N}_2\text{O}$, with the lowest deviations of <0.1 – 0.3 ‰ occurring when $\Delta\text{N}_2\text{O} = \sim 700$ ppb. Conversely, the standard deviations of triplicate sample measurements for $[\text{N}_2\text{O}]$ increased with increasing $\Delta\text{N}_2\text{O}$, rising from 0.04 – 0.09 ppb when $\Delta\text{N}_2\text{O} = \sim 0$ ppb (i.e. ambient conditions) to ~ 0.4 ppb when $\Delta\text{N}_2\text{O} = \sim 700$ ppb. All CRDS II $[\text{N}_2\text{O}]$ measurements had better 1σ repeatability than those acquired using GC. There was no clear distinction between CRDS II and IRMS triplicate repeatability, with both achieving triplicate repeatability ranging from 0.1 to 1 ‰ for most isotopic measurements. However, the repeatability of SP CRDS II measurements was mostly better than IRMS, achieving triplicate repeatability between 0.1 – 0.6 ‰, compared to 0.2 – 1 ‰ for IRMS.

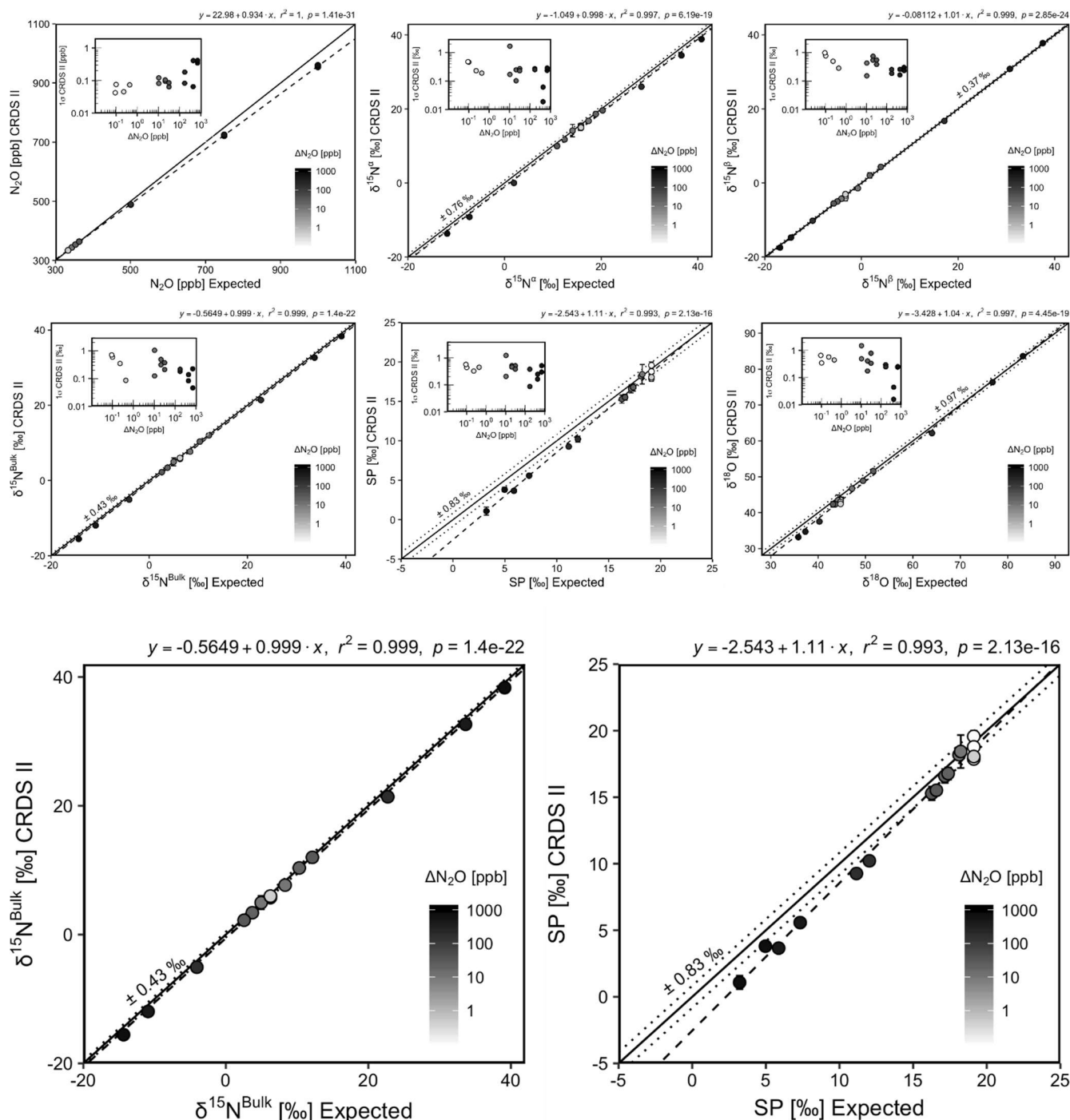


Fig. 114. Correlation diagrams for $\delta^{15}\text{N}^{\text{bulk}}$ and SP measurements at various $\Delta\text{N}_2\text{O}$ mole fractions analyzed by CRDS II plotted against expected values. The remaining plots for $[\text{N}_2\text{O}]$, $\delta^{15}\text{N}^{\alpha}$, $\delta^{15}\text{N}^{\beta}$ and $\delta^{18}\text{O}$ are provided in Supplementary Material 4 (Fig. S4-12). $[\text{N}_2\text{O}]$, $\delta^{15}\text{N}^{\alpha}$, $\delta^{15}\text{N}^{\beta}$, $\delta^{15}\text{N}^{\text{bulk}}$, SP and $\delta^{18}\text{O}$ measurements at various $\Delta\text{N}_2\text{O}$ mole fractions analyzed by the CRDS II plotted against expected values. The solid black line denotes the 1:1 line, while the dotted line indicates $\pm 1\sigma$ of the residuals from the 1:1 line. The dashed black line represents a linear fit to the data. Individual equations, coefficients of determination (r^2) and p -values are indicated above each plot. Each data point represents the mean and standard deviation (1σ) of triplicate measurements. The inset plots indicate the standard deviation (1σ) of the triplicate measurements achieved at different $\Delta\text{N}_2\text{O}$ mole fractions, and the 1:1 line is similarly a solid line.

QCLAS I

There was good agreement of $[\text{N}_2\text{O}]$ between QCLAS I and expected values, however the analyzer underestimated mole fractions at higher $\Delta\text{N}_2\text{O}$ during experiments 5 and 6. (Fig. 15). Unfortunately, it is clear

from the large spread of isotope values depicted in Fig. 12~~5~~ that the standardized calibration scheme selected for the two end-member mixing tests was insufficient for acquiring accurate and precise isotopic measurements using QCLAS I. For this reason, we urge researchers not to over-interpret such results, as the implementation of a QCLAS-specific calibration procedure (in-line with results from Sects. 3.1 and 3.3) would improve results dramatically. Nonetheless, QCLAS I obtained accurate results at higher N₂O mole fractions (indicated in red in [Figs. 12 and S4-13](#)~~Fig. 15~~), such that when $\Delta\text{N}_2\text{O} < 700$ ppb measurements were excluded, $\delta^{15}\text{N}^\alpha$, $\delta^{15}\text{N}^\beta$, $\delta^{15}\text{N}^{\text{bulk}}$ and SP were within ± 3.0 ‰, 1.4 ‰, 1.4 ‰ and 3.8 ‰ of calculated expected values, respectively. Similarly, QCLAS I showed good agreement with IRMS only at higher $\Delta\text{N}_2\text{O}$ (> 700 ppb; Fig. [S96-5](#)). Similar to OA-ICOS I, the standard deviations of QCLAS I triplicate isotope measurements decreased dramatically with increasing $\Delta\text{N}_2\text{O}$, improving from ~ 10 ‰ during experiments 1 and 2 to typically between 0.1–1 ‰ during experiments 5 and 6. Conversely, the standard deviations of triplicate sample measurements for [N₂O] increased with increasing $\Delta\text{N}_2\text{O}$, rising from < 0.1 ppb during experiments 1 through 4, to > 1 ppb during experiments 5 and 6. All QCLAS I [N₂O] measurements had better 1σ repeatability than those acquired using GC. QCLAS I had triplicate isotope measurement standard deviations comparable to IRMS only at higher $\Delta\text{N}_2\text{O}$ (> 700 ppb).

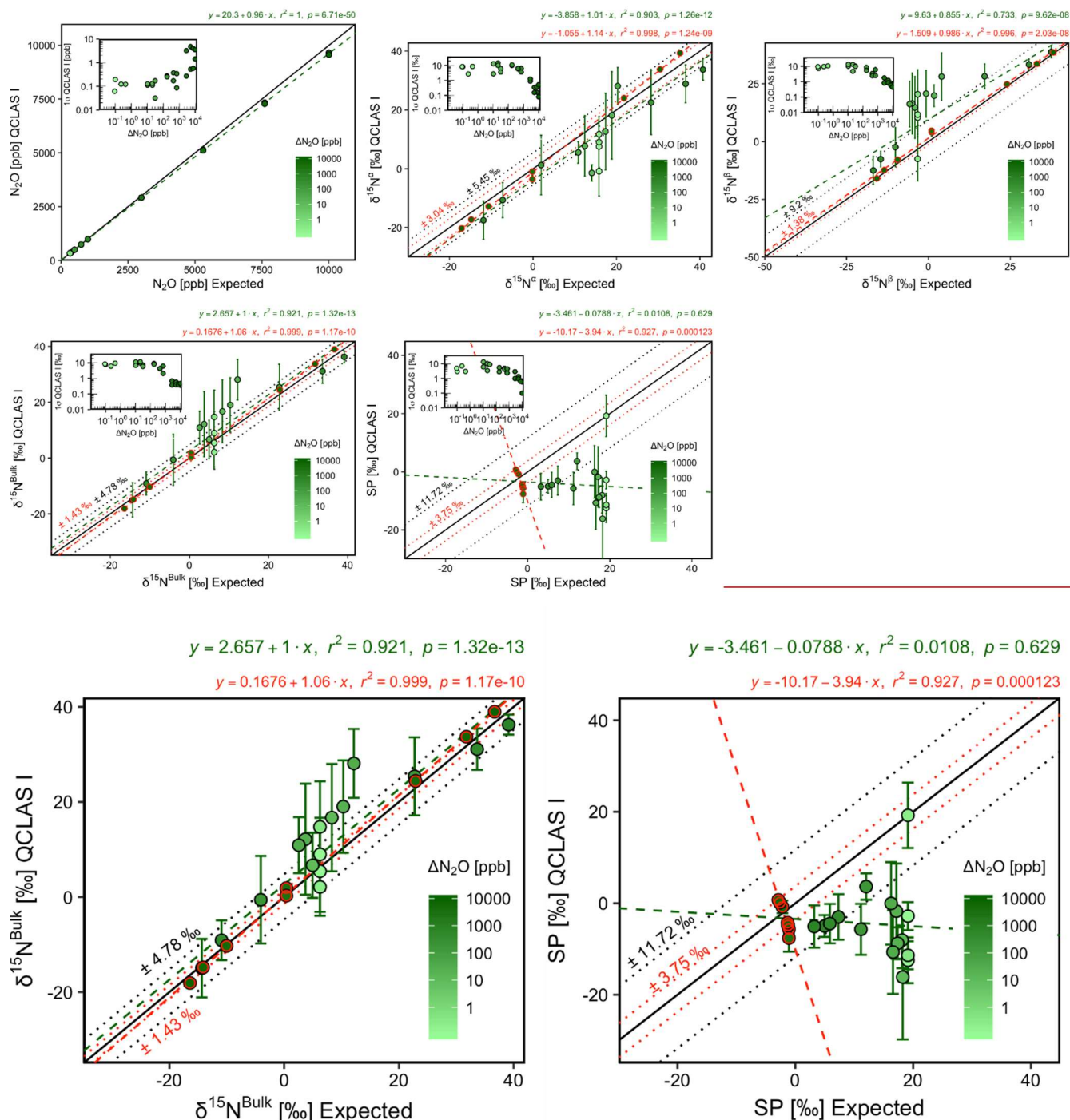


Fig. 125. Correlation diagrams for $\delta^{15}\text{N}^{\text{bulk}}$ and SP measurements at various $\Delta\text{N}_2\text{O}$ mole fractions analyzed by QCLAS I plotted against expected values. The remaining plots for $[\text{N}_2\text{O}]$, $\delta^{15}\text{N}^{\text{a}}$, $\delta^{15}\text{N}^{\text{b}}$ and $\delta^{18}\text{O}$ are provided in Supplementary Material 4 (Fig. S4-13). N_2O -mole fractions, $\delta^{15}\text{N}^{\text{a}}$, $\delta^{15}\text{N}^{\text{b}}$, $\delta^{15}\text{N}^{\text{bulk}}$ and SP measurements at various $\Delta\text{N}_2\text{O}$ -mole fractions analyzed by the QCLAS I plotted against expected values. The solid black line denotes the 1:1 line, while the dotted line indicates $\pm 1\sigma$ of the residuals from the 1:1 line. The dashed green line represents a linear fit to the data. Individual equations, coefficients of determination (r^2) and p -values are indicated above each plot. Each data point represents the mean and standard deviation (1 σ) of triplicate measurements. The inset plots indicate the standard deviation (1 σ) of the triplicate measurements achieved at different $\Delta\text{N}_2\text{O}$ mole fractions, and the 1:1 line is similarly a solid line. Results for Exp. 5-6 are highlighted in red, with the dashed red line indicating a linear fit to this data.

There was good agreement of N₂O mixing ratios between the TREX-QCLAS I and expected values (Fig. 16). Similarly, there was excellent agreement between the TREX-QCLAS I and calculated expected isotope values (all $r^2 > 0.97$; Figs. 13 and S4-14). Measurements for $\delta^{15}\text{N}^\alpha$, $\delta^{15}\text{N}^\beta$, $\delta^{15}\text{N}^{\text{bulk}}$ and SP were within ± 0.29 ‰, ± 0.32 ‰, ± 0.23 ‰ and ± 0.41 ‰ of expected values, respectively. $\delta^{18}\text{O}$ measurements were typically within ± 0.24 ‰ of expected values. Generally, the standard deviations of triplicate isotope measurements decreased with increasing $\Delta\text{N}_2\text{O}$, improving from typically 0.2–0.3 ‰ at low $\Delta\text{N}_2\text{O}$ mole fractions (ambient) to close to or better than 0.1 ‰ when $\Delta\text{N}_2\text{O}$ reached 30 ppb. Conversely, the standard deviations of triplicate sample measurements for $[\text{N}_2\text{O}]$ increased with increasing $\Delta\text{N}_2\text{O}$, rising from < 0.3 ppb to ~ 1 ppb. No comparison could be made between TREX-QCLAS I and IRMS measurements because TREX-QCLAS measurements were undertaken separately from the other instruments.

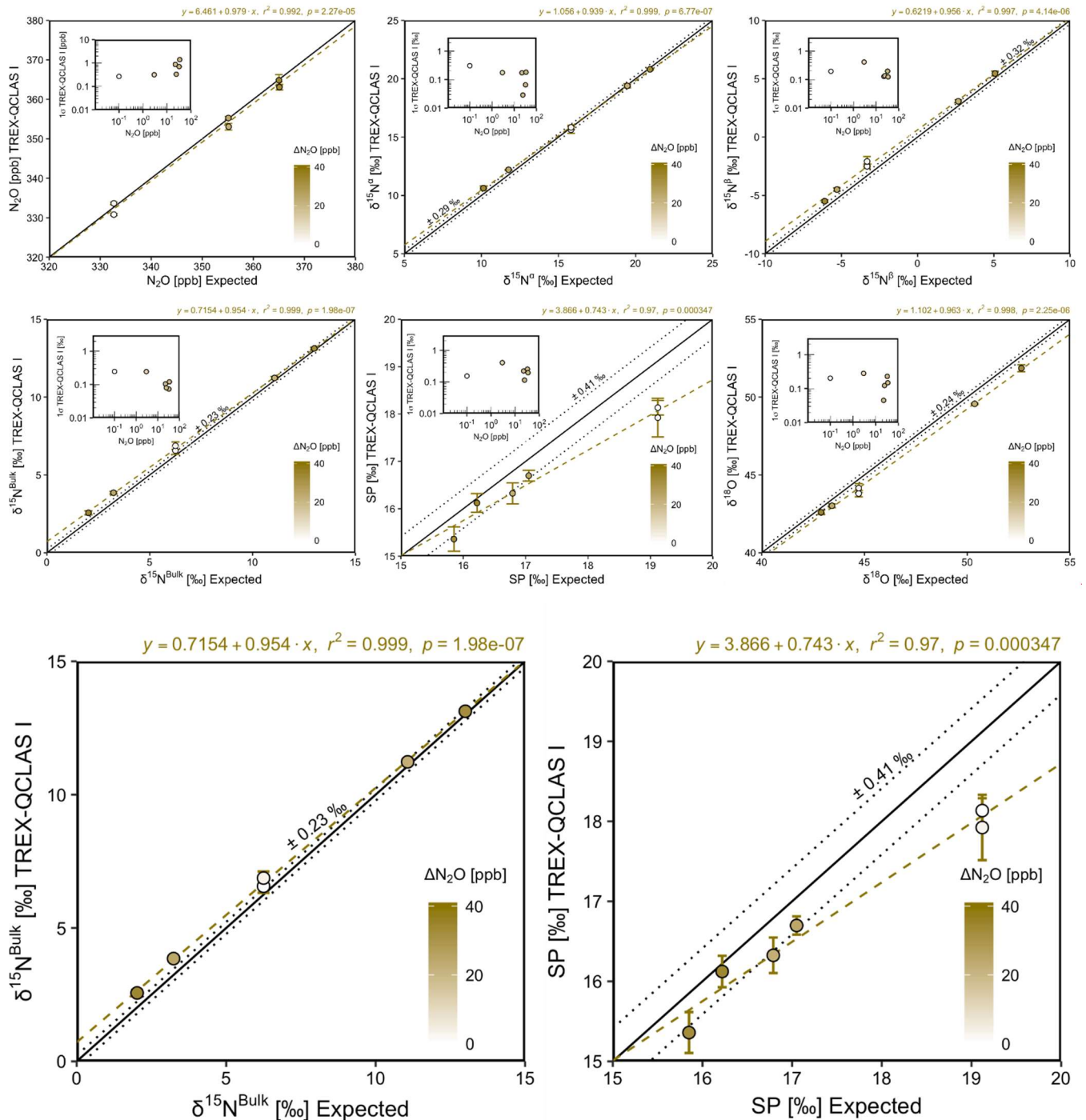


Fig. 136. Correlation diagrams for $\delta^{15}\text{N}^{\text{bulk}}$ and SP measurements at various $\Delta\text{N}_2\text{O}$ mole fractions analyzed by OA-ICOS I plotted against expected values. The remaining plots for $[\text{N}_2\text{O}]$, $\delta^{15}\text{N}^{\alpha}$, $\delta^{15}\text{N}^{\beta}$ and $\delta^{18}\text{O}$ are provided in Supplementary Material 4 (Fig S4-14). $[\text{N}_2\text{O}]$, $\delta^{15}\text{N}^{\alpha}$, $\delta^{15}\text{N}^{\beta}$, $\delta^{15}\text{N}^{\text{bulk}}$, SP and $\delta^{18}\text{O}$ measurements at various $\Delta\text{N}_2\text{O}$ mole fractions analyzed by the TREX-QCLAS I plotted against expected values. The solid black line denotes the 1:1 line, while the dotted line indicates $\pm 1\sigma$ of the residuals from the 1:1 line. The dashed green line represents a linear fit to the data. Individual equations, coefficients of determination (r^2) and p-values are indicated above each plot. Each data point represents the mean and standard deviation (1σ) of triplicate measurements. The inset plots indicate the standard deviation (1σ) of the triplicate measurements achieved at different $\Delta\text{N}_2\text{O}$ mole fractions, and the 1:1 line is similarly a solid line.

3.7.2 Source identification using Keeling analysis

Despite the excellent agreement between expected and measured values across all experiments for OA-ICOS I, CRDS I and II, and TREX-QCLAS I, the extrapolated *source* intercept values acquired using Keeling analysis showed large standard errors, especially for Experiments 1 and 2 ($\Delta\text{N}_2\text{O} = 30$ ppb) (Figs. 14 and S4-157; Table 10 Supplementary Material 10). This was mostly due to the small mole fraction range (i.e. large inverse mole fraction range) over which the regression line was extrapolated in order to acquire the intercept value. The cause of the erroneous intercepts values was likely two-fold: (1) the extrapolated source was highly susceptible to measurements acquired at background levels, and due to the inherent greater uncertainty associated with measurements acquired at ambient N_2O mole fractions, intercepts can be skewed accordingly; and (2) any further non-linearity that could not be taken into account in the three-point concentration dependence correction applied. Overall, this implies that N_2O isotope source studies using laser spectroscopy focusing on near-ambient N_2O variations remain a challenging undertaking, and one should expect large uncertainty in source estimates over small mole fraction changes.

For Experiments 3 through 6, however, the accuracy of the source intercept and its standard error improved dramatically for all analyzers on account of the decreasing uncertainty in measurement. OA-ICOS I and both CRDS analyzers typically achieved within $\pm 2\text{--}5\%$ of the assigned values for $\delta^{15}\text{N}^{\alpha}$, $\delta^{15}\text{N}^{\beta}$, $\delta^{15}\text{N}^{\text{bulk}}$, SP and $\delta^{18}\text{O}$, and had performance comparable to or better than the GC-IRMS approach (Figs. 14 and S4-15, 17). Similarly, the standard error of all intercepts decreased dramatically for Experiments 3 through 6, and all analyzers typically achieved better than $\pm 1\%$ standard error on derived intercepts in Experiments 5 and 6.

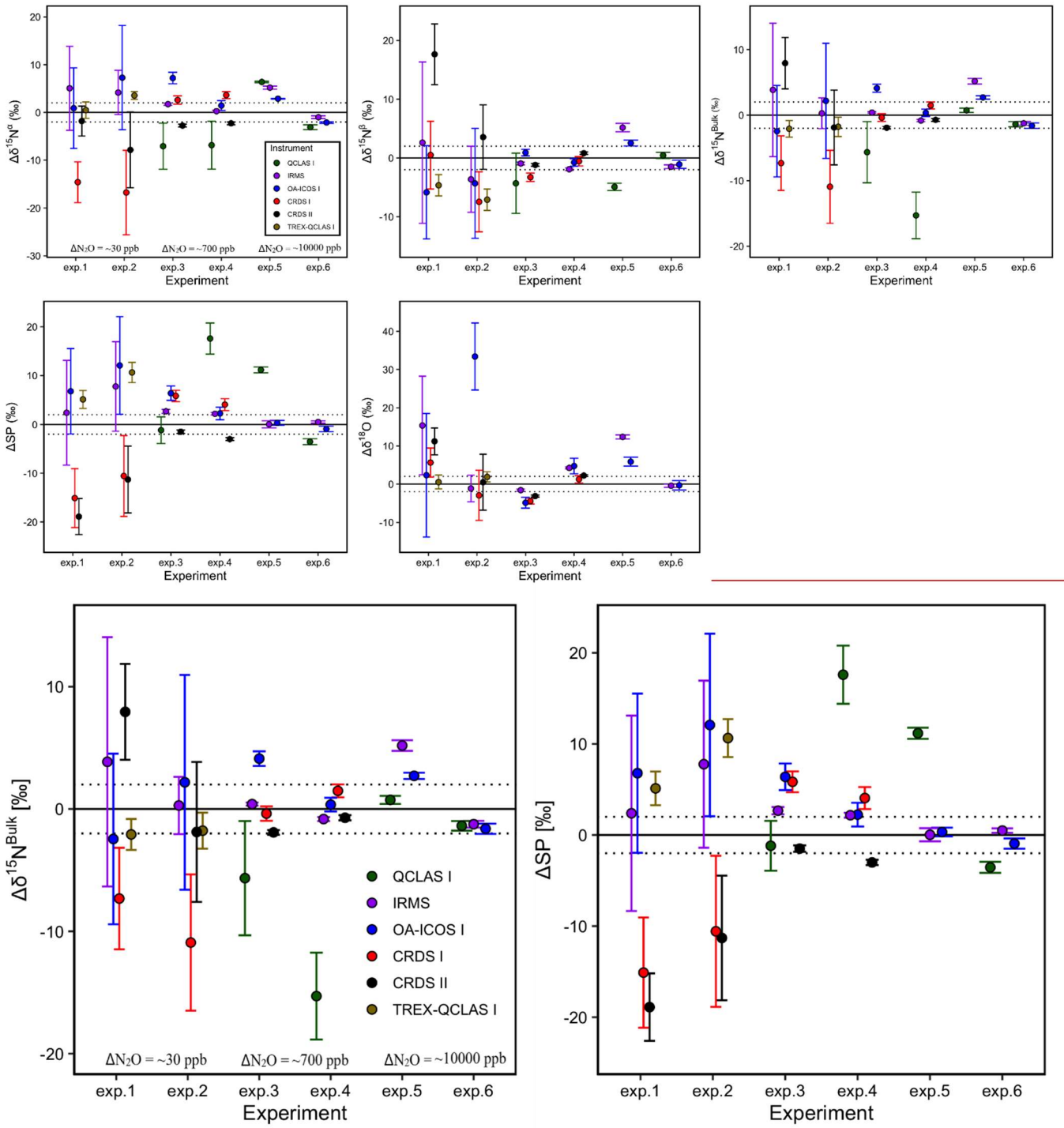


Fig. 147. $\Delta\delta^{15}\text{N}^{\alpha}$, $\Delta\delta^{15}\text{N}^{\beta}$, $\Delta\delta^{15}\text{N}^{\text{bulk}}$, and ΔSP and $\Delta\delta^{18}\text{O}$ ($\text{Estimated}_{\text{Source}} - \text{True}_{\text{Source}}$) values derived from the OA-ICOS I (blue), CRDS I (red), CRDS II (black), QCLAS I (green) and IRMS (purple) via Keeling analysis of the two end-member mixing scenario. The remaining plots for $\delta^{15}\text{N}^{\alpha}$, $\delta^{15}\text{N}^{\beta}$ and $\delta^{18}\text{O}$ are provided in Supplementary Material 4 (Fig. S4-15). $\text{Estimated}_{\text{Source}} = \text{True}_{\text{Source}}$ is indicated by a solid black line at $y = 0$, and the dotted lines indicated $\pm 2\%$ deviation from $y = 0$. The change in concentration exceeding that of the background gas is indicated for experiments 1-2 ($\Delta\text{N}_2\text{O} = \sim 30$ ppb), 3-4 ($\Delta\text{N}_2\text{O} = \sim 700$ ppb) and 5-6 ($\Delta\text{N}_2\text{O} = \sim 10000$ ppb). Note: the QCLAS I results for experiments 1 and 2 are not depicted to maintain clarity, as they exceed the selected y-axis scale.

Table 10. Intercept values obtained by the four analyzers from the Keeling analysis. The error reported is 1 standard error. A 3-point concentration correction was applied to the data. Error ($\text{Source}_{\text{Estimated}} - \text{Source}_{\text{True}}$) represents the error (‰) between the *estimated* source values and the *true* source values. $\Delta\text{N}_2\text{O}$ represents the average concentration difference (ppb) between the highest concentration in each experiment and the *background* based on the measurements recorded by each analyzer.

Experiment sequence	$\Delta\text{N}_2\text{O}$ [ppb]	Instrument					Error ($\text{Source}_{\text{Estimated}} - \text{Source}_{\text{True}}$)				
		OA-ICOS-I									
		$\delta^{15}\text{N}^a$ [‰]	$\delta^{15}\text{N}^b$ [‰]	$\delta^{15}\text{N}^{\text{bulk}}$ [‰]	SP [‰]	$\delta^{18}\text{O}$ [‰]	$\delta^{15}\text{N}^a$ [‰]	$\delta^{15}\text{N}^b$ [‰]	$\delta^{15}\text{N}^{\text{bulk}}$ [‰]	SP [‰]	$\delta^{18}\text{O}$ [‰]
1—Enriched	31.42	71.15 ± 8.44	80.04 ± 7.93	75.62 ± 6.97	-8.84 ± 8.74	131.2 ± 16.16	0.89	-5.84	-2.45	6.79	2.35
2—Depleted	31.26	-37.4 ± 10.91	-37.19 ± 9.34	-36.59 ± 8.78	0.28 ± 10.02	58.65 ± 8.78	7.27	-4.32	2.18	12.08	33.40
3—Depleted	694.22	-18.53 ± 1.19	-22.7 ± 0.56	-20.56 ± 0.60	4.27 ± 1.46	26.49 ± 1.41	7.21	0.92	4.12	6.39	-4.85
4—Enriched	701.46	54.64 ± 1.03	57.21 ± 0.63	55.94 ± 0.56	-2.51 ± 1.30	107.3 ± 2.06	1.43	-0.75	0.35	2.24	4.75
5—Enriched	9831.51	53.3 ± 0.07	56.62 ± 0.49	54.96 ± 0.26	-3.33 ± 0.48	105.1 ± 1.17	2.88	2.54	2.71	0.33	5.88
6—Depleted	9933.59	-26.46 ± 0.16	-24.02 ± 0.70	-25.26 ± 0.42	-2.35 ± 0.56	31.49 ± 1.21	-2.11	-1.08	-1.62	-0.94	-0.30
CRDS-I											
1—Enriched	29.37	55.66 ± 4.27	86.39 ± 5.76	70.75 ± 4.15	-30.73 ± 6.05	134.5 ± 3.81	-14.60	0.51	-7.32	-15.10	5.65
2—Depleted	29.21	-61.43 ± 8.86	-40.32 ± 5.10	-49.69 ± 5.57	-22.37 ± 8.29	22.32 ± 6.54	-16.76	-7.45	-10.92	-10.57	-2.93
3—Depleted	646.99	-23.14 ± 0.86	-26.89 ± 0.73	-25.05 ± 0.59	3.72 ± 1.15	26.89 ± 0.78	2.60	-3.27	-0.37	5.84	-4.45
4—Enriched	651.93	56.83 ± 0.74	57.41 ± 0.8	57.07 ± 0.53	-0.69 ± 1.21	103.8 ± 0.95	3.62	-0.55	1.48	4.06	1.27
CRDS-II											
1—Enriched	29.55	68.45 ± 3.15	103.53 ± 5.16	86.01 ± 3.92	-34.52 ± 3.7	140.05 ± 3.52	-1.81	17.65	7.94	-18.89	11.21
2—Depleted	29.41	-52.51 ± 7.94	-29.32 ± 5.47	-40.65 ± 5.72	-23.1 ± 6.84	25.76 ± 7.31	-7.84	3.55	-1.88	-11.30	0.51
3—Depleted	620.28	-28.49 ± 0.30	-24.8 ± 0.22	-26.59 ± 0.19	-3.61 ± 0.35	28.23 ± 0.24	-2.76	-1.18	-1.91	-1.49	-3.11
4—Enriched	626.24	50.94 ± 0.30	58.78 ± 0.21	54.87 ± 0.21	-7.76 ± 0.29	104.75 ± 0.25	-2.27	0.82	-0.72	-3.01	2.25
QCLAS-I											
1—Enriched	30.52	185.3 ± 84.81	157.7 ± 74.91	172.3 ± 68.04	26.11 ± 59.38	-	115.0	71.81	94.27	41.74	-
2—Depleted	30.48	106.5 ± 68.41	103.3 ± 111.5	102.7 ± 82.67	2.23 ± 76.5	-	151.1	136.2	141.5	14.03	-
3—Depleted	648.35	-32.8 ± 4.83	-27.92 ± 5.12	-30.33 ± 4.67	-3.3 ± 2.74	-	-7.07	-4.30	-5.65	-1.18	-
4—Enriched	654.63	46.36 ± 5.03	34.08 ± 2.84	40.29 ± 3.55	12.85 ± 3.19	-	-6.85	-23.88	-15.30	17.60	-
5—Enriched	9231.17	56.8 ± 0.17	49.17 ± 0.63	52.99 ± 0.33	7.51 ± 0.61	-	6.38	-4.91	0.74	11.17	-
6—Depleted	9323.02	-27.44 ± 0.48	-22.49 ± 0.53	-25.02 ± 0.39	-4.96 ± 0.61	-	-3.09	0.45	-1.38	-3.55	-
Trex-QCLAS-I											
1—Enriched	32.38	73.95 ± 1.71	86.49 ± 1.80	80.20 ± 1.27	-12.54 ± 1.85	134.3 ± 1.81	0.48	-4.64	-2.10	5.12	0.55
2—Depleted	34.14	-44.84 ± 0.83	-41.78 ± 1.83	-43.31 ± 1.47	-3.02 ± 2.08	25.96 ± 1.33	3.55	-7.09	-1.79	10.64	1.90
GC-IRMS											
1—Enriched	30.14	75.31 ± 8.78	88.49 ± 13.71	81.93 ± 10.19	-13.24 ± 10.73	144.2 ± 12.88	5.06	2.61	3.86	2.39	15.35
2—Depleted	30.43	-40.50 ± 4.63	-36.49 ± 5.61	-38.48 ± 2.34	-4.02 ± 9.17	24.12 ± 3.46	4.17	-3.62	0.27	7.77	-1.13
3—Depleted	668.62	-24.00 ± 0.23	-24.55 ± 0.25	-24.28 ± 0.12	0.55 ± 0.40	29.77 ± 0.27	1.74	-0.93	0.40	2.67	-1.57
4—Enriched	674.33	53.48 ± 0.19	56.05 ± 0.23	54.76 ± 0.16	-2.57 ± 0.27	106.7 ± 0.26	0.26	-1.91	-0.82	2.17	4.24
5—Enriched	8540.91	55.62 ± 0.33	59.25 ± 0.73	57.44 ± 0.44	-3.63 ± 0.72	111.5 ± 0.51	5.20	5.17	5.19	0.03	12.37
6—Depleted	8958.53	-25.35 ± 0.29	-24.43 ± 0.32	-24.89 ± 0.28	-0.92 ± 0.24	31.38 ± 0.39	-1.00	-1.49	-1.24	0.49	-0.41

15 4 Discussion

4.1 Factors affecting the precision and accuracy of N_2O isotopocule measurements using laser spectroscopy

A summary of results is presented in Table 8. Our results highlight that the precision at which laser-based analyzers acquire N_2O isotopocule measurements is a function of N_2O mole fraction, the selected measuring and averaging times and calibration frequency according to measurement stability. The degree

of accuracy obtained using different laser spectrometers is ultimately a function of the robustness of corrections aimed at removing matrix and trace gas effects, and the selected calibration procedure aimed at standardizing the data to international scales. The temperature sensitivities of all analyzers tested necessitates that, especially when such instruments are deployed in the field, laser spectrometers in general be operated under temperature-controlled conditions (such as in maintained field stations), and/or their dependence adequately characterized and corrected. The degree of accuracy obtained using different laser spectrometers is ultimately a function of the robustness of corrections aimed at removing matrix and trace gas effects, and the selected calibration procedure aimed at standardizing the data to international scales.

Table 8. Summary of main findings presented in this study.

Detection scheme (model; manufacturer)	OA-ICOS I (N2OIA-30e-EP)	CRDS I & II (G5131-i)	QCLAS I (CW-QC-TILDAS-SC-D)	TREX-QCLAS I (CW-QC-TILDAS-76-CS)
Allan precision (300 s)				
$\delta^{15}\text{N}^a$, $\delta^{15}\text{N}^b$, $\delta^{18}\text{O}$ [‰]				
326.5 ppb N_2O	0.79 – 1.69	0.32 – 0.46	0.39 – 3.45 ^{a)}	n.d.
~ 1000 ppb N_2O	0.28 – 0.67	0.21 – 0.89	0.19 – 0.83 ^{a)}	n.d.
~ 10000 ppb N_2O	0.12 – 0.17	n.d.	0.02 – 0.48 ^{a)}	n.d.
Repeatability (326.5 ppb N_2O)				
N_2O [ppb]	0.07	0.26 – 0.30	0.16	1.29
$\delta^{15}\text{N}^a$, $\delta^{15}\text{N}^b$, $\delta^{18}\text{O}$ [‰]	1.19 – 2.17	0.52 – 0.83	5.35 – 8.57	0.37 – 0.60
Temperature effect (326.5 ppb N_2O)				
N_2O [ppb K^{-1}]	0.01	0.02	0.10	n.d.
$\delta^{15}\text{N}^a$, $\delta^{15}\text{N}^b$, $\delta^{18}\text{O}$ [‰ K^{-1}]	0.36 – 2.60	0.25 – 0.65	31.29 – 37.32	n.d.
N_2O mole fraction dependence				
$\delta^{15}\text{N}^a$, $\delta^{15}\text{N}^b$, $\delta^{18}\text{O}$ [‰ ppb ($\Delta 1/\text{N}_2\text{O}$)]	-8296 – 2544	-458 – 1353	-66386 – 15833	n.d.
O_2 matrix effect (330 ppb N_2O)				
N_2O [ppb % ⁻¹ (ΔO_2)]	-0.044	0.24 – 0.305	0.351	n.s.
$\delta^{15}\text{N}^a$, $\delta^{15}\text{N}^b$, $\delta^{18}\text{O}$ [‰ % ⁻¹ (ΔO_2)]	0.874 – 1.270	-0.279 – (-1.364)	-1.111	n.s.
CO_2 trace gas effects (330 ppb N_2O)				
N_2O [ppb ppm ⁻¹ (ΔCO_2)]	0.0011	0.0005	n.s.	n.s.
$\delta^{15}\text{N}^a$, $\delta^{15}\text{N}^b$, $\delta^{18}\text{O}$ [‰ ppm ⁻¹ (ΔCO_2)]	-0.009 – 0.026	n.s. – (-0.0019)	n.s. – 0.0154	n.s.
CH_4 trace gas effects (330 ppb N_2O)				
N_2O [ppb ppm ⁻¹ (ΔCH_4)]	n.s. ^{b)}	-0.039 – (-0.056)	n.s. ^{b)}	n.s. ^{b)}
$\delta^{15}\text{N}^a$, $\delta^{15}\text{N}^b$, $\delta^{18}\text{O}$ [‰ ppm ⁻¹ (ΔCH_4)]	0.173	0.085 – 2.50	n.s.	n.s.
CO trace gas effects (330 ppb N_2O)				
N_2O [ppb ppm ⁻¹ (ΔCO)]	-0.29	-0.15 – (-0.24)	-0.19	n.s.
$\delta^{15}\text{N}^a$, $\delta^{15}\text{N}^b$, $\delta^{18}\text{O}$ [‰ ppm ⁻¹ (ΔCO)]	n.s.	-0.53 – (-2.41)	n.s. – (-4.04)	n.s.

a) Includes QCLAS I, II and III

b) Likely due to inaccuracies during dynamic dilution (see text for details)

n.d. not determined

n.s. not statistically significant at $p < 0.05$ and/or $r^2 < 0.5$

All spectrometers tested displayed temperature effects on isotope measurements, which can be attributed to differences in the lower state energies of the probed N_2O isotopocule lines (Supplementary Material 11) (e.g. Wächter et al. 2008). The temperature sensitivities of all analyzers tested necessitates that, especially when deployed in the field, they be operated under temperature-controlled conditions (such as in maintained field stations).

The experiments performed in this study were undertaken using a standardized protocol. Calibration was performed on isotope δ values derived from raw uncalibrated isotopocule amount fractions, thus requiring

[N₂O] dependence corrections. Alternative approaches aimed at calibrating isotopocule amount fractions prior to deriving δ values were not included in our study, but have the potential to remove the need for this correction (e.g. Wen et al., 2013; Flores et al., 2017; Griffith, 2018) if appropriate reference materials become available. The experiments performed in this study were undertaken using a standardized protocol, including a two point δ calibration, with which we could compare instrument performance. In cases where calibrations are performed on the derived isotope ratios or δ values, [N₂O] dependence corrections should span the range of expected N₂O mole fractions and account for non-linear effects (e.g. Winther et al. 2018). Alternative calibration approaches based on isotopocule concentrations or ratio calibration procedures were not included in our study, but have the potential to remove the need for this correction (e.g. Wen et al., 2013; Flores et al., 2017; Griffith, 2018). Isotopocule calibration approaches would require a set of N₂O standard gases with high accuracy mole fractions in addition to assigned δ values.

All analyzers tested in this study showed significant effects from changing O₂ composition of the gas matrix. Although the magnitude of this effect ultimately varied across the analysers and was dependent on N₂O mixing ratios, the effect of a change in O₂ composition of 20.5 % was typically on the order of 10 to 30 % for δ values. Similar O₂ dependencies have been reported by Erler et al. (2015) for CRDS N₂O isotope laser spectrometers, as well as for CRDS H₂O isotope analyzers (Johnson and Rella, 2017). The underlying reason for this effect is differences in N₂ versus O₂ (and Ar) broadening parameters of the probed N₂O isotopocule lines. In short, the N₂, O₂ (and Ar) broadening parameters depend on rotational quantum numbers of the respective N₂O lines (Henry et al., 1985; Supplementary Material 11). Thus, differences in the rotational quantum numbers for a pair of isotopocules (e.g. ¹⁴N¹⁵N¹⁶O / ¹⁴N¹⁴N¹⁶O) relate to a difference in their N₂, O₂ and Ar broadening parameters. Consequently, differences in the O₂ or Ar content of the sample gas matrix and that of the reference gas affect measured isotope ratios and lead to changes in apparent delta values. Nonetheless, Notably, the magnitude of effects reported for the CRDS analyzers in this study varied across CRDS I (a 2015 model) and CRDS II (a 2018 model), as well as from those reported by Erler et al. (2015). Therefore, we recommended that in applications where O₂ concentrations vary, such as groundwater, estuaries, stratified waterbodies, and incubation studies, researchers test individual analyzers for their specific dependencies to allow for correction. This is especially important given that N₂O production and reduction processes in such environments are strongly controlled by O₂ availability. Although the Ar effects characterized in this study were not large, it is nonetheless recommended as a precautionary measure that researchers ensure, where possible, the standard calibration gas Ar composition is similar to that of the sample gas.

The CO₂ effects for OA-ICOS and CH₄ effects for CRDS analyzers must be considered for applications of these analyzers where CO₂ and CH₄ may also co-vary, such as during diel atmospheric monitoring, in

soil-flux chamber measurements, incubation studies and even waterbodies (e.g. Erler et al. 2015). These effects need to be either characterized and corrected for by the user, or the interfering gas quantitatively removed. To our knowledge, there is currently no commercially-available technique to remove CH₄ from a gas stream without affecting N₂O, and therefore independent co-analysis of CH₄ is ultimately required to correct for these effects post-measurement. Similarly, while water vapor effects can in theory be characterized and corrected for all instruments, we recommend that researchers remove water vapor from the gas stream prior to analysis. Although not tested here, other studies have highlighted possible spectral interference effects associated with elevated H₂S and volatile organic compounds (Erler et al., 2015; Ostrom and Ostrom, 2017), but these may also be removed from gas streams using chemical traps (e.g. Cu and activated carbon traps, respectively).

The scaling of gas matrix and trace gas effects with [N₂O] has important implications for any measurement setup that relies on post-measurement correction equations. An equation developed to correct for CH₄ effects that was derived using a [N₂O] of 330 ppb should not be implemented for a sample gas containing 990 ppb N₂O. For example, as shown in Fig. 8, the measured interference effect on $\delta^{15}\text{N}^a$ measurements acquired using CRDS II for 10 ppm [CH₄] at 330 ppb N₂O was 24.9 ‰, while at 990 ppb N₂O it was 8.1 ‰, resulting in a 16.8 ‰ difference. The scaling of interference effects from trace gases has been reported previously for CO₂/CH₄ laser spectrometers (Assan et al., 2017; Malowany et al., 2015). This underlines the usefulness of removing H₂O, CO₂ and CO with scrubbers prior to measurement, as this removes the need for correction equations to begin with and the scaling of corrections that can ensue. We are unaware of any studies that have shown that O₂ interferences caused by pressure broadening linewidth effects change as a function of N₂O mole fraction. While we were unable to describe the scaling of the O₂ effect sufficiently using correction functions based on theoretical deductions, empirical equations based on experimental testing such as those developed in Sects. 3.5.2 and 3.6.2, could be implemented by researchers when co-variation in both O₂ and N₂O in the sample gas is expected. Alternatively, as shown in this study, matrix and/or trace gas effects can be removed by automated N₂O preconcentration devices such as TREX (Ibraim et al., 2018; Mohn et al., 2010), similar to IRMS. However, such devices are not commercially available, complex to build and operate, and restrict sample frequency.

4.2 Pre-measurement considerations

Our study clearly shows that knowledge/estimation of the matrix and trace gas composition of both reference standards and sample gases, and the differences between them, are critical for accurate N₂O isotopocule analysis using laser spectroscopy. We acknowledge, however, that this may be difficult to predict in certain applications without prior testing of the sample gas, and therefore researchers should err on the side of caution.

As a pre-requisite to acquiring measurements using N₂O isotope laser spectrometers, researchers will be required to consider the accessory gas mixtures required to characterize their instrument. For applications with significant variations in matrix (O₂, Ar) or trace gas (CO₂, CH₄, CO) compositions, researchers will

5 require gas mixtures containing the gas of interest in order to characterize the associated interference effects for their laser spectrometer. This also necessitates that appropriate interference detectors are implemented, especially O₂ and CH₄ analyzers given that these effects cannot be mitigated using chemical traps.

10 In this study, interference effects, and the associated scaling of these effects according to the co-measured N₂O mole fraction, were derived via dynamic dilution with various gas mixtures using MFCs. This allowed for the introduction of a wide range of gas mixtures to the analyzers for interference testing, and consequently only a small amount of gas mixtures were required for all of the experiments outlined in Sect. 2.4. In comparison, a much larger number of individual gas mixtures would have been required had

15 they been prepared using static dilution techniques (see Erler et al. 2015). The scaling of interference effects were sufficiently distinguished by undertaking testing at three different N₂O mole fractions (N₂O = 330, 660 and 990 ppb), and we therefore recommend this as a minimum criterion for researchers wishing to characterize this effect.

20 Researchers should also consider the sample gas volume required for a given measurement application using a specific laser spectrometer. In our experience, ensuring that five laser cavity cell volumes have been flushed prior to measurement is *best practice* to negate any memory effects when these instruments are operated using continuous flow-through configurations (as opposed to discrete sample measurements in a closed laser cavity). By following this procedure and using the operating parameters selected in this

25 study (Table 1), the sample gas volume required for a single 300 s measurement is approximately 80 mL for CRDS II, 150 mL for CRDS I, 600 mL for OA-ICOS I and 1200 mL for QCLAS I. By comparison, TREX-QCLAS I requires approximately 5 L of sample gas to allow for N₂O preconcentration. These sample gas volumes represent typical numbers for atmospheric applications; however, instrument parameter settings such as flow rate and cell pressure, which ultimately change the required sample

30 volume, can be optimized depending on the measurement application. This is particularly the case for QCLAS instruments, which can be operated with different user-adjustable settings. For applications requiring discrete sample analysis (e.g. the headspace analysis of $\delta^{15}\text{N}$ and $\delta^{18}\text{O}$ in N₂O derived from dissolved NO₃⁻), high N₂O concentration gas samples with lower volumes can be introduced to these

35 instruments using injection ports and dilution gases (e.g. Soto et al., 2015; Wassenaar et al., 2018); however we did not test these capabilities in our study.~~Researchers should also consider the sample gas volume required for a given measurement application using a specific laser spectrometer. In our~~

experience, ensuring that five laser cavity cell volumes have been flushed prior to measurement is *best practice* to negate any memory effects during a measurement run. By following this procedure and using the operating parameters selected in this study, the sample gas volume required for a single 300-s measurement is approximately 84 mL for CRDS II, 147 mL for CRDS I, 603 mL for OA-ICOS I and 1170 mL for QCLAS I. The different sample volumes required for CRDS I and CRDS II is due to the different selected flow rates. By comparison, TREX-QCLAS I requires approximately 5 L of sample gas to allow for N₂O preconcentration. Thus, users should carefully consider the available volume of the sample gas, although the possibility exists to dilute high concentration samples to increase gas volume. Researchers should also ensure that gas samples contain N₂O within the operational ranges of the different laser spectrometers (Table 1).

4.3 Measurement workflow

In-line with our results, we propose a step-by-step workflow that can be followed by researchers to acquire N₂O isotopocule measurements: (Fig. 15). This workflow seeks to cover all sources of potential error tested in our study. Not all steps will be applicable because interference effects vary across analyzers. For QCLAS analyzers, which offer high versatility, interference effects can also be approached by multi-line analysis, inclusion of interfering spectral lines or adaption of pressure broadening parameters in the spectral fitting algorithm. For specific applications, such as incubation experiments with He, accessory injection units and setups using TREX, related actions have to be taken. While we tested several mono-variant (e.g. changes in [CH₄] at constant [N₂O]) and some bi-variant (e.g. changes in [CH₄] and [N₂O]) systems in our study, more complex systems (e.g. changes in [CH₄], [O₂] and [N₂O]) were not tested, and deviations from additive behavior are to be expected. Depending on the desired precision, users may vary the measurement and averaging times, and calibration frequency.

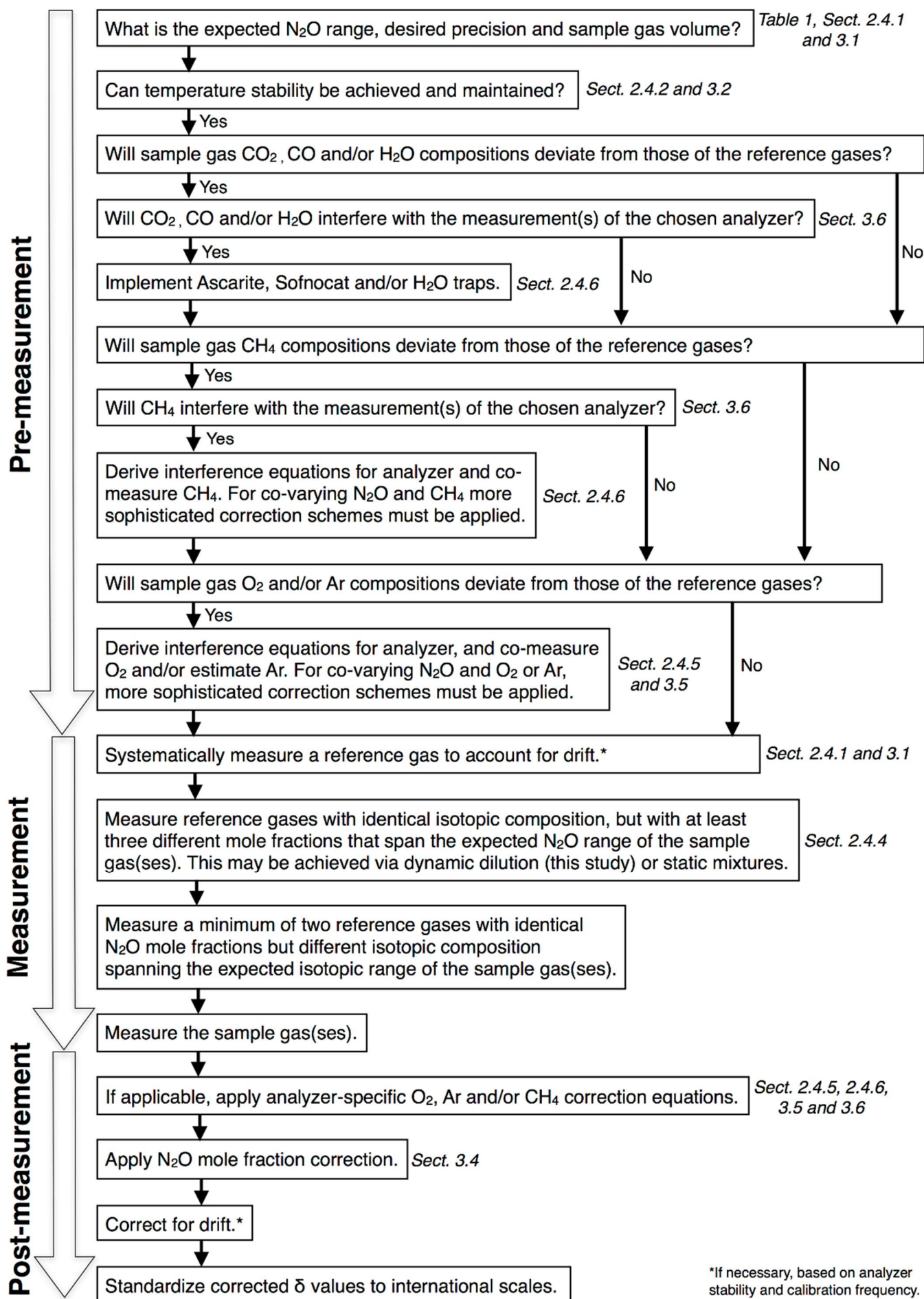


Fig. 15. Proposed measurement workflow for the operation of N₂O isotope laser spectrometers. Relevant sections of this study are shown next to each step.

1. ~~Prior to any measurement, consider the expected N₂O range, desired precision, volume of sample gas required and temperature stability, and evaluate whether the preceding is implementable with the desired laser spectrometer.~~
2. ~~Implement H₂O, CO₂ and CO scrubbers into the measurement setup.~~
3. ~~Consider whether the O₂, Ar and/or CH₄ composition of the sample gas is likely to differ to that of the reference gas. If no, proceed to Step 5.~~
4. ~~Co-analyze O₂ and CH₄ in the sample gas so that post-measurement correction can be made. Appropriate calibration of O₂ and CH₄ analyzers should be undertaken. Ar compositional differences can be estimated based on the reference standard gas matrix composition.~~
5. ~~During the measurement run, analyze a minimum of two reference gases whose isotopic composition span the expected isotope compositions. Systemic measurement of a gas cylinder can be used to account for drift. If measurements are to be calibrated on derived ratio or δ values, mole fraction dependence must be characterized using a minimum three-point procedure, although more points may be required to account for non-linear effects. The frequency at which this step is implemented should be in line with the analyzer stability.~~
6. ~~Analyze the sample gas. Best precision can be gained with optimized analysis time and replication of analysis.~~
7. ~~Quantify the difference in [O₂], [Ar] and/or [CH₄] between the sample and reference gas. If [N₂O] = ~330 ppb, go to step 8. If [N₂O] > ~330 ppb, go to Step 9. If there is no difference in [O₂], [Ar] and/or [CH₄] between the sample and reference gas, go to Step 10.~~
8. ~~Apply analyzer-specific matrix and/or trace gas corrections derived when the co-measured [N₂O] = ~330 ppb. Interference effect equations may be derived prior to or post sample gas measurement.~~
9. ~~Apply analyzer specific matrix and/or trace gas coefficients to scale correction equations according to [N₂O]. Interference effect equations may be derived prior to or post sample gas measurement, and effects should be derived at a minimum three N₂O mole fractions (for example, when N₂O = 330, 660 and 990 ppb).~~
10. ~~Correct data, if applicable, for [N₂O] dependence.~~
11. ~~If required, apply drift correction.~~
12. ~~Standardize δ values to international scales using desired method (e.g. Gröning, 2018; Wen et al. 2013).~~

4.4 What degree of accuracy can be achieved using this workflow?

The simulated two end-member mixing experiments conducted in this study show that, when the workflow proposed above is applied, accuracy within $\pm 0.5\%$ can be achieved for TREX-QCLAS, ± 0.4 – 1.6% for CRDS analyzers, and ± 1.6 – 3.6% for OA-ICOS analyzers. Likewise, the comparison between the laser spectrometers and IRMS highlights that cross-technique compatibility within ± 1 – 2.5% can be

achieved for most N₂O isotopocule measurements. However, it is clear that the balanced (i.e. non analyzer-specific) approach applied for the purpose of this comparative study did not cater to QCLAS I. Therefore, a more specific calibration protocol for the QCLAS I will likely yield better performance, as shown in [Supplementary Material 3 Table 6](#). It is worth noting that, although the results of our study are representative of the performance of the instruments tested, the magnitude of reported effects and performances are likely to vary within the same analyzer models.

Whilst the laboratory-simulated mixing experiment is not fully representative of naturally-occurring two end-member mixing *per se*, the results are useful in comparing intercept accuracy and uncertainty amongst analyzers and against IRMS. Our results show that large uncertainties exist for N₂O source apportionment using Keeling analysis performed at near-ambient N₂O mole fractions. Given the amount of corrections that are required in the experiment, we have not detailed individual analyzer uncertainty budgets to quantify individual sources of error on the intercept, as it is beyond the scope of this study. Nonetheless, the reduction of uncertainty with increasing Δ N₂O shown in experiments 1–6 in Sect. 3.7 has also been shown in previous studies (e.g. Wolf et al., 2015). Therefore, by extension, it is reasonable to assume that the current largest source of uncertainty for ambient N₂O measurements using laser spectroscopy is the inherent signal-to-noise ratio of the measurement.

5 Conclusions

In this study, we characterized and compared N₂O isotope laser-based analyzers with the three most common detection schemes, including OA-ICOS, CRDS and QCLAS. Our results show a number of factors that need to be carefully considered to ensure precise and accurate measurements of N₂O isotopocules using laser spectroscopy. The performance of N₂O isotope laser spectrometers depends on a complex interplay between instrumental precision, drift, matrix gas composition and associated spectral interferences that ultimately vary as a function of N₂O mole fraction. On this basis, we echo recommendations from Ostrom and Ostrom (2017), who cautioned not to underestimate the need for the careful consideration of analyzer-specific corrections. These analyzers clearly do not represent “plug and play” devices – instead, one needs to carefully consider the desired application, precision and accuracy, and develop appropriate calibration strategies to achieve these outcomes.

Consequently, we recommend calibration schemes that have: (1) a calibration frequency that is adequate for constraining instrument drift over experimental period/long-term measurements; (2) temperature stability during measurement, or the temperature effect adequately characterized and corrected; (3) a three-point or higher [N₂O] effect correction that spans the range of expected [N₂O] (if calibration relies on raw δ values derived from uncalibrated isotopocule amount fractions; i.e. a δ -calibration

~~approach relies on ratio or δ values, rather than isotopocule abundance~~); and (4) accounted for the differences in matrix and trace gas composition between the sample gas and reference gases, whereby either analyzer-specific interference corrections have been carefully characterized and applied, or where possible interfering substances (CO_2 , CO , H_2O) removed using chemical traps. Correcting for interference effects becomes significantly more complicated once $[\text{N}_2\text{O}]$ exceed ambient levels, requiring a multitude of analyzer- and gas-specific constants that inevitably increase the number of gas mixtures required by the user, as well as the uncertainty of the measurement. Researchers should therefore strive to implement measurement setups that require as few corrections as possible, and this will inherently decrease the combined uncertainty in the measurement.

~~It is important to note that the results of this study should be interpreted for these analyzer models only, and results are likely to vary slightly across the same make. Newer analyzers and models may yield better performance than reported here. As illustrated by the noticeable improvement between the CRDS I (2015 model) and CRDS II (2018 model), it is foreseeable that the performance of N_2O isotope laser spectrometers will continue to improve into the future. Future studies should focus on quantifying the error contributions to N_2O isotopocule analysis using laser spectroscopy.~~

Author contributions. SH and JL, guided by JM, designed the study, established the setup and coordinated the experiments. Responsibilities on the analyzers were as follows: SH, BK and DC OA-ICOS; JL and TB CRDS I; LX and BW QCLAS I and CRDS II; JW and KZ TREX-QCLAS I; MB and JS QCLAS II, QCLAS III and GC-IRMS. JM prepared the non-commercial gas mixtures used in this study. LY referenced the δ values of applied gas mixtures to international scales. SH and JL performed the main data analysis and together with JM developed correction algorithms. SH and JL wrote the manuscript with input from all co-authors.

Data availability. All data are available from the corresponding author upon request.

Competing interests. The authors declare that they have no conflict of interest.

Acknowledgements. We extend our thanks to Doug Baer, Rob Provencal and Frederick Despagne from ABB Los Gatos Research Inc., Renato Winkler, Magdalena Hofmann and Paulos Getachew from Picarro Inc., and Dave Nelson and Barry McManus from Aerodyne Research Inc. for their helpful discussions and assistance concerning the analyzers. We thank Christoph Zellweger for his assistance analysing matrix gas cylinders and providing the Picarro G2401 for matrix interference testing, and the NABEL laboratory at Empa for providing the dew point generator for water vapor testing. We want to thank Kristýna Kantnerová from Empa and Daniel Zindel from ETH for the synthesis of ^{18}O -labelled N_2O .

This study was supported by the European Metrology Programme for Innovation and Research (EMPIR) 16ENV06 project “Metrology for Stable Isotope Reference Standards (SIRS)”. The EMPIR initiative is co-funded by the European Union's Horizon 2020 research and innovation programme and the EMPIR Participating States. Furthermore, this research was supported by grants from the Cotton Research and Development Corporation (CRDC), and was facilitated by an Endeavour Research Fellowship acquired by Stephen Harris from the Australian Government. Stephen Harris is supported by PhD scholarships from the Australian Government, the Australian Institute of Nuclear Science and Engineering (AINSE), Australian Nuclear Science and Technology Organisation (ANSTO) and CRDC. The UNSW Sydney N₂OIA-30e-EP was purchased using funds from the Australian National ~~Groundwater Infrastructure Scheme~~Collaborative Research Infrastructure Strategy (NCRIS) Groundwater Infrastructure Project. Jing Wei and Longfei Yu were supported by the Swiss National Science Foundation (SNSF) within grant CRSII5_170876 and 200021_163075 as well as the ~~by the~~ EMPAPOSTDOCS-II programme, which received funding from the European Union’s Horizon 2020 research and innovation programme under the Marie Skłodowska-Curie grant agreement number 754364.

References

- ABB-Los Gatos Research Inc.: Off-Axis Integrated Cavity Output Spectroscopy (OA-ICOS), available at <http://www.lgrinc.com/advantages/>, 2019.
- Allan, D.: Statistics of atomic frequency standards, *Proc. IEEE*, 54, 221–230, 1966.
- Anderson, B., Bartlett, K., Frolking, S., Hayhoe, K., Jenkins, J., and Salas, W.: Methane and Nitrous Oxide Emissions from Natural Sources, Office of Atmospheric Programs, US EPA, EPA 430-R-10-001, Washington DC, 2010.
- Assan, S., Baudic, A., Guemri, A., Ciais, P., Gros, V., and Vogel, F.R.: Characterization of interferences to in situ observations of $\delta^{13}\text{CH}_4$ and C_2H_6 when using a cavity ring-down spectrometer at industrial sites, *Atmos. Meas. Tech.*, 10, 2077–2091, doi: 10.5194/amt-10-2077-2017, 2017.
- Baer, D. S., Paul, J. B., Gupta, M., and O’Keefe, A.: Sensitive absorption measurements in the near-infrared region using off-axis integrated-cavity-output spectroscopy, *Appl. Phys. B-Lasers O.*, 75, 261–265, doi:10.1007/s00340-002-0971-z, 2002.
- Baggs, E.M.: A review of stable isotope techniques for N₂O source partitioning in soils: recent progress, remaining challenges and future considerations, *Rapid Communications in Mass Spectrometry*, 22, 1664–1672, doi: 10.1002/rcm.3456, 2008.
- Berden, G., Peeters, R. and Meijer, G.: Cavity ring-down spectroscopy: Experimental schemes and applications, *Int. Rev. Phys. Chem.*, 19, 565–607, doi: 10.1080/014423500750040627, 2000.
- Bernard, S., Röckmann, T., Kaiser, J., Barnola, J.-M., Fischer, H., Blunier, T., and Chappellaz, J.: Constraints on N₂O budget changes since pre-industrial time from new firn air and ice core isotope measurements, *Atmos. Chem. Phys.*, 6, 493–503, doi:10.5194/acp-6-493-2006, 2006.

- Bouwman, A. F., Boumans, L. J. M., and Batjes N. H.: Modeling global annual N₂O and NO emissions from fertilized fields, *Global Biogeochem. Cycles*, 16, 1080, doi:10.1029/2001GB001812, 2002.
- 5 Bowling, D. R., Burns, S. P., Conway, T. J., Monson, R. K., and White, J. W. C.: Extensive observations of CO₂ carbon isotope content in and above a high-elevation subalpine forest, *Global Biogeochem. Cy*, 19, GB3023, doi:10.1029/2004gb002394, 2005.
- 10 Bowling, D. R., Sargent, S. D., Tanner, B. D., and Ehleringer, J. R.: Tunable diode laser absorption spectroscopy for stable isotope studies of ecosystem-atmosphere CO₂ exchange, *Agr. Forest Meteorol.*, 118, 1–19, doi:10.1016/s0168-1923(03)00074-1, 2003.
- 15 Brase, L., Bange, H.W., Lendt, R., Sanders, T., and Dähnke, K.: High Resolution Measurements of Nitrous Oxide (N₂O) in the Elbe Estuary, *Front. Mar. Sci.*, 4, 162, doi:10.3389/fmars.2017.00162, 2017.
- Buchen, C., Lewicka-Szczebak, D., Flessa, H. and Well, R.: Estimating N₂O processes during grassland renewal and grassland conversion to maize cropping using N₂O isotopocules, *Rapid Commun Mass Spectrom*, 32, 1053–1067, doi:10.1002/rcm.8132, 2018.
- 20 Decock, C. and Six, J.: How reliable is the intramolecular distribution of ¹⁵N in N₂O to source partition N₂O emitted from soil?, *Soil Biol. Biochem.*, 65, 114–127, doi: 10.1016/j.soilbio.2013.05.012, 2013.
- 25 Denk, T.R., Mohn, J., Decock, C., Lewicka-Szczebak, D., Harris, E., Butterbach-Bahl, K., Kiese, R., and Wolf, B.: The nitrogen cycle: A review of isotope effects and isotope modeling approaches, *Soil Biol Biochem.*, 105, 121–137, doi:10.1016/j.soilbio.2016.11.015, 2017.
- 30 Denman, K. L., Brasseur, G., Chidthaisong, A., Ciais, P., Cox, P. M., Dickinson, R. E., Hauglustaine, D., Heinze, C., Holland, E., Jacob, D., Lohmann, U., Ramachandran, S., da Silva Dias, P. L., Wofsky, S. C., and Zhang, X.: Couplings between changes in the climate system and biogeochemistry, in: *Climate change 2007, the physical science basis, contribution of working group I to the Fourth Assessment Report of the Intergovernmental Panel on Climate Change*, edited by: Solomon, S., Qin, D., Manning, M., Chen, Z., Marquis, M., Averyt, K. B., Tignor, M., and Miller, H. L., Cambridge University Press, Cambridge, United Kingdom and New York, NY, USA, 499–587, 2007.
- 35 Erler, D.V., Duncan, T.M., Murray, R., Maher, D.T., Santos, I.R., Gatland, J.R., Mangion, P., and Eyre, B.D.: Applying cavity ring-down spectroscopy for the measurement of dissolved nitrous oxide mole fractions and bulk nitrogen isotopic composition in aquatic systems: Correcting for interferences and field application, *Limnol Oceanogr Methods*, 13, 391–401, doi:10.1002/lom3.10032, 2015.
- 40 Eyer, S., Tuzson, B., Popa, M.E., Van Der Veen, C., Röckmann, T., Rothe, M., Brand, W.A., Fisher, R., Lowry, D., Nisbet, E.G., and Brennwald, M.S.: Real-time analysis of δ¹³C- and δD-CH₄ in ambient air with laser spectroscopy: method development and first intercomparison results, *Atmos. Meas. Tech.*, 9, 263–280, doi:10.5194/amt-9-263-2016, 2016.
- 45 Flores, E., Viallon, J., Moussay, P., Griffith, D.W., and Wielgosz, R.I.: Calibration strategies for FT-IR and other isotope ratio infrared spectrometer instruments for accurate δ¹³C and δ¹⁸O measurements of CO₂ in air, *Anal. Chem.*, 89, 3648–3655, doi:10.1021/acs.analchem.6b05063, 2017.
- 50 Forster, P., Ramaswamy, V., Artaxo, P., Berntsen, T., Betts, R., Fahey, D. W., Haywood, J., Lean, J., Lowe, D. C., Myhre, G., Nganga, J., Prinn, R., Raga, G., Schulz, M., and Van Dorland, R.: *Climate Change 2007: Changes in Atmospheric Constituents and in Radiative Forcing*, The Physical Science Basis: Contribution of Working Group I to the Fourth Assessment Report of the Intergovernmental Panel on Climate Change, edited by: Solomon, S., Qin, D., Manning, M., Chen, Z., Marquis, M., Averyt, K. B., Tignor, M., and Miller, H. S., Cambridge University Press, Cambridge, UK, New York, NY, USA, 2007.

- 5 Friedrichs, G., Bock, J., Temps, F., Fietzek, P., Körtzinger, A., and Wallace, D.W.: Toward continuous monitoring of seawater $^{13}\text{CO}_2/^{12}\text{CO}_2$ isotope ratio and pCO_2 : Performance of cavity ringdown spectroscopy and gas matrix effects, *Limnol Oceanogr–Meth*, 8, 539–551, doi: 10.4319/lom.2010.8.539, 2010.
- 10 Griffis, T. J., Baker, J. M., Sargent, S. D., Tanner, B. D., and Zhang, J.: Measuring field-scale isotopic CO_2 fluxes with tunable diode laser absorption spectroscopy and micrometeorological techniques, *Agr. Forest Meteorol.*, 124, 15–29, doi:10.1016/j.agrformet.2004.01.009, 2004.
- 15 Griffith, D. W. T., Deutscher, N. M., Caldwel, C., Kettlewell, G., Riggensbach, M., and Hammer, S.: A Fourier transform infrared trace gas and isotope analyser for atmospheric applications, *Atmos. Meas. Tech.*, 5, 2481–2498, doi:10.5194/amt-5-2481-2012, 2012.
- 20 Griffith, D. W.: Calibration of isotopologue-specific optical trace gas analysers: a practical guide, *Atmos. Meas. Tech.*, 11, 6189–6201, doi:10.5194/amt-11-6189-2018, 2018.
- 25 Gröning, M.: TEL Technical Note No. 01. SICalib User Manual (Stable Isotope Calibration for routine δ -scale measurements) Ver 2.16j, 2018.
- 30 Harris, E., Henne, S., Hüglin, C., Zellweger, C., Tuzson, B., Ibraim, E., Emmenegger L., and Mohn J.: Tracking nitrous oxide emission processes at a suburban site with semicontinuous, in situ measurements of isotopic composition, *J. Geophys. Res. Atmospheres*, 122, 1850–1870, doi: 10.1002/2016JD025906, 2017.
- 35 Harris, E., Joss, A., Emmenegger, L., Kipf, M., Wolf, B., Mohn, J. and Wunderlin, P.: Isotopic evidence for nitrous oxide production pathways in a partial nitrification-anammox reactor, *Water Res.*, 83, 258–270, doi:10.1016/j.watres.2015.06.040, 2015a.
- 40 Harris, E., Nelson, D.D., Olszewski, W., Zahniser, M., Potter, K.E., McManus, B.J., Whitehill, A., Prinn, R.G., and Ono, S.: Development of a spectroscopic technique for continuous online monitoring of oxygen and site-specific nitrogen isotopic composition of atmospheric nitrous oxide, *Anal. Chem.*, 86, 1726–1734, doi:10.1021/ac403606u, 2014.
- 45 Harris, E., Zeyer, K., Kegel, R., Müller, B., Emmenegger, L. and Mohn, J.: Nitrous oxide and methane emissions and nitrous oxide isotopic composition from waste incineration in Switzerland, *Waste Manage.*, 35, 135–140, doi:10.1016/j.wasman.2014.10.016, 2015b.
- 50 Heil, J., Wolf, B., Brüggemann, N., Emmenegger, L., Tuzson, B., Vereecken, H., and Mohn, J.: Site-specific ^{15}N isotopic signatures of abiotically produced N_2O , *Geochim. Cosmochim. Ac.*, 139, 72–82, doi: 10.1016/j.gca.2014.04.037, 2014.
- Henry, A., Margottin-Maclou, M., and Lacome, N.: N_2 - and O_2 -broadening parameters in the ν_3 band of $^{14}\text{N}_2^{16}\text{O}$, *J. Mol. Spectrosc.*, 111, 291–300, doi:10.1016/0022-2852(85)90006-2, 1985.
- 55 Ibraim, E., Harris, E., Eyer S., Tuzson, B., Emmenegger, L., Six, J., and Mohn, J.: Development of a field-deployable method for simultaneous, real-time measurements of the four most abundant N_2O isotopocules, *Isotopes Environ Health Stud.*, 54, 1–5, doi: 10.1080/10256016.2017.1345902, 2018.
- 60 Ibraim, E., Wolf, B., Harris, E., Gasche, R., Wei, J., Yu, L., Kiese, R., Eggleston, S., Butterbach-Bahl, K., Zeeman, M., and Tuzson, B.: Attribution of N_2O sources in a grassland soil with laser spectroscopy based isotopocule analysis, *Biogeosci.*, 16, 3247–3266, doi:10.5194/bg-16-3247-2019, 2019.

- Ishijima, K., Sugawara, S., Kawamura, K., Hashida, G., Morimoto, S., Murayama, S., Aoki, S., and Nakazawa, T.: Temporal variations of the atmospheric nitrous oxide mole fraction and its $\delta^{15}\text{N}$ and $\delta^{18}\text{O}$ for the latter half of the 20th century reconstructed from firn air analyses, *J Geophys. Res. Atmos.*, 112, D3, doi: 10.1029/2006JD007208, 2007.
- 5 Ji, Q., Grundle, D.S.: An automated, laser-based measurement system for nitrous oxide isotope and isotopomer ratios at nanomolar levels, *Rapid Commun Mass Spectrom.*, 33, 1553–1564, doi:10.1002/rcm.8502, 2019.
- 10 Johnson, J. E. and Rella, C. W.: Effects of variation in background mixing ratios of N_2 , O_2 , and Ar on the measurement of $\delta^{18}\text{O}\text{--H}_2\text{O}$ and $\delta^2\text{H}\text{--H}_2\text{O}$ values by cavity ring-down spectroscopy, *Atmos. Meas. Tech.*, 10, 3073–3091, <https://doi.org/10.5194/amt-10-3073-2017>, 2017.
- Keeling, C. D.: The mole fraction and isotopic abundances of atmospheric carbon dioxide in rural areas, 15 *Geochim. Cosmochim. Acta*, 13, 322–334, doi:10.1016/0016-7037(58)90033-4, 1958.
- Koba, K., Osaka, K., Tobari, Y., Toyoda, S., Ohte, N., Katsuyama, M., Suzuki, N., Itoh, M., Yamagishi, H., Kawasaki, M., and Kim, S.J.: Biogeochemistry of nitrous oxide in groundwater in a forested ecosystem elucidated by nitrous oxide isotopomer measurements, *Geochim. Cosmochim. Acta*, 73, 3115–20 3133, doi:10.1016/j.gca.2009.03.022, 2009.
- Kong, X., Duan, Y., Schramm, A., Eriksen, J., Holmstrup, M., Larsen, T., Bol, R., and Petersen, S.O.: Mitigating N_2O emissions from clover residues by 3, 4-dimethylpyrazole phosphate (DMPP) without adverse effects on the earthworm *Lumbricus terrestris*, *Soil Biol. Biochem.*, 104, 95–107, 25 doi:10.1016/j.soilbio.2016.10.012, 2017.
- Köster, J. R., Cárdenas, L., Senbayram, M., Bol, R., Well, R., Butler, M., Mühling, K. H., and Dittert, K.: Rapid shift from denitrification to nitrification in soil after biogas residue application as indicated by nitrous oxide isotopomers, *Soil Biol. Biochem.*, 43, 1671–1677, doi: 10.1002/rcm.6434, 2011.
- 30 Köster, J. R., Well, R., Tuzson, B., Bol, R., Dittert, K., Giesemann, A., Emmenegger, L., Manninen, A., Cárdenas, L., and Mohn, J.: Novel laser spectroscopic technique for continuous analysis of N_2O isotopomers – application and intercomparison with isotope ratio mass spectrometry, *Rapid Commun. Mass Spectrom.*, 27, 216–222, doi:10.1002/rcm.6434, 2013.
- 35 Lebegue, B., Schmidt, M., Ramonet, M., Wastine, B., Yver Kwok, C., Laurent, O., Belviso, S., Guemri, A., Philippon, C., Smith, J., and Conil, S.: Comparison of nitrous oxide (N_2O) analyzers for high-precision measurements of atmospheric mole fractions, *Atmos. Meas. Tech.*, 9, 1221–1238, doi:10.5194/amt-9-1221-2016, 2016.
- 40 Lee, A., Winther, M., Priemé, A., Blunier, T., and Christensen, S.: Hot spots of N_2O emission move with the seasonally mobile oxic-anoxic interface in drained organic soils, *Soil Biol. and Biochem.*, 115, 178–186, doi:10.1016/j.soilbio.2017.08.025, 2017.
- 45 Lewicka-Szczebak, D., Well, R., Köster, J. R., Fuß, R., Senbayram, M., Dittert, K., and Flessa, H.: Experimental determinations of isotopic fractionation factors associated with N_2O production and reduction during denitrification in soils, *Geochim. Cosmochim. Ac.*, 134, 55–73, doi: 10.1016/j.gca.2014.03.010, 2014.
- 50 Lewicka-Szczebak, D., Well, R., Bol, R., Gregory, A. S., Matthews, G. P., Misselbrook, T., Whalley, W. R., and Cardenas, L. M.: Isotope fractionation factors controlling isotopocule signatures of soil-emitted N_2O produced by denitrification processes of various rates, *Rapid Commun. Mass Spectr.*, 29, 269–282, doi: 10.1002/rcm.7102, 2015.

- Li, X., Sørensen, P., Olesen, J.E., and Petersen, S.O.: Evidence for denitrification as main source of N₂O emission from residue-amended soil, *Soil Biol. Biochem.*, 92, 153–160, doi:10.1016/j.soilbio.2015.10.008, 2016.
- 5 Li, P., Wang, S., Peng, Y., Liu, Y., and He, J.: The synergistic effects of dissolved oxygen and pH on N₂O production in biological domestic wastewater treatment under nitrifying conditions, *Environ. Technol.*, 36, 1623–1631, doi: 10.1080/09593330.2014.1002862, 2015.
- 10 Malowany, K., Stix, J., Van Pelt, A., and Lucic, G.: H₂S interference on CO₂ isotopic measurements using a Picarro G1101-i cavity ring-down spectrometer, *Atmos. Meas. Tech.*, 8, 4075–4082, doi: 10.5194/amt-8-4075-2015, 2015.
- 15 Miller, J.B., and Tans, P.P.: Calculating isotopic fractionation from atmospheric measurements at various scales, *Tellus*, 55, 207–214, doi:10.1034/j.1600-0889.2003.00020.x, 2003.
- Minamikawa, K., Nishimura, S., Nakajima, Y., Osaka, K.I., Sawamoto, T., and Yagi, K.: Upward diffusion of nitrous oxide produced by denitrification near shallow groundwater table in the summer: a lysimeter experiment, *Soil Sci. Plant Nutr.*, 57, 719–732, doi: 10.1080/00380768.2011.625556, 2011.
- 20 Mohn, J., Guggenheim, C., Tuzson, B., Vollmer, M. K., Toyoda, S., Yoshida, N., and Emmenegger, L.: A liquid nitrogen-free preconcentration unit for measurements of ambient N₂O isotopomers by QCLAS, *Atmos. Meas. Tech.*, 3, 609–618, doi:10.5194/amt-3-609-2010, 2010.
- 25 Mohn, J., Tuzson, B., Manninen, A., Yoshida, N., Toyoda, S., Brand, W. A., and Emmenegger, L.: Site selective real-time measurements of atmospheric N₂O isotopomers by laser spectroscopy, *Atmos. Meas. Tech.*, 5, 1601–1609, doi:10.5194/amt-5-1601-2012, 2012.
- 30 Mohn, J., Wolf, B., Toyoda, S., Lin, C. T., Liang, C. M., Brüggemann, N., Wissel, H., Steiker, A. E., Dyckmans, J., Szwed, L., Ostrom, N. E., Casciotti, K. L., Forbes, M., Giesemann, A., Well, R., Doucett, R. R., Yarnes, C. T., Ridley, A. R., Kaiser, J., and Yoshida, N.: Inter-Laboratory assessment of nitrous oxide isotopomer analysis of isotopomer analysis by isotope ratio mass spectrometry and laser spectroscopy: current status and perspectives, *Rapid Commun. Mass Spectr.*, 28, 1995–2007, doi: 10.1002/rcm.6982, 2014.
- 35 Mosier, A., Kroeze, C., Nevison, C., Oenema, O., Seitzinger, S. and Van Cleemput, O.: Closing the global N₂O budget: nitrous oxide emissions through the agricultural nitrogen cycle, *Nutr. Cycl. Agroecosys.*, 52, 225–248, doi:10.1023/A:1009740530221, 1998.
- 40 Murray, R., Erler, D., Rosentreter, J., Maher, D., and Eyre, B.: A seasonal source and sink of nitrous oxide in mangroves: Insights from mole fraction, isotope, and isotopomer measurements, *Geochim. Cosmochim. Acta*, 238, 169–192, doi:10.1016/j.gca.2018.07.003, 2018.
- 45 Nara, H., Tanimoto, H., Tohjima, Y., Mukai, H., Nojiri, Y., Katsumata, K., and Rella, C.W.: Effect of air composition (N₂, O₂, Ar, and H₂O) on CO₂ and CH₄ measurement by wavelength-scanned cavity ring-down spectroscopy: calibration and measurement strategy, *Atmos. Meas. Tech.*, 5, 2689–2701, doi:10.5194/amt-5-2689-2012, 2012.
- 50 Nikolenko, O., Orban, P., Jurado, A., Morana, C., Jamin, P., Robert, T., Knöller, K., Borges, A.V., and Brouyère, S.: Dynamics of greenhouse gases in groundwater: hydrogeological and hydrogeochemical controls. *Appl Geochem.*, 105, 31–44, doi:10.1016/j.apgeochem.2019.04.009, 2019.
- NOAA/ESRL: Combined Nitrous Oxide data from the NOAA/ESRL Global Monitoring Division, 2019.

- Ogawa, M., and Yoshida, N.: Intramolecular distribution of stable nitrogen and oxygen isotopes of nitrous oxide emitted during coal combustion, *Chemosphere*, 61, 877–887, doi:10.1016/j.chemosphere.2005.04.096, 2005.
- 5 Ostrom N., and Ostrom, P.: Mining the isotopic complexity of nitrous oxide: a review of challenges and opportunities, *Biogeochemistry*, 132, 359–372, doi:10.1007/s10533-017-0301-5, 2017.
- Ostrom, N.E. and Ostrom, P.H.: The Isotopomers of Nitrous Oxide: Analytical Considerations and Application to Resolution of Microbial Production Pathways, in: *Handbook of Environmental Isotope Geochemistry Volume 1*, edited by: Baskaran, M., Springer Berlin Heidelberg, Berlin, Heidelberg, 453–476, 2011.
- 10 Ostrom, N.E., Gandhi, H., Coplen, T.B., Toyoda, S., Böhlke, J.K., Brand, W.A., Casciotti, K.L., Dyckmans, J., Giesemann, A., Mohn, J., and Well, R.: Preliminary assessment of stable nitrogen and oxygen isotopic composition of USGS51 and USGS52 nitrous oxide reference gases and perspectives on calibration needs, *Rapid Commun Mass Spectrom*, 32, 1207–1214, doi:10.1002/rcm.8157, 2018.
- 15 Ostrom, N. E., Pitt, A., Sutka, R., Ostrom, P. H., Grandy, A. S., Huizinga, K. M., and Robertson, G. P.: Isotopologue effects during N₂O reduction in soils and in pure cultures of denitrifiers, *J. Geophys. Res.*, 20 112, G02005, doi:10.1029/2006JG000287, 2007.
- Pang, J., Wen, X., Sun, X. and Huang, K.: Intercomparison of two cavity ring-down spectroscopy analyzers for atmospheric ¹³CO₂/¹²CO₂ measurement, *Atmos. Meas. Tech.*, 9, 3879–3891, doi:10.5194/amt-9-3879-2016, 2016.
- 25 Park, S., Croteau, P., Boering, K.A., Etheridge, D.M., Ferretti, D., Fraser, P.J., Kim, K.R., Krummel, P.B., Langenfelds, R.L., Van Ommen, T.D. and Steele, L.P.: Trends and seasonal cycles in the isotopic composition of nitrous oxide since 1940, *Nat. Geosci.*, 5, 261, doi:10.1038/NGEO1421, 2012.
- 30 Pataki, D. E., Bowling, D. R., Ehleringer, J. R., and Zobitz, J. M.: High resolution atmospheric monitoring of urban carbon dioxide sources, *Geophys. Res. Lett.*, 33, L03813, doi:10.1029/2005gl024822, 2006.
- Peng, L., Ni, B.J., Erler, D., Ye, L., and Yuan, Z.: The effect of dissolved oxygen on N₂O production by ammonia-oxidizing bacteria in an enriched nitrifying sludge, *Water Res.*, 66, 12–21, doi:10.1016/j.watres.2014.08.009, 2014.
- 35 Picarro Inc.: Cavity Ring-Down Spectroscopy (CRDS), available at <https://www.picarro.com/company/technology/crds>, 2019.
- 40 Potter, K.E., Ono, S., and Prinn, R.G.: Fully automated, high-precision instrumentation for the isotopic analysis of tropospheric N₂O using continuous flow isotope ratio mass spectrometry, *Rapid Commun Mass Spectrom*, 27, 1723–1738, doi:10.1002/rcm.6623, 2013.
- Prokopiou, M., Martinerie, P., Sapart, C.J., Witrant, E., Monteil, G., Ishijima, K., Bernard, S., Kaiser, J., Levin, I., Blunier, T., and Etheridge, D.: Constraining N₂O emissions since 1940 using firn air isotope measurements in both hemispheres, *Atmos Chem Phys*, 17, 4539–4564, doi:10.5194/acp-17-4539-2017, 2017.
- 45 Pérez, T., Garcia-Montiel, D., Trumbore, S., Tyler, S., Camargo, P.D., Moreira, M., Piccolo, M., and Cerri, C.: Nitrous oxide nitrification and denitrification ¹⁵N enrichment factors from Amazon forest soils, *Ecol Appl*, 16, 2153–2167, doi: 10.1890/1051-0761(2006)016[2153:NONADN]2.0.CO;2, 2006.
- 50

- Pérez, T., Trumbore, S.E., Tyler, S.C., Matson, P.A., Ortiz-Monasterio, I., Rahn, T., and Griffith, D.W.T.: Identifying the agricultural imprint on the global N₂O budget using stable isotopes, *J Geophys Res Atmos.*, 106, 9869–9878, doi:10.1029/2000JD900809, 2001.
- 5 R Core Team.: R: A language and environment for statistical computing. R Foundation for Statistical Computing, Vienna, Austria. URL <https://www.R-project.org/>, 2017.
- Ravishankara, A. R., Daniel, J. S., and Portmann, R. W.: Nitrous oxide (N₂O): the dominant ozone-depleting substance emitted in the 21st century, *Science*, 326, 123–125, 2009.
- 10 Rella, C. W., Chen, H., Andrews, A. E., Filges, A., Gerbig, C., Hatakka, J., Karion, A., Miles, N. L., Richardson, S. J., Steinbacher, M., Sweeney, C., Wastine, B., and Zellweger, C.: High accuracy measurements of dry mole fractions of carbon dioxide and methane in humid air, *Atmos. Meas. Tech.*, 6, 837–860, doi:10.5194/amt-6-837-2013, 2013.
- 15 Röckmann, T., and Levin I.: High-precision determination of the changing isotopic composition of atmospheric N₂O from 1990 to 2002, *J. Geophys. Res.*, 110, D21304, doi:10.1029/2005JD006066, 2015.
- 20 Rothman, L.S., Jacquemart, D., Barbe, A., Benner, D.C., Birk, M., Brown, L.R., Carleer, M.R., Chackerian Jr, C., Chance, K., Coudert, L.E.A., and Dana, V.: The HITRAN 2004 molecular spectroscopic database, *J Quant Spectrosc Radiat Transf.*, 96, 139–204, doi:10.1016/j.jqsrt.2004.10.008, 2005.
- 25 Soto, D.X., Koehler, G., and Hobson, K.A.: Combining denitrifying bacteria and laser spectroscopy for isotopic analyses ($\delta^{15}\text{N}$, $\delta^{18}\text{O}$) of dissolved nitrate, *Anal. Chem.*, 87, 7000–7005, doi:10.1021/acs.analchem.5b01119, 2015.
- 30 Sutka, R. L., Ostrom, N. E., Ostrom, P. H., Breznak, J. A., Gandhi, H., Pitt, A. J., and Li, F.: Distinguishing nitrous oxide production from nitrification and denitrification on the basis of isotopomer abundances, *Appl. Environ. Microb.*, 72, 638–644, doi:10.1128/AEM.72.1.638-644.2006, 2006.
- 35 Sutka, R. L., Ostrom, N. E., Ostrom, P. H., Gandhi, H., and Breznak, J. A.: Nitrogen isotopomer site preference of N₂O produced by *Nitrosomonas europaea* and *Methylococcus capsulatus* bath, *Rapid Commun. Mass Sp.*, 17, 738–745, doi:10.1002/rcm.968, 2003.
- 40 Tian, H., Chen, G., Lu, C., Xu, X., Ren, W., Zhang, B., Banger, K., Tao, B., Pan, S., Liu, M., Zhang, C., Bruhwiler, L., and Wofsy, S.: Global methane and nitrous oxide emissions from terrestrial ecosystems due to multiple environmental changes, *Ecosyst. Health Sustain.*, 1, 1–20, doi:10.1890/ehs14-0015.1, 2015.
- Tuzson, B., Mohn, J., Zeeman, M.J., Werner, R.A., Eugster, W., Zahniser, M.S., Nelson, D.D., McManus, J.B., and Emmenegger, L.: High precision and continuous field measurements of $\delta^{13}\text{C}$ and $\delta^{18}\text{O}$ in carbon dioxide with a cryogen-free QCLAS, *Appl. Phys. B*, 92, 451, doi:10.1007/s00340-008-3085-4, 2008.
- 45 Toyoda S., Yoshida N., and Koba K.: Isotopocule analysis of biologically produced nitrous oxide in various environments, *Mass Spectrom. Rev.*, 36, 135–160, doi: 10.1002/mas.21459, 2017.
- Toyoda, S. and Yoshida, N.: Determination of nitrogen isotopomers of nitrous oxide on a modified isotope ratio mass spectrometer, *Anal. Chem.*, 71, 4711–4718, doi:10.1021/ac9904563, 1999.
- 50 Toyoda, S., Kuroki, N., Yoshida, N., Ishijima, K., Tohjima, Y., and Machida T.: Decadal time series of tropospheric abundance of N₂O isotopomers and isotopologues in the Northern Hemisphere obtained by

- the long-term observation at Hateruma Island, Japan, *J. Geophys. Res. Atmos.*, 118, 3369–3381, doi:10.1002/jgrd.50221, 2013.
- Toyoda, S., Mutoke, H., Yamagishi, H., Yoshida, N., and Tanji, Y.: Fractionation of N₂O isotopomers during production by denitrifier, *Soil Biol. Biochem.*, 37, 1535–1545, doi:10.1016/j.soilbio.2005.01.009, 2005.
- Toyoda, S., Yano, M., Nishimura, S., Akiyama, H., Hayakawa, A., Koba, K., Sudo, S., Yagi, K., Makabe, A., Tobari, Y., Ogawa, N. O., Ohkouchi, N., Yamada, K., and Yoshida, N.: Characterization and production and consumption processes of N₂O emitted from temperate agricultural soils determined via isotopomer ratio analysis, *Glob. Biogeochem. Cy.*, 25, GB2008, doi: 10.1029/2009GB003769, 2011.
- Verhoeven, E., Barthel, M., Yu, L., Celi, L., Said-Pullicino, D., Sleutel, S., Lewicka-Szczebak, D., Six, J., and Decock, C.: Early season N₂O emissions under variable water management in rice systems: source-partitioning emissions using isotope ratios along a depth profile, *Biogeosci.*, 16, 383–408, doi:10.5194/bg-16-383-2019, 2019.
- Verhoeven, E., Decock, C., Barthel, M., Bertora, C., Sacco, D., Romani, M., Sleutel, S., and Six, J.: Nitrification and coupled nitrification-denitrification at shallow depths are responsible for early season N₂O emissions under alternate wetting and drying management in an Italian rice paddy system, *Soil Biol. Biochem.*, 120, 58–69, doi:10.1016/j.soilbio.2018.01.032, 2018.
- Vogel, F. R., Huang, L., Ernst, D., Giroux, L., Racki, S., and Worthy, D. E. J.: Evaluation of a cavity ring-down spectrometer for in situ observations of ¹³CO₂, *Atmos. Meas. Tech.*, 6, 301–308, doi:10.5194/amt-6-301-2013, 2013.
- Wächter, H., Mohn, J., Tuzson, B., Emmenegger, L., and Sigrist, M.W.: Determination of N₂O isotopomers with quantum cascade laser based absorption spectroscopy, *Optics express*, 16, 9239–9244, doi:10.1364/OE.16.009239, 2008.
- Wassenaar, L.I., Douence, C., Altabet, M.A., and Aggarwal, P.K.: N and O isotope ($\delta^{15}\text{N}^{\alpha}$, $\delta^{15}\text{N}^{\beta}$, $\delta^{18}\text{O}$, $\delta^{17}\text{O}$) analyses of dissolved NO₃⁻ and NO₂⁻ by the Cd-azide reduction method and N₂O laser spectrometry, *Rapid Commun. Mass Spectr.*, 32, 184–194, doi:10.1002/rcm.8029, 2018.
- Wei J., Zhou M., Vereecken H., and Brüggemann N.: Large variability in CO₂ and N₂O emissions and in ¹⁵N site preference of N₂O from reactions of nitrite with lignin and its derivatives at different pH. *Rapid Commun. Mass Sp.*, 31, 1333–1343, doi:10.1002/rcm.7912, 2017.
- Well, R., Eschenbach, W., Flessa, H., von der Heide, C., and Weymann, D.: Are dual isotope and isotopomer ratios of N₂O useful indicators for N₂O turnover during denitrification in nitrate-contaminated aquifers? *Geochim. Cosmochim. Acta* 90, 265–282, doi:10.1016/j.gca.2012.04.045, 2012.
- Well, R. and Flessa, H.: Isotopologue signatures of N₂O produced by denitrification in soils, *J. Geophys. Res.*, 114, G02020, doi:10.1029/2008JG000804, 2009.
- Well, R., Flessa, H., Jaradat, F., Toyoda, S., and Yoshida, N.: Measurement of isotopomer signatures of N₂O in groundwater, *J. Geophys. Res.* 110, G02006, doi:10.1029/2005JG000044, 2005.
- Well, R., Flessa, H., Xing, L., Xiaotang, J., and Römheld, V.: Isotopologue ratios of N₂O emitted from microcosms with NH₄⁺ fertilized arable soils under conditions favoring nitrification, *Soil Biol. Biochem.*, 40, 2416–2426, doi:10.1016/j.soilbio.2008.06.003, 2008.

- Wen, X.-F., Meng, Y., Zhang, X.-Y., Sun, X.-M., and Lee, X.: Evaluating calibration strategies for isotope ratio infrared spectroscopy for atmospheric $^{13}\text{CO}_2/^{12}\text{CO}_2$ measurement, *Atmos. Meas. Tech.*, 6, 1491–1501, doi:10.5194/amt-6-1491-2013, 2013.
- 5 Werle, P.O., Mücke, R., and Slemr, F.: The limits of signal averaging in atmospheric trace-gas monitoring by tunable diode-laser absorption spectroscopy (TDLAS), *Applied Physics B*, 57, 131–139, doi:10.1007/BF00425997, 1993.
- Werner, R. A. and Brand, W. A.: Referencing strategies and techniques in stable isotope ratio analysis,
 10 *Rapid Commun. Mass Spectrom.*, 15, 501–519, doi:10.1002/rcm.258, 2001.
- Winther, M., Balslev-Harder, D., Christensen, S., Priemé, A., Elberling, B., Crosson, E., & Blunier, T.: Continuous measurements of nitrous oxide isotopomers during incubation experiments, *Biogeosciences*, 15, 767–780, doi:10.5194/bg-15-767-2018, 2018.
- 15 Wolf, B., Merbold, L., Decock, C., Tuzson, B., Harris, E., Six, J., Emmenegger L., and Mohn J.: First on-line isotopic characterization of N_2O above intensively managed grassland, *Biogeosciences*, 12, 2517–2531, doi: 10.5194/bg-12-2517-2015, 2015.
- 20 Wunderlin, P., Lehmann, M. F., Siegrist, H., Tuzson, B., Joss, A., Emmenegger, L., and Mohn, J.: Isotope signatures of N_2O in a mixed microbial population system: constraints on N_2O producing pathways in wastewater treatment, *Environ. Sci. Technol.*, 47, 1339–1348, doi: 10.1021/es303174x, 2013.
- Wunderlin, P., Mohn, J., Joss, A., Emmenegger, L., and Siegrist, H.: Mechanisms of N_2O production in
 25 biological wastewater treatment under nitrifying and denitrifying conditions, *Water Res.*, 46, 1027–37, doi: 10.1016/j.watres.2011.11.080, 2012.
- Yamamoto, A., Uchida, Y., Akiyama, H., and Nakajima, Y.: Continuous and unattended measurements of the site preference of nitrous oxide emitted from an agricultural soil using quantum cascade laser
 30 spectrometry with intercomparison with isotope ratio mass spectrometry, *Rapid Commun. Mass Spectr.*, 28, 1444–1452, doi:10.1002/rcm.6916, 2014.
- Yoshida, N. and Toyoda, S.: Constraining the atmospheric N_2O budget from intramolecular site
 35 preference in N_2O isotopomers, *Nature*, 405, 330–334, doi:10.1038/35012558, 2000.
- Yue, F.J., Li, S.L., Liu, C.Q., Mostofa, K.M., Yoshida, N., Toyoda, S., Wang, S.L., Hattori, S., and Liu, X.L.: Spatial variation of nitrogen cycling in a subtropical stratified impoundment in southwest China, elucidated by nitrous oxide isotopomer and nitrate isotopes, *Inland Waters*, 8, 186–195, doi: 10.1080/20442041.2018.1457847, 2018.